A VIRTUAL-CAM BASED CONTROL METHODOLOGY

FOR FREE-PISTON ENGINES

By

CHAO YONG

Dissertation

Submitted to the Faculty of the

Graduate School of Vanderbilt University

in partial fulfilment of the requirements

for the degree of

DOCTOR OF PHILOSOPHY

in

Mechanical Engineering

August 2011

Nashville, Tennessee

Approved:

Professor Eric J. Barth

Professor Michael Goldfarb

Professor Nilanjan Sarkar

Professor Robert J. Webster

Professor George E. Cook

i

To my parents

ACKNOWLEDGEMENTS

TABLE OF CONTENTS

LIST OF FIGURES AND TABLES

Page

ABSTRACT

The free-piston engine has been widely investigated and variety of free-piston engines have been developed for a number of applications due to their advantages in comparison to conventional internal combustion (IC) engines: 1) the free-piston reduces the mechanical friction losses from side loading of piston due to the crank. 2) The engine can be started/stopped on demand so that the engine's fuel efficiency can be improved by eliminating the idle operation in conventional IC engines. 3) The absence of a crankshaft-connecting rod mechanism gives the engine variable stroke lengths to allow the controller for optimizing the engine efficiency by using variable compression/expansion ratios.

In conventional internal combustion engines, valves are opened and closed using a cam surface. The cam positions are kinematically related to the piston positions through the crankshaft and timing belt. In contrast, there is no crankshaft or kinematic cam surface in a free-piston engine to physically realize this mechanism because the piston is not connected to a crank and cam. In addition, a free-piston engine has variable stroke lengths and therefore it presents a challenge for active piston motion and precise stroke length control. Inspired by the crank and cam mechanism in conventional engines, this work proposes a virtual-cam based approach to connect free-piston motion to valve controls in an electronic control context. The primary functionality of the virtual cam control framework is to create repetitive but variable indices for the exhaust/injection valves and spark timing similar to the function of physical cams in conventional engines. Since the cam is virtually created, it can be dynamically rebuilt to comply with cycle-to-cycle variations such as engine load and stroke length. This index rebuilding procedure is

based on a cycle-to-cycle adjustment method that uses the information obtained from previous cycles to adjust the cam parameters.

Measurement of the piston position in free-piston engines is often difficult, whereas the cylinder pressure can be more easily measured. From a control's perspective, pressure, power and energy of a control volume directly represent the dynamics of the engine and the piston. Therefore, this work investigates using pressure measurements and pressure dynamics in the virtual-cam control approach. Specific details of this method such as measurement of critical positions, e.g. Top Dead Center (TDC) and Bottom Dead Center (BDC), are shown. Moreover, a novel term of "breathe-in duration" is used for evaluating the pump performance for a free-piston engine air compressor so that measurement of the stroke length and calculation of expansion ratio are replaced by it.

A comprehensive lumped-parameter model of an experimental Free Liquid-Piston Engine Compressor (FLPEC) was built and validated. The proposed control method was first demonstrated in simulation of the FLPEC. The simulation results were promising, thus an experimental evaluation of the proposed control scheme was conducted on a High Inertance Free Liquid Piston Compressor (HIFLPC). Experimental results of the injection control, exhaust control and overall engine operation presented within this manuscript showed an overall satisfactory engine performance, especially: 1) overall engine efficiency was significantly improved from experimental results of manually tuned tests; 2) wide operation range in terms of the reservoir pressure was achieved; 3) the controller was shown to be capable of adjusting the engine operational frequency upon request. Based on the experimental results, this control framework should be capable of serving as a favourable control scheme for other free-piston engines.

Chapter I

FREE-PISTON ENGINES AND CONTROL

The free-piston engine has been widely investigated since it was first proposed by R.P. Pescara in 1928. A variety of free-piston engines have been developed for a number of applications due to their advantages in comparison to conventional internal combustion (IC) engines. Some of these advantages are: 1) the free-piston reduces the mechanical friction losses from side loading of piston due to the crank. In some configurations, such as the free liquid-piston engine developed by Riofrio and Barth [2][3], the piston friction is largely eliminated by using a liquid free-piston. 2) The engine does not require idle cycles. In other words, it can be started/stopped upon request so that the engine's fuel efficiency can be improved by eliminating the idle operation in conventional IC engines. 3) The absence of a crankshaft-connecting rod mechanism gives the engine variable stroke lengths. This feature will allow the controller to optimize the engine efficiency by using variable compression/expansion ratios.

However, in addition to these advantages, the unique features of the free-piston engine also present a control challenge due to the non-crank mechanism. In this chapter, a brief review of the free-piston engine concept and applications is provided, followed by a discussion of the control challenges.

1.1   Free-piston engines

A free-piston engine is typically a linear combustion engine. The piston used in the engine is called free because it is not connected to a crankshaft and not kinematically

1

limited in its motion as in conventional combustion engines. Based on the piston/cylinder configuration, free-piston engines are typically divided into three categories: single piston, dual piston and opposed piston. A less common fourth category, gas generators, is also discussed in some literature. For a more detailed description of these configurations, one can refer to a comprehensive review recently provided by R. Mikalsen and A.P. Roskilly [4].

In the early 1930's, a German company named Junkers developed a free-piston air compressor that was used by the German navy during World War 2 to provide compressed air for submarines [5]. Later, a US company called Worthington continued this Junker design without major design changes [6]. In 1950's, the automobile industry conducted research on utilizing the advantages of the free-piston engine concept, aiming for automobile scale applications. For instance, General Motors (GM) developed two free-piston gas generators [7]. However, the results of their test were quite disappointing. According to Specht [8], the problems included control difficulties and high maintenance costs but they did not dismiss the free-piston engines as a concept. Ford carried out similar efforts in free-piston engine developments in 1950's without success [9]. An important reason for these efforts being unsuccessful was the lack of a proper mechanical control mechanism, since electronic control was not available at the time.

Further research on the free-piston engines was largely abandoned in the mid-20th century partially because of these unsuccessful attempts. Along with the advance in modern control technologies, however, the free-piston engine concept has again drawn the interest of a number of research groups. Control systems and their implementation

have gained more popularity in reported modern free-piston engine development, as opposed to earlier approaches that focused primarily on engine design. Achten et al. [10] at Innas reported the implementation of an advanced control system for a hydraulic free-piston engine pump, which has a 20% fuel efficiency increase compared to conventional engines due to the reduction of friction losses from crank and active loads. However, the simplicity of the mechanical design set high requirements for the control system. To investigate the control challenge, Tikkanen et al. [11-12] described the design and control of a dual hydraulic free-piston engine pump. In a more recent approach, Kværner ASA developed a modern two-stroke high-speed diesel free-piston engine aimed at marine applications [13]. By using modern electronic control technologies, experimental results on the single cylinder of the diesel combustion unit were reported in [14], showing that Top Dead Center (TDC) and Bottom Dead Center (BDC) were controlled to be stabilized at their set-points. Authors of [13-14] concluded that the modern electric control technology provides the "required processing capacity and resolution to implement the required control system functionality" of modern free-piston engines.

Mikalsen and Roskilly [4] described more free-piston engines applications in a comprehensive overview. They concluded that since the free-piston engine is "restricted to the two-stroke operating principle", and therefore heavily reliant on scavenging in order to achieve proper combustion characteristics, "accurate control of piston motion currently represents one of the biggest challenges for developers of free-piston engines." In order to investigate the control challenges of free-piston engines, a discussion of their unique features is carried out in the next section.

1.2   Unique features of free-piston engines

In order to control the stroke length and the piston dynamics, the sum forces on either side of the piston (mainly from the pressures on the piston) need to be controlled. However, accurate pressure control, especially combustion pressure control is difficult. To address the control challenge imposed by these difficulties, the knowledge of the piston dynamics is utilized in the controller. Therefore, the free piston dynamics are first discussed in the next sub-section.

1.2.1   Free-piston dynamics

In conventional engines, the piston is connected by the crank to the flywheel. This mechanism serves as a mechanical piston motion control system. The inertia of the flywheel acts as energy storage that provides power for the compression stroke. It lacks control flexibility but provides full piston motion and position control. Moreover, the crank mechanism also defines the boundary of the piston motion, i.e. TDC and BDC. This configuration allows a fixed stroke and consequently a fixed expansion ratio. Conversely, in the free-piston engine, the piston is free and its stroke length is not restricted by the crank mechanism. It gives the free-piston engine more control flexibility for complying with different loads. However, it also presents a control challenge for accurate piston motion control.

Typically, a combustion chamber and a load chamber (or bounce chamber) will be on opposite sides of the piston, as shown in Figure 1.1 (a). The moment when the piston is at TDC is the initial point of combustion. During the power stroke, high pressure resulting from the combustion pushes the piston to the load side, thereby sending power

to the load and pressurizing the bounce chamber; during the return stroke, the pressurized bounce chamber or some other type of returning force acts on the piston to ensure a reciprocating motion of the piston. BDC is defined as the piston position at which the piston stops at the end of the power stroke. TDC and BDC together define the stroke length. If a bounce device other than a gas bounce chamber is used, the piston motion characteristic is slightly different but the same principle will remain applicable.
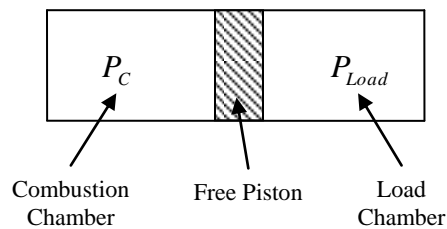
(a) A simplified single piston engine
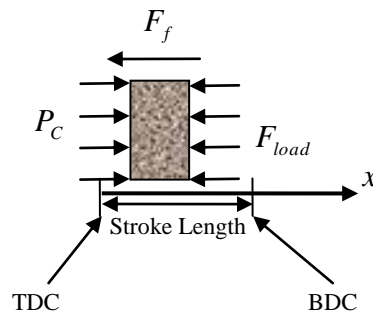
(b) Piston dynamics and stroke

Figure 1.1 Piston dynamics of single piston free-piston engine

By using pressure sensors, the piston dynamics can be modelled based on the measured pressures together with the frictions and loads acting on the piston. Figure 1.1(b) shows the forces acting upon the piston. Applying Newton's second law to the moving piston, the dynamics can be described as,

$$\sum_i F_i = m_p \frac{d^2 x}{dt^2} = P_C A - F_f - F_{load} \qquad (1.1)$$

where P_C is the combustion pressure, A is cross sectional area of the piston, F_f is the friction force and F_{load} is the force from the load, x denotes the position of the mover (piston). The stroke length during the power stroke is $x_{BDC} - x_{TDC}$.

Eq. (1.1) implies that precise piston motion control requires accurate pressure control of P_C and control of the load force F_{load}. However, since the combustion process is not directly controllable, the combustion pressure dynamics are also not directly controllable. TDC and BDC, as shown in Figure 1.1, are not fixed positions as in conventional engines. For stroke length control or expansion (compression) ratio control, more specifically, controlling the piston to reach particular positions of TDC and BDC is of more interest than the precise piston motion profile control along the piston path. Development of practical TDC/BDC control methods for such purpose is more important for good thermodynamic efficiency, avoiding piston-wall collision and so on, which is the focus in this work.

1.2.2 Frequency control

In conventional engines, the stroke length is fixed. Thus, the frequency control in such engines is essentially speed control. For a free-piston engine using a gas bounce chamber or a spring-like return device, the period of an engine cycle is strongly influenced by its passive dynamics of the spring-mass nature. The combustion process only has slight impact on the engine frequency in free-piston engines. Therefore, the frequency of the free-piston engine is typically limited in a small range. However, free-

piston engines do not have idle cycle as conventional engines do, and therefore the piston can be controlled to stop at the end of the return cycle. In this way, the engine frequency can be controlled by stopping the engine for a certain amount of time before the next power stroke, i.e. postpone the combustion for next cycle.

1.2.3 Free-piston engine loads
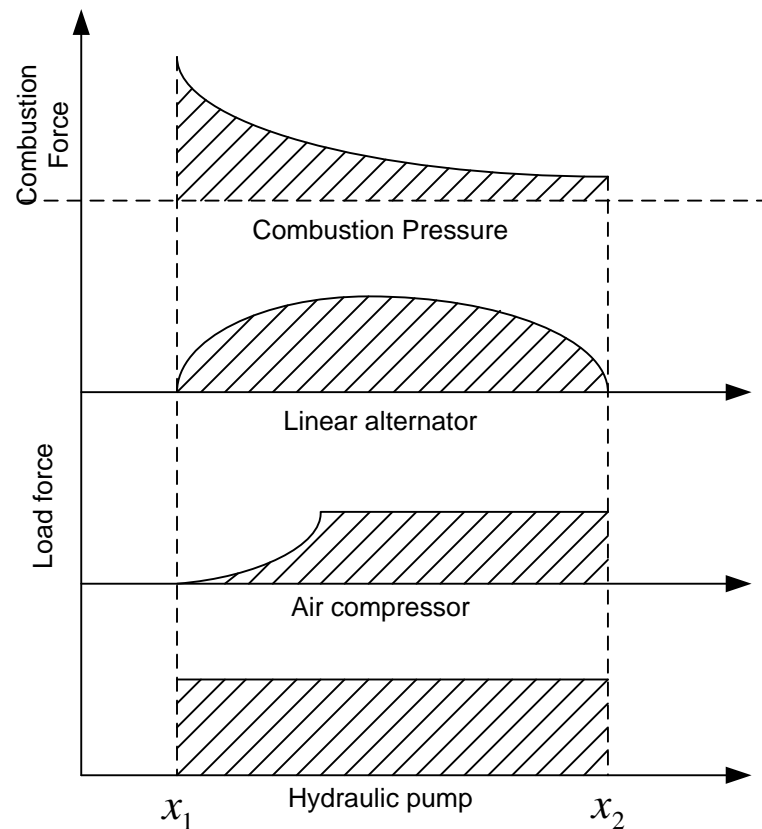
Figure 1.2 Characteristics of free-piston engine loads [15].

The position-varying loads acting on the piston of a given free-piston engine are different and therefore it also present a control challenge. As shown in Figure 1.2 [15], the load forces for the same combustion pressure dynamics (top) in different free-piston

engine applications. It is desired to have a linear load, more controllable load as seen with the hydraulic pump, so that the piston dynamics is relatively easier to control. Therefore, the difficulty lies in developing a proper expansion ratio (stroke length) control for devices with non-linear loads.

1.2.4   Combustion process in free-piston engines

The combustion process in free-piston engines, as reported by different researchers, has shown: 1) it is significantly faster than that in the conventional combustion engines due to the direct coupling of the combustion cylinder to the low inertia moving components; 2) it has cleaner emissions for a spark ignited free-piston engine than crankshaft engines; 3) the in-cylinder heat transfer is also different from conventional engines. Refer to [4] for more detailed discussions.

From a control perspective, a particular feature of free-piston engines is that the combustion process strongly influences the stroke length. The amount of fuel injection determines the stroke length and the energy delivered to the loads. For optimal efficiency, the energy input is desired to match the energy output requirement. Therefore, fuel mass injection control is a crucial control input for engine efficiency and stroke length control.

1.3   Control of free-piston engines

Combustion expansion ratio control is the most important control objective for free-piston engines. This control objective is a combination of TDC and BDC positions control. As shown in Eq. (1.2), TDC and BDC together define the expansion ratio λ_c,

$$\lambda_c = \frac{x_{BDC}}{x_{TDC}} \tag{1.2}$$

TDC is the initial piston position in the power stroke. Even small variations in the initial volume of the combustion chamber lead to large changes in the expansion ratio. On the other end of the stroke, the BDC position also affects the compression ratio, but does so much less than TDC position.

In order to control TDC, BDC and the resulting stroke length, a variety of approaches in the past have been attempted by regulating one or more of the following control inputs: 1) amount of air/fuel injection; 2) exhaust opening timing; 3) exhaust closing timing; 4) ignition timing and 5) load. Load, however, is not directly controllable in most free-piston applications, and it is therefore not considered as a controllable input in this work. The four considered control inputs listed above will be addressed in order.

The amount of the fuel mass is the energy input to the engine which is converted to energy output in the form of work done on the load. This amount needs to be regulated in such a way that the engine will correspondingly output the power required by certain loads. S. Tikkanen reported a control approach for this purpose which is applied to a dual hydraulic free-piston engine [12]. The controller is based on energy balance, i.e., the input energy (result of fuel combustion) equals the output energy, in the form of the piston mechanical energy and compression energy. In this approach, timing/estimation of the valve and injection, expansion ratio and engine operation are controlled based on energy conservation. Simulation results show good control performance, but experimental tests were not performed on the real device. This control approach requires full knowledge of the engine, including friction and load. This requirement makes the energy-balance-based method difficult to practically implement. Moreover, the

measurement of the load energy is possible for the hydraulic engine pump but not always feasible for other applications such as air compressors.

Some free-piston engines, such as the free-piston engine generator developed by Mikalsen and Roskilly [4], have a scavenging port for exhausting. Active exhaust control is not required for such engines. By eliminating the exhaust port design, there is more stroke flexibility. However, this requires an accurate exhaust valve control dealing with variable BDC positions. A good example is the control strategy for a free-piston gas generator developed by the Norwegian company Kværner ASA. Johansen T.A. et al [13][14]. The authors developed an electronic cam and crankshaft based control strategy dealing with the control of a free-piston diesel engine. The control target is a multi-cylinder free-piston diesel engine that consists of a free-piston gas generator, a turbocharger and a power turbine. This engine has 8 cylinders with 8MW total power output. The control system in their work includes valve and injector timing, piston motion control and a supervisory control. During the engine operation, the piston position and pressures are measured in real time. An estimator is then used to predict piston motion so that the valve timing controller can send the control signals in advance to compensate the time delays of the actuators and injector. Piston motion control deals with the TDC and BDC position control. Experimental results show a satisfactory level of engine performance controlled when using this method. The timing control and piston motion control used by T.A. Johansen et al are based on estimations of the piston position and the gas mass in the power chamber. Therefore, the accuracy of such control method is strongly influenced by that of the estimator. The authors did not show the performance

of these estimators and how the estimation accuracy affects the timing control. The feasibility of estimating piston and pressure dynamics may become a more crucial question for much smaller scale than this 8MW engine.

Besides piston motion control, engine speed or frequency control is also one of the control goals. For instance, for hydraulic free-piston engines to allow flow control, they require a wide speed range. For such purpose, Achten et al [10] reported a Pulse Pause Modulation scheme for frequency control of hydraulic free-piston engines. This control method pauses the piston at BDC by using a controllable hydraulic cylinder as rebound device. Only when the hydraulic rebound device is released, upwards motion of the piston can be resumed. The stored energy in the rebound chamber is released for compression. This type of frequency control in free-piston engines is possible because the piston position in each stroke is not frequency-dependent.

In a very recent work, Mikalsen and Roskilly [17][18] investigated the feasibility of classical control strategies for the free-piston engine generator developed at Newcastle University. The control strategies include decentralized PID control, pseudo-derivative feedback control and disturbance feedforward control. They concluded "further research into free-piston engine control is required to solve the significant control challenges associated with such engines".

As one can see, the reported control approaches are typically application specific and thus, the feasibilities of these reported methods are limited to particular engines. For instance, accurate estimation of piston dynamics used in [17] [18] is not always achievable; full knowledge of the engine dynamics and controlled loads are not available

for applications other than hydraulic pumps [12]. In contrast, in conventional combustion engines the crankshaft mechanism provides a universal piston motion and valve timing control framework. Injection, compression, and valve timings strictly correspond to certain piston positions, controlled by the crankshaft and cams regardless of the load and cylinder pressure variations. Inspired by crank and cam mechanism in conventional engines, the purpose of this work is to develop a general control framework for free-piston engine control that mimics this crankshaft mechanism without losing control flexibility. Using computer/electronic control, the crank and cam mechanism can be virtually created and dynamically adjusted to fulfill the control objectives such as optimizing the engine efficiency and expansion ratio. In the next chapter, the development of such a framework is described in detail.

Chapter II

VIRTUAL-CAM BASED CONTROL FOR FREE-PISTON ENGINES

The term of virtual cam used here refers to the repetitive but variable timing control indices in a computer/electronic based controller. Modern computer technology provides a convenient way to electronically control intake/exhaust valves. In the engine control community, researchers have been interested in control of camless engine which would yield higher efficiency [19]. The camless valve actuation systems offer potential benefits since valve positions can be controlled independently rather than using an engine-dependent camshaft [20]. The free-piston engine can easily take advantage from such technology by its camless nature.

The proposed virtual-cam based controller has a primary functionality of opening/closing valves similarly to the physical cam of conventional engines. That is, cams trigger the open/close actuations of the control valves at certain piston positions. In conventional engines, the piston is connected by the crank to the flywheel. This mechanism mechanically serves as the piston motion control system. The crank mechanism also defines the boundary of the piston motion, i.e. TDC and BDC. The rotary dynamics of the crankshaft are fully constrained by the piston dynamics. This mechanism can drive the crankshaft to rotate a full revolution because the connected piston travel distance is fixed during one engine cycle.

As illustrated in Figure 2.1 (a), the piston position is used to generate cam timing in conventional engines, but this mechanism is not available in free-piston engines. The

piston motion is now actively controlled and absolute positions of the piston can no longer be used to trigger the valve actuations. The proposed virtual cam mechanism uses a self-driven crankshaft that locates the virtual cams at relative positions (TDC/BDC for instance) for valve timings. The cam characteristics are adjusted based on the measurement of the engine dynamics and the evaluation of the engine performance, as shown in Figure 2.1(b). The angular speed of the virtual camshaft determines the period of a cycle. The operational frequency of the engine can be manually input or can be automatically adjusted by the system level controller based on evaluation of the engine performance.
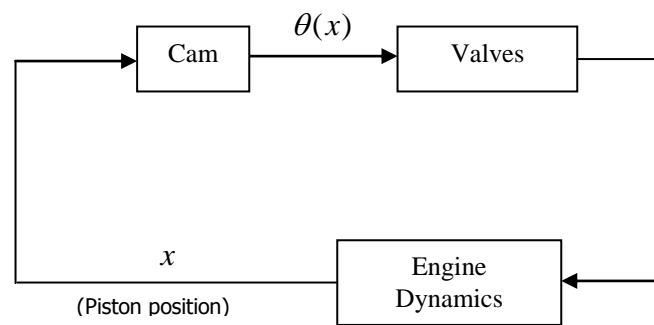
(a) Physical cam control scheme in conventional engines
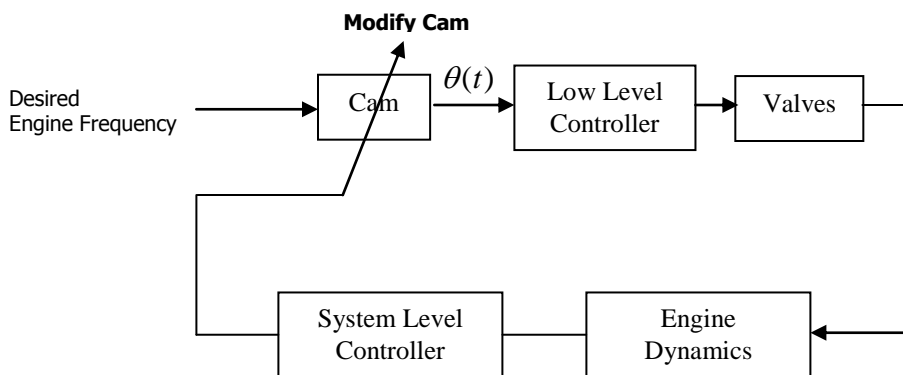
(b) Virtual-cam based control scheme for free-piston engines

Figure 2.1 Comparison between physical cam and virtual cam schemes

2.1 Virtual-cam for free-piston engine control

2.1.1 Virtual cam construction
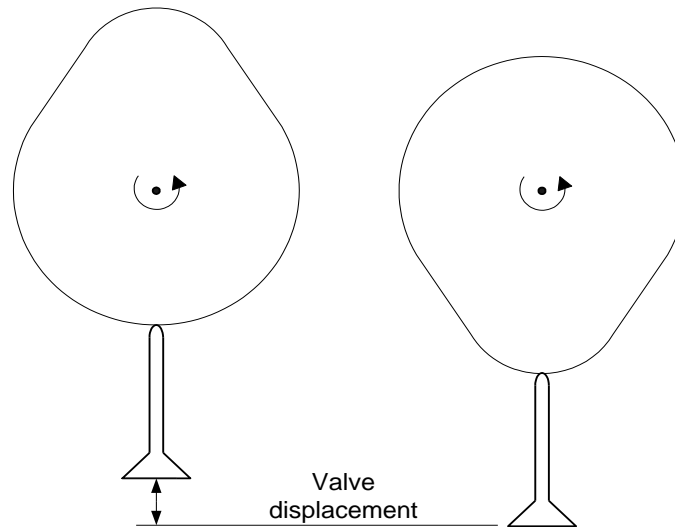
Figure 2.2 Cam and valve

By definition, a cam is a projecting part of a rotating wheel or a shaft that strikes a lever at one or more points in its circular path, as shown in Figure 2.2. In automobile engines, timing belts are used to connect the crankshaft with the camshaft so that rotary motion of the engine is translated into the reciprocating motion of the cam to operate the intake and exhaust valves. Cams in engine control can be characterized by their displacement diagrams, which reflect the changing position the valve would make as the cam rotates about a fixed axis. The valve displacement is fully defined by the displacement diagram (the shape of its periphery) of the corresponding cam. Figure 2.2 shows the valve displacement from close position (left) to open position (right) along with the cam rotation. During the open/close motion, the cam shape and the rotary motion of the cam together characterize the dynamics of the valve.

(a) Virtual cam position   (b) Virtual cam shape
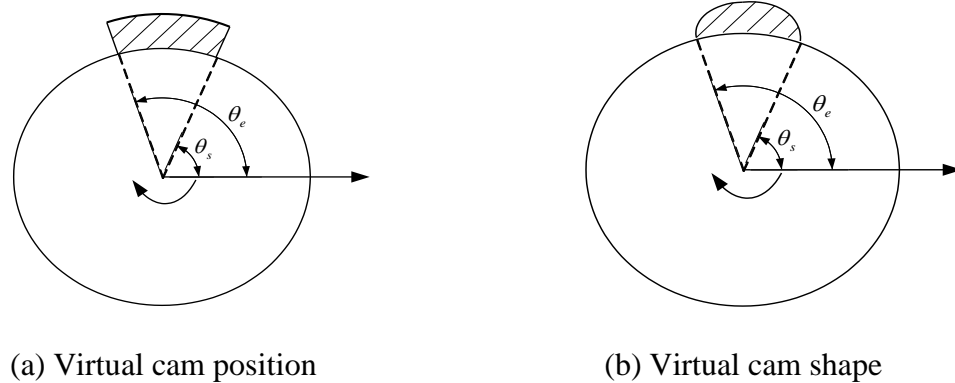
Figure 2.3 Basic cam configurations

Based on above discussion, one can see that a cam has two basic properties: 1) position, including start and end positions; 2) shape of its periphery that defines the corresponding valve open/close dynamics. The position of a cam, denoted by $\{\theta_s, \theta_e\}$, defines the time to open and close the corresponding valve.

The cam starts to push valve open at opening angle θ_s and closes the valve at closing angle θ_e. Figure 2.3(a) illustrates a cam lobe which would produce a square-wave shape that only defines the timings for opening/closing the valve at $\{\theta_s, \theta_e\}$. In Figure 2.3(b), its periphery is designed and shaped to generate certain valve response dynamics while the cam duration is still $\{\theta_s, \theta_e\}$. Furthermore, the cam position is advanced by a low level controller to compensate for valve lifter dynamics and ignition delay if they are known or measured in the previous engine cycles. To illustrate, consider Figure 2.4(a) which shows the command signals sent to a free liquid-piston engine [2-3]. The solid line is the air/fuel injection command, the dashed line is the spark signal and the dotted line is the exhaust valve command signal. Valve lift dynamics are shown in Figure 2.4(b). In order to achieve desired dynamic response of the valve lifter, the low-level controller can

control the shape of the cam's periphery. Specifically, the voltage for controlling the valve lifting and landing forms the "shape" of the virtual cam.
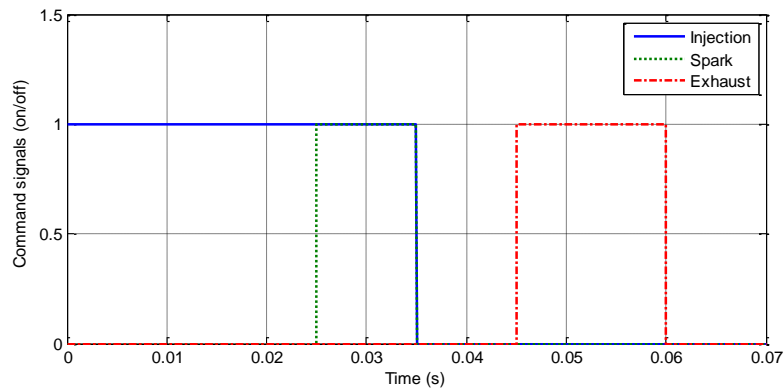
(a) Control commands
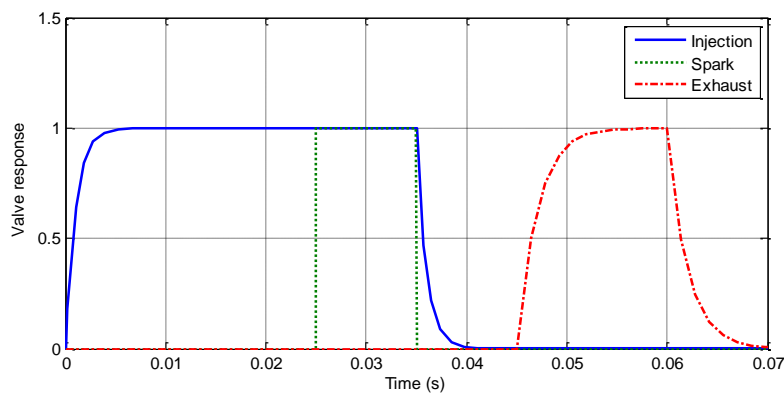
(b) Actual system responses to the control commands

Figure 2.4 Delay and dynamics response

Conventional engines have multiple valves and every valve has a dedicated cam. All the cams are typically fabricated on a camshaft, which is a cylindrical rod running the length of the cylinder bank with a number of oblong lobes or cams protruding from it, one for each valve, as shown in Figure 2.5(a). The cams force the valves to open by pressing on a valve, or on some intermediate mechanism, as they rotate. In the virtual

cam context, all cams can be similarly projected on one rotating virtual camshaft, as illustrated in Figure 2.5(b). Since this camshaft is virtually created, it is self-spinning at an angular velocity ω. One revolution of this virtual camshaft corresponds to one engine cycle. If f_{engine} is the operational frequency of the engine, the following equation holds,

$$f_{engine} = \frac{\omega}{2\pi} \tag{2.1}$$

Hence, the operating frequency of the engine could be simply modulated by controlling the angular velocity ω while using a constant R. When the angular velocity ω is changed to change the engine frequency from f_1 to f_2, the new virtual cam positions θ_2 under the new operational frequency need to be corresponding changed by $\theta_2 = f_2\theta_1/f_1$. Thus, the timings are kept same in the time domain.

(a) A typical camshaft   (b) Virtual camshaft

Figure 2.5 Physical camshaft and virtual camshaft

As a summary, the working principles of the proposed virtual cam control scheme are: 1) one revolution of the virtual camshaft corresponds to one engine cycle, thus the frequency of the engine is controlled by the angular velocity of the virtual camshaft; 2)

18

the opening/closing timing of each valve is defined by the valve's virtual cam position duplex $\{\theta_s, \theta_e\}$; 3) the shape of a virtual cam defines the control output, such as voltage (or current) for electronic valves; 4) all the virtual cam and camshaft parameters are re-defined at the end of each engine cycle. Thus all timings can be adjusted by changing the cam parameters.

Based on the proposed virtual cam framework, a control strategy is required to adaptively adjust cam function from cycle to cycle. In the next section, the controller design will be discussed in detail.

2.1.2 Control structure

The cycle-to-cycle rebuilding of the virtual cam structure provides a convenient way for repetitive/iterative engine control strategies. The repeating timing indices are now represented by cam parameters $\{\theta_s, \theta_e\}$ at a certain camshaft angular speed ω. The main control task for the virtual cam is to adaptively modify the cam geometry over the engine cycles to comply with varying strokes, loads, etc.

For general engine control, a number of inputs and outputs to the system need to be defined. Typically, main inputs to the engine include the signals to the air/fuel injection system, which determine fuel injection timing and the mass of fuel to be injected, and the signals to the exhaust valve(s), the timings of which affect the stroke length and expansion (compression) ratio. The main disturbance for free-piston engines is the engine load, which is considered uncontrollable in this work.

On the high level control, a system level control is required to optimize the engine performance with respect to fuel efficiency and exhausting timings for a given operating

point. In conventional engines, this is achieved by adjusting fuel injection timing and valve timings. For free-piston engines, optimization of the engine performance also includes expansion (compression) ratio, i.e. stroke length control.
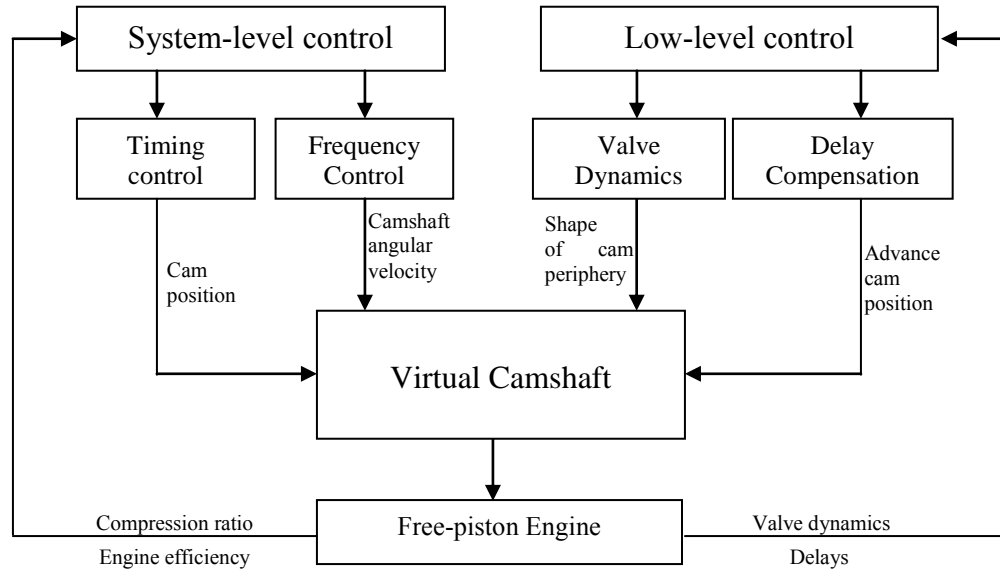
Figure 2.6 Virtual-cam based free-piston engine control structure

By using the concept of the virtual cam and camshaft, the control structure is illustrated in Figure 2.6. The key part of the control structure is the virtual camshaft that includes multiple virtual-cams for multiple valves. The system level controller dictates the opening/closing timings for valves and the engine frequency, which are virtual cam position $\{\theta_s, \theta_e\}$ and camshaft angular speed ω, respectively. The low level controller deals with the valve lifter dynamics control and delay compensation. At the end of each engine cycle, the virtual cams are rebuilt and the resulting control outputs are sent to the free-piston engine. The rebuilding method is based on the analysis of the engine performance including stroke length, engine efficiency and other factors that will be

discussed further in the next section. Meanwhile, valve response dynamics and delays are measured and fed back to the low-level controller.

This structure of the control mechanism naturally bridges system level control with lower level control. Consider an electromechanical valve actuator in camless engines, which has been studied by numerous researchers [19][20]. The control design for an electromechanical valve actuator is the virtual cam design in our context. The system level controller sends out the open/close commands, i.e. $\{\theta_s, \theta_e\}$. The corresponding cam is then 'shaped' by the low level controller to realize desired effects such as the soft landing of the valve [21].

2.2   Virtual cam repeating index rebuild

Since the low-level control is engine and valve specific, it will be omitted from the discussion of the general control methodology of the virtual-cam framework. This work thus focuses on the system-level control for virtual-cam rebuilding. In a typical free-piston engine, optimizing the amount of the fuel mass injected and the exhaust valve timings are the main control objectives. These objectives are controlled to achieve desired engine efficiency and stroke length.

Similar to conventional IC engines, a free-piston engine typically has at least one combustion chamber, providing energy input for the power stroke, and a load chamber (or a bounce chamber), as shown on the left in Figure 2.6. A load chamber is used to deliver energy to loads and a bounce chamber is used to assist returning piston back. For direct air/fuel injection engines such as some HCCI free-piston engines, the air/fuel mixture is directly injected into the combustion chamber through an injection valve.

Upon combustion, the piston is pushed towards the load (bounce) side by the high-pressure combustion products. This is called a power stroke, at the end of which the piston stops at BDC, as shown on the right in Figure 2.7. The initiation of return stroke is indicated by the return of the piston towards the combustion side. During the return stroke, the exhaust valve should be opened so that the combustion products can be exhausted. Using this simplified model described here, the system-level control method can be developed based on the thermodynamic analysis of the engine.
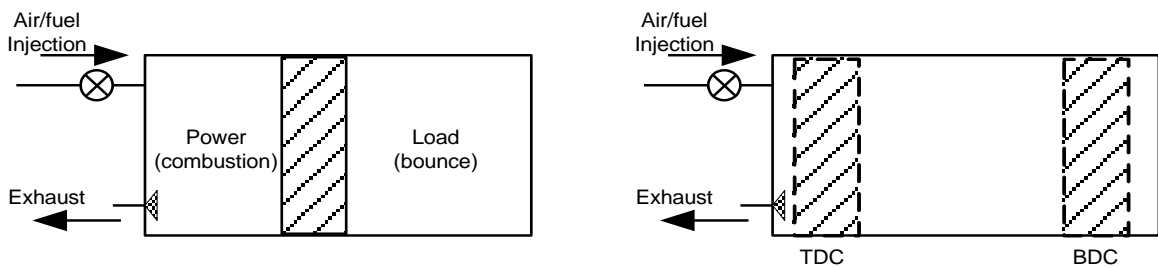
Figure 2.7 A simplified illustration of the free-piston engine

2.2.1 Fuel injection control

In conventional IC engines, the mass of fuel injection per cycle influences the engine speed and power output. This is likewise the case in free-piston engines. The mass of injected fuel also affects the stroke length and the expansion ratio in the combustion chamber. Varying the mass of fuel injected will not only influence the combustion energy that will be delivered to the load and stored in the bounce chamber, but it will also affect the TDC and BDC positions.

The fuel injection control is necessary to optimize the energy input for a specific load and to achieve a certain stroke length so that the optimal engine efficiency can be achieved. Generally, the overall engine efficiency is given by,

$$\eta_f = \frac{E_{out}}{E_{in}} \tag{2.2}$$

where E_{in} is the energy input per cycle and E_{out} is the energy output per cycle. The original amount of chemically stored energy in the injected mass of air/fuel mixture is given by,

$$E_{in} = m_c \Delta H_r \tag{2.3}$$

where m_c is the mass of the fuel injected into the combustion chamber and ΔH_r is computed from the lower heating value of the stoichiometric combustion of the fuel. By using an electronic on/off valve, the energy investment is proportional to the mass of the fuel injected, given by Eq. (2.4),

$$E_{in} = \Delta H_r \int_0^{t_{inj}} \dot{m}_c dt \tag{2.4}$$

Therefore, regulating the duration of the injection t_{inj} can control the input energy for each cycle. In order to derive the control law for the injection control, an energy analysis in the combustion chamber was carried out.

The power stroke of the combustion chamber can be divided into two stages as: 1) air/fuel injection period; 2) combustion and expansion period, or called power period. The states of the combustion chamber are illustrated in Figure 2.8. The initial time is

denoted by t_0 when the injection begins, the end of the injection or the beginning of the power period is at time t_1, and the end of the power stroke is at time t_2.
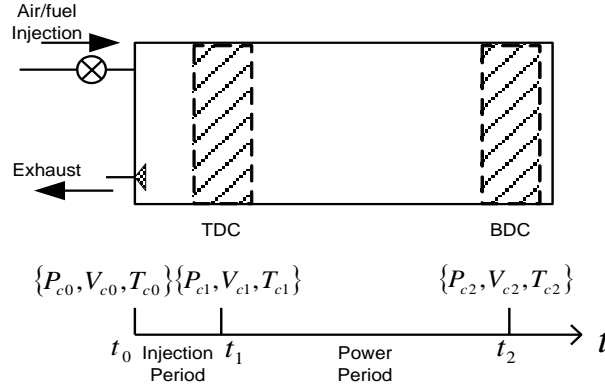
Figure 2.8 States of the combustion chamber

A power balance equates the energy storage rate to the energy flux rate crossing the control volume (CV) of the combustion chamber boundaries. The rate form of the first law of thermodynamics is given as follows:

$$\dot{U}_c = \dot{H}_c + \dot{Q}_c - \dot{W}_c \tag{2.5}$$

where $\dot{U}_c$ is the rate of change of internal energy, $\dot{H}_c$ is the net enthalpy flow rate into the CV, $\dot{Q}_c$ is the net heat flux rate into the CV, and $\dot{W}_c$ is the rate of work done by the gas in the CV. Expressions for $\dot{H}_c$ and $\dot{W}_c$ are given as,

$$\dot{H}_c = \sum \dot{m}_c \left(c_{p_{in/out}} \right)_c \left(T_{in/out} \right)_c \tag{2.6}$$

$$\dot{W}_c = P_c \dot{V}_c \tag{2.7}$$

where $\dot{m}_c$ is the mass flow rate entering (positive sign) or leaving (negative sign) the CV, $c_{p_{in/out}}$ and $T_{in/out}$ are the constant-pressure specific heat and the temperature of the

24

substance entering or leaving the CV, respectively, P_c, V_c and T_c are the pressure, volume and temperature in the CV, respectively, c_v is the constant-volume specific heat of the substance in the CV, and γ is the ratio of specific heats of the substance in the CV.

During injection period, assuming the temperature change is negligible, i.e. $T_{c0} \rightarrow T_{c1} = const$, the change of the internal energy can be calculated by,

$$\int_{t_0}^{t_1} \dot{U}_{c1} dt = \int_{t_0}^{t_1} \dot{m}_c c_p T_{c1} dt - \int_{t_0}^{t_1} P_c \dot{V}_c dt \tag{2.8}$$

During the power period after combustion, there is no mass flow in/out the combustion chamber, i.e. $\dot{m}_c = 0$, if the exhaust valve is closed. Therefore, the internal energy change is given by,

$$\int_{t_1}^{t_2} \dot{U}_{c2} dt = \int_{t_1}^{t_2} \dot{Q}_c dt - \int_{t_1}^{t_2} P_c \dot{V}_c dt \tag{2.9}$$

Assuming the combustion efficiency is denoted by η_c, the energy released by combustion is proportional to the total fuel mass injected, given by,

$$\int_{t_1}^{t_2} \dot{Q}_c dt = \eta_c \Delta H_r m_c = \eta_c \Delta H_r \int_{t_0}^{t_1} \dot{m}_c dt \tag{2.10}$$

Based on the assumption of constant temperature of $\dot{T}_{c1} = 0$ during the injection period, Integrating Eq. (2.5) over the entire period from t_0 to t_2 yields,

$$\int_{t_0}^{t_2} \dot{U}_c dt = \int_{t_0}^{t_1} \dot{U}_{c1} dt + \int_{t_1}^{t_2} \dot{U}_{c2} dt = \int_{t_0}^{t_1} \dot{m}_c c_p T_c dt + \eta_c \Delta H_r \int_{t_0}^{t_1} \dot{m}_c dt - \int_{t_0}^{t_2} P_c \dot{V}_c dt \tag{2.11}$$

The fundamental internal energy equation in the combustion chamber is given by,

$$\dot{U}_c = m_c c_v \dot{T}_c + \dot{m}_c c_v T_c \tag{2.12}$$

Integrating both sides of the equation yields,

$$\int_{t_0}^{t_2} \dot{U}_c dt = \int_{t_0}^{t_2} m_c c_v \dot{T}_c dt + \int_{t_0}^{t_2} \dot{m}_c c_v T_c dt \tag{2.13}$$

During the injection period, the temperature is assumed to be constant, which yields,

$$\int_{t_0}^{t_1} m_c c_v \dot{T}_c dt = 0 \tag{2.14}$$

During the power period, there is no mass flow in/out the combustion chamber, which gives,

$$\int_{t_1}^{t_2} \dot{m}_c c_v T_c dt = 0 \tag{2.15}$$

Therefore, Eq. (2.13) can be written as,

$$\int_{t_0}^{t_2} \dot{U}_c dt = \int_{t_1}^{t_2} m_c c_v \dot{T}_c dt + \int_{t_0}^{t_1} \dot{m}_c c_v T_c dt \tag{2.16}$$

Equating the right sides of Eq. (2.11) and Eq. (2.16) yields,

$$\int_{t_1}^{t_2} m_c c_v \dot{T}_c dt + \int_{t_0}^{t_1} \dot{m}_c c_v T_{c1} dt = \int_{t_0}^{t_1} \dot{m}_c c_p T_c dt + \eta_c \Delta H_r \int_{t_0}^{t_1} \dot{m}_c dt - \int_{t_0}^{t_2} P_c \dot{V}_c dt \tag{2.17}$$

Rearranging Eq. (2.17) yields,

$$\left[(c_v - c_p) T_{c1} - \eta_c \Delta H_r \right] \int_{t_0}^{t_1} \dot{m}_c dt = - \int_{t_1}^{t_2} m_c c_v \dot{T}_c dt - \int_{t_0}^{t_2} P_c \dot{V}_c dt \tag{2.18}$$

Two terms at the right side of Eq. (2.18) can be replaced as following. The net energy increase in the combustion chamber, bounded by constant mass, is only a function of its net temperature increase.

$$\Delta U_{c2} = \int_{t_1}^{t_2} m_c c_v \dot{T}_{c2} dt = m_c c_v T_{c1} - m_c c_v T_{c2} \tag{2.19}$$

where T_{c1} is the temperature at the end of injection period and T_{c2} is the temperature in the final state, respectively. During the power period, the internal energy change of the combustion chamber can be calculated using,

$$\Delta U_{c2} = \frac{P_{c1}V_{c1}}{\gamma - 1}\left(\left(\frac{V_{c2}}{V_{c1}}\right)^{k-1} - 1\right) \tag{2.20}$$

where the expansion ratio of the combustion chamber R_c is calculated by,

$$R_c = \frac{V_{c2}}{V_{c1}} \tag{2.21}$$

The *PV* work done by the combustion gas is delivered to the load by the piston. Thus,

$$\int_{t_0}^{t_2} P_c \dot{V}_c dt = -\int_{t_0}^{t_2} f_{load}(t)\dot{x}_p dt \tag{2.22}$$

where $f_{load}(t)$ is the force from the load and x_p is the piston position, and $\dot{x}_p = \dot{V}_c/A$.

The load force is proportional to the piston displacement. Therefore, the larger expansion of the combustion chamber results in more energy being delivered to the load.

Letting the constant $k_m = (c_v - c_p)T_{c1} - \eta_c \Delta H_r$ and substituting Eq. (2.20-2.22) into Eq. (2.18) yields,

$$k_m \int_{t_0}^{t_1} \dot{m}_c dt = P_{c1}V_{c1}\left(R_c^{k-1} - 1\right) + \int_{t_0}^{t_2} f_{load}(t)\dot{x}_p dt \tag{2.23}$$

Using Eq. (2.23), the control law for fuel mass injection can be derived. First, the fuel mass influences the expansion ratio of the combustion chamber. A larger piston displacement (or a larger stroke length) is achieved by injecting a larger mass of fuel under a certain load. Second, a higher loading force requires more energy input for the piston to move a certain stroke length. It is also important to note that the physical configuration of the engine limits the maximum stroke length. Hence, the basic idea behind the control of fuel mass injection is to inject the minimum mass of fuel per cycle while achieving the desired expansion ratio or stroke length.

The control input is the injection duration of $t_0 \rightarrow t_1$, which essentially determines the quantity of the fuel mass injected or the energy input to the engine. The energy output is represented by two terms on the right side of Eq. (2.23). The primary goal of the fuel mass control is to balance Eq. (2.23) so that the energy input in each cycle is sufficient but not excessive to achieve a certain stroke length under a certain load. Rearranging Eq. (2.23) yields,

$$\int_{t_0}^{t_1} \dot{m}_c dt = \frac{P_{c1}V_{c1}}{k_m V_{c1}^{\gamma-1} A^{\gamma-1}}\left(x_{c2}^{\gamma-1} - x_{c1}^{k-1}\right) + \frac{1}{k_m}\int_{t_0}^{t_2} f_{load}(t)\dot{x}_p dt \tag{2.24}$$

where the piston position at the end of power stroke x_{c2} defines the BDC position and A is the cross section area of the piston. In the kth engine cycle, the above equation can be written as,

$$m_c[k] = E_x[k]\left(x[k]_{c2}^{k-1} - x[k]_{c1}^{k-1}\right) + E_L[k]L[k] \tag{2.25}$$

where

$$E_x[k] = \frac{P_{c1}[k]V_{c1}[k]}{k_m V_{c1}[k]^{\gamma-1} A^{k-1}} \tag{2.26}$$

$$E_L[k] = \frac{1}{k_m} \tag{2.27}$$

$$L[k] = \int_{t_0}^{t_2} f_{load}[k](t)\dot{x}_p dt \tag{2.28}$$

Eq. (2.25) quantifies the fuel mass required for desired stroke length of $x_{c2}[k] - x_{c1}[k]$ under the load profile of $L[k]$ in the kth cycle. Therefore, a desired constant stroke length is first set for the controller, denoted by x_d. Then the amount of energy necessary to push the piston to travel for the desired stroke length can be

calculated. For an air compressor, this position is where the compression chamber has zero volume, meaning all of the air in the compression chamber is pumped out. During engine operation, the load varies from cycle to cycle. Thus, the fuel mass injected should be accordingly adjusted to accommodate these variations.

In order to adaptively rebuild the virtual cam for the fuel mass injection, this work proposes a cycle-to-cycle based dynamic control method. The adjustment of the fuel mass is based on the evaluation of the engine performance in the previous cycle and the current loads (or predicted loads in the next cycle). A linear formulation of the dynamic control algorithm reads as,

$$m_f[k+1] = m_f[k] + E_x(x_d - x_{stroke}[k]) + E_L(L[k+1] - L[k]) \qquad (2.29)$$

where $m_f[k]$ is the fuel mass injected in the kth cycle, x_d is the desired stroke length, $x_{stroke}[k]$ is the measured stroke length in the kth cycle, $E_x(x_d - x_{stroke}[k])$ is the weighted stroke length error. The weighting constant E_x has the same order of magnitude and unit as $E_x[k]$ in Eq. (2.26). $L[k]$ is the load in the kth cycle; $L[k+1]$ is the predicted load in the next cycle. $E_L(L[k+1] - L[k])$ weights the load variation with the constant E_L which has the same order of magnitude and unit as $E_L[k]$ in Eq. (2.27). The control principle is illustrated in Figure 2.9.
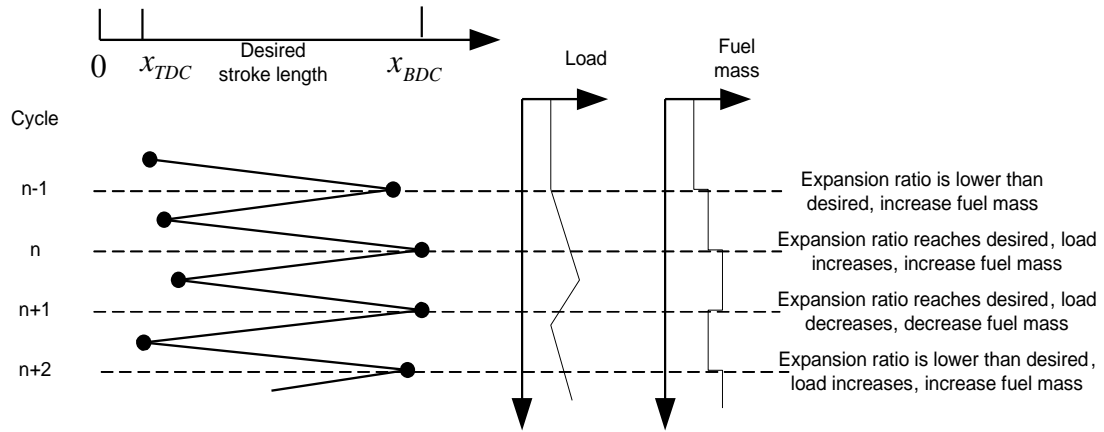
Figure 2.9 Expansion ratio and fuel mass control

The amount of air/fuel mixture used per cycle is determined by adaptively adjusting the injection duration for a desired stroke length and the load based on how it is expected to vary in the next cycle. The adjustment is made effective by changing the corresponding virtual cam parameters of $\{\theta_s, \theta_e\}_{fuel}$, i.e., a longer duration of fuel injection is achieved by increasing $\theta_s \to \theta_e$ for a given operating frequency.

2.2.2 Exhaust timing control

Exhaust valve timings can strongly influence TDC of free-piston engines. At the end of the power stroke, it is desired to open the exhaust valve of the combustion chamber so that the combustion products can be immediately exhausted. In some free-piston engines [5-10], scavenge ports are used for this purpose. In more recently developed free-piston engines, such as [19] [24], active on/off exhaust valves are used to achieve better controllability. If the exhaust valve is not opened when the return stroke begins, the trapped combustion products in the combustion chamber will be compressed and will act as a gas spring resisting the return of the piston. This will cause a portion of

the energy (stored in the bounce chamber or other return device) to be wasted on compressing the combustion gas. The return stroke length is thus shorter, resulting in a larger initial TDC, and consequently, a smaller expansion ratio in the next cycle.

For most free-piston engines, combustion and expansion happen very quickly, so the control process needs to be fast enough to comply with the rapid engine operation. However, sensor measurements and operations conducted on these signals are delayed by filters. Furthermore, solenoid electronic valves cannot be instantaneously opened/closed fully as there are restricted by their response dynamics. These facts make it impossible to use a given engine cycle's sensor data to time the opening/closing of the valve in that cycle. When the TDC/BDC is determined, the time at which the control command needs to be sent out has already passed. Therefore, control can not be carried out in real-time. These kinds of delay problems have been investigated in conventional engine control [19] [20]. A potential solution is to predict the dynamics of the piston in real-time, allowing for the control commands to be accordingly sent out in advance to compensate for the delays [13-14]. This method, however, requires additional intensive computations and handles disturbances poorly. Therefore, an adaptive control algorithm is proposed in this work for adjusting virtual cam parameters from cycle to cycle.

As mentioned before, the virtual cam for each subsequent cycle is rebuilt at the end of cycle preceding it. This allows delays and dynamic response to be integrated into the rebuilding process in which the cam lobes are accordingly adjusted. Therefore, based on the knowledge of previous control results, the virtual cam parameters can be gradually adjusted at the end of each cycle such that the timings approach their ideal values.

At the end of a return stroke, the ideal exhaust valve timing $\{\theta_{oi}, \theta_{ci}\}_{ex}$ can be obtained by measuring the time when the piston reaches TDC and BDC, which can be determined by measuring piston positions directly. The ideal virtual cam positions are denoted by θ_{oi} for open and θ_{ci} for close. Meanwhile, the actual time when the open/close control signals are sent to the engine are also known, denoted by $\{\theta_{oa}, \theta_{ca}\}_{ex}$. Directly applying the ideal timings in previous cycle to the next cycle is not practical due to the cycle-to-cycle variations that include different TDC/BDC and consequently ideal exhaust timings. Thus, the exhaust timing adjustment is carried out in a first order proportional control manner, given by

$$\theta_{oa}[k+1] = \theta_{oa}[k] + \beta_o(\theta_{oi}[k] - \theta_{oa}[k]) \tag{2.30}$$

$$\theta_{ca}[k+1] = \theta_{ca}[k] + \beta_c(\theta_{ci}[k] - \theta_{ca}[k]) \tag{2.31}$$

where $\beta_o(\theta_{oi}[k] - \theta_{oa}[k])$ weights the previous exhaust valve open timing error, $\beta_c(\theta_{ci}[k] - \theta_{ca}[k])$ weights the previous exhaust valve close timing error.

In Equations (2.30) and (2.31), if $\beta_o = 1$ and $\beta_c = 1$, it will be directly applying the optimal timings achieved in current cycle to the next cycle. It is not practical due to the reason mentioned above. Hence, a gradual adjustment, with $\beta_o, \beta_c \neq 1$, is used to reduce $\theta_{oi}[k] - \theta_{oa}[k]$ and $\theta_{ci}[k] - \theta_{ca}[k]$ with successive cycles without causing the system to undergo sudden changes. Figure 2.10 illustrates the working principle of the proposed exhaust control strategy. The errors between actual and ideal opening/closing timings are measured in the current cycle and reduced in the following cycle by Equations (2.30-2.31).
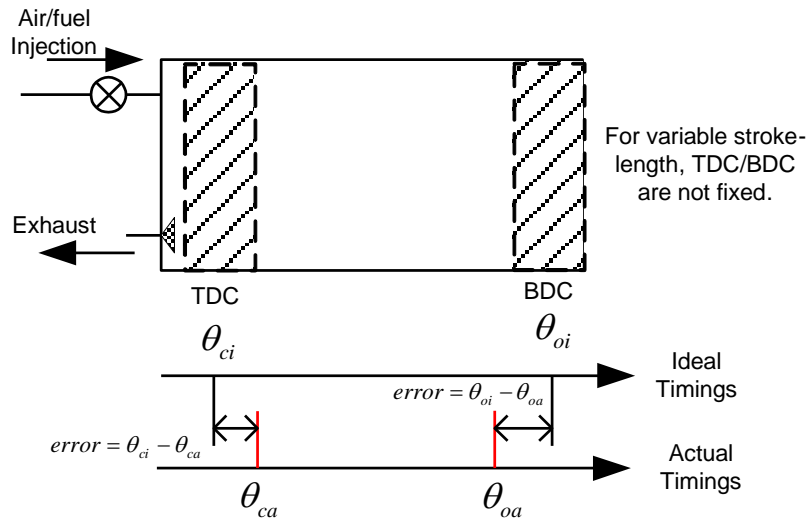
Figure 2.10 Cycle-to-cycle exhaust timing control

2.3   Pressure-based control approach

In order to use those control laws derived above, piston position measurement is required. However, this measurement is not always available in all free-piston engines. For instance, the free liquid-piston engine compressor [2][3] has no piston rod, and the piston's position is controlled by trapping it between two varying control volumes. In its case, pressure dynamics can be used to infer piston dynamics as the latter is difficult to practically measure.

For many decades, cylinder pressure has been used by engineers for various applications of internal combustion engines. J. D. Powell [22] discussed how to address the air/fuel ratio control problem by using cylinder peak pressure, and showed the benefits of using cylinder pressure for timing and engine control. Additionally, the use of cylinder pressure for combustion misfire detection was also discussed by [22]. P. Yoon et al. [23] presented a closed-loop control of spark advance and air/fuel ratio in SI engines

using the cylinder pressure. The peak pressure and the time at which it occurred in each cycle were analyzed and used for controlling the air/fuel ratio and spark timing.

The chamber pressure provides an alternative way to examine the piston dynamics and using pressure for free-piston engine control purpose has never been reported. The fast response of modern electronic pressure sensors and the computational capabilities of microprocessors allow the use pressure as a fundamental engine variable for engine control. Hence, this work will be the first to investigate the possibility of using pressures for assisting the proposed virtual-cam based control method.

During the power stroke while the exhaust valve is closed, pressure dynamics are directly caused by compression and expansion in the bounce chamber and the combustion chamber. The fundamental internal energy equation of a gas is given by,

$$\Delta U_g = mc_v \Delta T \qquad (2.32)$$

which states that the net energy increase ΔU_g in a control volume (bounded by constant mass m) is only a function of its net temperature increase ΔT, assuming that no heat or enthalpy fluxes occur. For a control volume that is changing its states, above equation can be expanded to,

$$\Delta U_g = mc_v T_o - mc_v T_f \qquad (2.33)$$

where T_o is the temperature at the initial state and T_f is the temperature at the final state, respectively. Applying the ideal gas law, Eq. (2.33) can be written as,

$$\Delta U_g = \frac{mRT_o}{\gamma - 1} - \frac{mRT_f}{\gamma - 1} \qquad (2.34)$$

where R and γ are the gas constant and the ratio of specific heats of the gas, respectively. Further, using the ideal gas law, the following substitution can be made,

$$\Delta U_g = \frac{P_f V_f}{\gamma - 1} - \frac{P_o V_o}{\gamma - 1} \tag{2.35}$$

where P_o and V_o are the original pressure and volume, and P_f and V_f are the pressure and volume at the final state, respectively. For a free-piston air compressor, the final state is when the pump pressure exceeds the reservoir pressure and the pump begins. Assuming this process is adiabatic, the following expression holds,

$$P_o V_0^{\gamma} = P_f V_f^{\gamma} \tag{2.36}$$

By substituting Eq. (2.36) to Eq. (2.35) and rearranging the terms yields following two equations,

$$\Delta U_g = \frac{P_o V_o}{\gamma - 1}\left(\left(\frac{V_f}{V_o}\right)^{\gamma - 1} - 1\right) \tag{2.37}$$

$$\Delta U_g = \frac{P_o V_o}{\gamma - 1}\left(\left(\frac{P_f}{P_o}\right)^{\frac{\gamma - 1}{\gamma}} - 1\right) \tag{2.38}$$

Since V_f/V_o is the expansion ratio of the combustion chamber, Eq. (2.37) shows the relation between the expansion energy and the expansion ratio of the combustion chamber. Eq. (2.38) shows the relation between expansion energy and pressure ratio. These two equations correlate the pressure dynamics to the control target, that is, the expansion ratio (proportional to the stroke length). Differentiating both sides of Eq.

(2.36) yields the instantaneous power P_w done by the control volume at the final state (or at any time),

$$P_w = \frac{P_o^{\frac{1}{\gamma}} V_o}{\gamma} P_f^{\frac{\gamma-1}{\gamma}} \dot{P}_f \qquad (2.39)$$

Using Equations (2.37-2.39) and analyzing the engine performance in term of energy and power, the proper timings for engine control can be obtained. As shown in Eq. (2.39), the power of a control volume is related to its pressure dynamics. When $\dot{P}_f$ becomes zero, power is at its maximum or minimum for a given stroke. The gas stops doing work on the piston so that the velocity of the piston becomes zero ($\dot{x}_{piston}=0$) as well. In this way, Eq. (2.39) correlates the power of gas to the dynamics of the piston. When the piston's $\dot{x}_{piston}=0$, it is typically BDC or TDC which are of interest to the controller. When the chamber is not sealed, the above relationship between pressure dynamics and piston dynamics are still true, i.e. $\dot{P}_f = 0$ while $\dot{x}_{piston}=0$. In all above equations, γ (for adiabatic process) can be replaced by a constant k if it is a polytrophic process.

To illustrate above discussion, the following consider example of capturing interested piston positions using energy and power analysis. When the piston reaches either BDC or TDC, kinetic energy of the piston becomes zero. Therefore, the piston stops doing work on the control volume, and the control volume starts to do work on the piston. This can be seen from the power P_w crossing zero and switching its direction, as shown in Figure 2.11. This figure shows the pressure dynamics in the combustion

chamber and the work done by the combustion products. The data is from simulations of the free liquid-piston engine compressor (FLPEC), which will be introduced in the next chapter. When the piston comes to the BDC, pressure reaches its peak (local maximum) and power crosses zero from negative to positive and $\dot{P}_f = 0$ while $\dot{x}_{piston} = 0$.
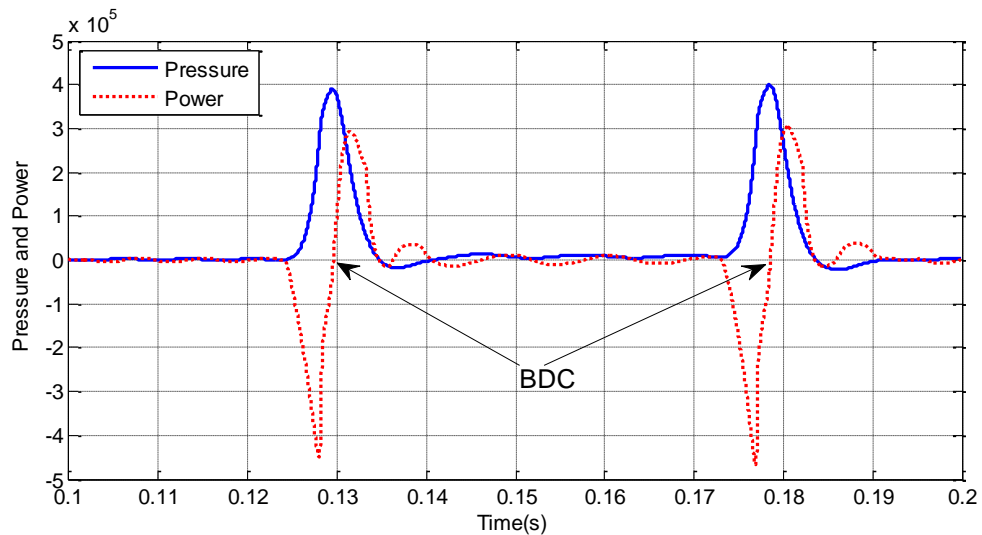
Figure 2.11 Pressure dynamics and power of the expansion chamber in FLPEC [2] [3]

Most opening/closing valve actuations occur at critical positions such as BDC and TDC. By opening the exhaust valves, gas in previously sealed control volume is quickly released in the form of mass flowing out of the chamber. Upon scavenging, energy in a cylinder is released so that this control volume can reduce its negative work on the piston. In this way, the piston can move "more freely" without being pushed by the compressed air in the cylinder. In additional to pinpointing critical positions such as TDC and BDC, pressure dynamics can be used to analyze piston dynamics influenced by control or disturbances.

37

2.4   Conclusions

This chapter introduced the working principles of the virtual-cam based control structure. A cycle-to-cycle based dynamic adjustment method for the cam parameters was proposed for the injection control and exhaust control. Control laws for injection and exhaust were derived in a general free-piston engine control context. In addition, the possibility of using pressure dynamics for free-piston engine control was also discussed. Before implementing the proposed control structure on a real device, it will be tested and validated in simulation. Therefore, the next chapter introduces modeling of a Free Liquid-Piston Engine Compressor (FLPEC). The simulation test results of the controller will be provided in chapter 4.

Chapter III

MODLEING AND SIMULATION OF A FREE-PISTON ENGINE COMPRESSOR

In this chapter, a prototype of an experimental free-liquid piston engine compressor [24] is introduced and its modeling and simulation are provided. The proposed virtual-cam control framework is tested and validated in simulation of this device first. Experimental testing of the control method was conducted on a later version the free-piston engine compressor prototype [25].

3.1 Free-Liquid Piston Engine Compressor (FLPEC)

Motivated by high energy and power densities, pneumatic power supply and actuation systems are being investigated by various researchers [26][27] for untethered robotic applications requiring controlled human-scale power motion output. Such systems utilize linear pneumatic actuators that have approximately an order of magnitude better volumetric power density and five times better mass specific power density than state of the art electrical motors [28]. Regarding power supply, on-board air supply has shown to be a non-trivial issue, since standard air compressors are too heavy for the intended target scale, as are portable tanks with enough compressed air (stored energy) to supply the actuators for a useful duration of time. To address this problem, a free liquid-piston engine compressor (FLPEC) with a separated combustion chamber has been developed by Riofrio and Barth [24] to provide an on-board supply of compressed air.

The FLPEC discussed in this chapter is a compact internal combustion engine with a free-piston configuration, dynamically arranged to match the load of compressing

and pumping air. The combined benefits of a high-energy density fuel, the efficiency of the device, the compactness and low weight of the device, and the use of the device to drive lightweight linear pneumatic actuators (as compared with similar power electric motors) is projected to provide at least an order of magnitude greater total system energy density (power supply and actuation) than state of the art power supply (batteries) and actuators (electric motors) appropriate for human-scale power output [24].
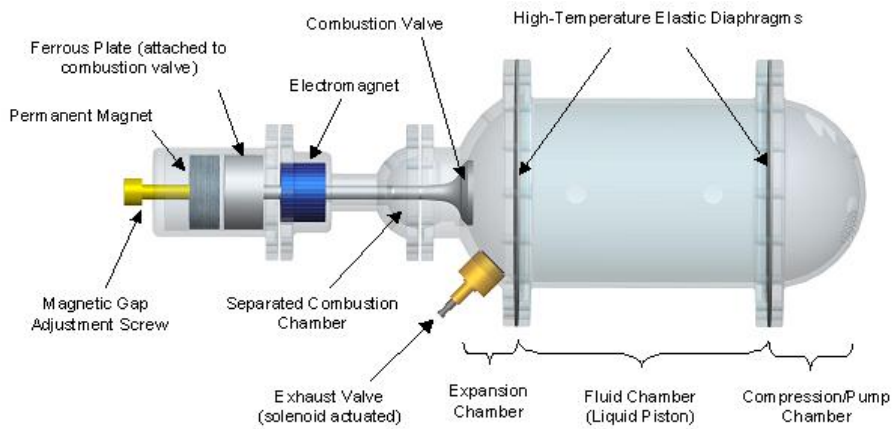
(a) Conceptual model of the FLPEC
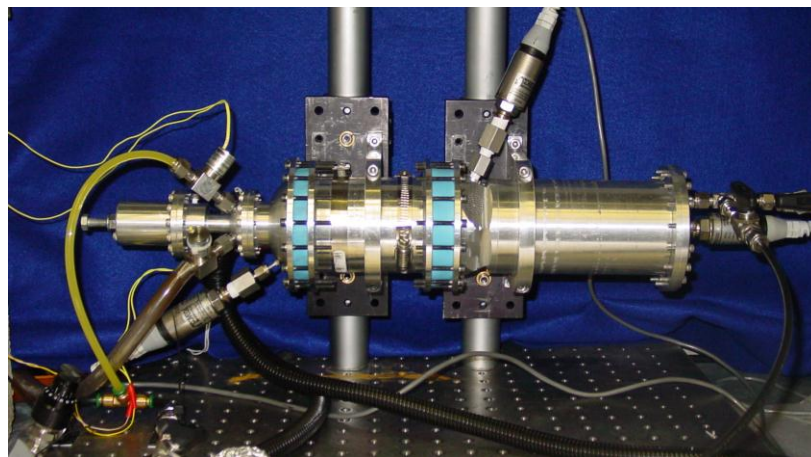
(b) Fabricated engine

Figure 3.1 The free liquid-piston engine compressor configuration [24]

The FLPEC is shown in Figure 3.1. It consists of a combustion chamber, an expansion chamber, a liquid piston, and a compression/pumping chamber. The combustion chamber is separated from the expansion chamber by a magnetically latching valve that seals in the face of high pressure air and fuel injected into the chamber, and opens in the face of higher pressure combustion products. The expansion chamber allows for the combustion products to perform PV work on a free-piston consisting of a liquid slug trapped between two high-temperature elastomeric diaphragms. Please refer to [24] for more details.

3.2   Dynamic system model of the FLPEC

The FLPEC was modeled as a lumped-parameter model with a level of fidelity appropriate for only those states of interest, and with accuracy adequate for control purposes. Therefore the system is simplified as the forced mass-spring-damper system shown in Figure 3.2. A control volume (CV) approach was taken to model the pressure and temperature dynamics in the combustion constant-volume chamber (subscript "c"), the expansion chamber (subscript "e"), and the compression chamber (subscript "p"). Mass flow rates were modeled through all six channels: 1) air/fuel injection mass flow through a controlled on/off valve ($\dot{m}_{inj}$), 2) breathe-in check-valve inlet mass flow into the combustion chamber ($\dot{m}_1$), 3) mass flow through the magnetically-latched combustion valve between the combustion and expansion chambers ($\dot{m}_2$), 4) mass flow through the exhaust valve of the expansion chamber ($\dot{m}_3$), and 5) inlet ($\dot{m}_4$) and 6) outlet ($\dot{m}_5$) check-valve mass flow of the compression chamber.   The arrows in Figure 2 indicate the directions of the mass flow, where $\dot{m}_2$ and $\dot{m}_3$ are modeled as two-way flow

dependent upon time varying upstream and downstream pressures. Finally, the inertial dynamics of the liquid piston and the combustion valve were included to relate the time-based behavior of all three control volumes.
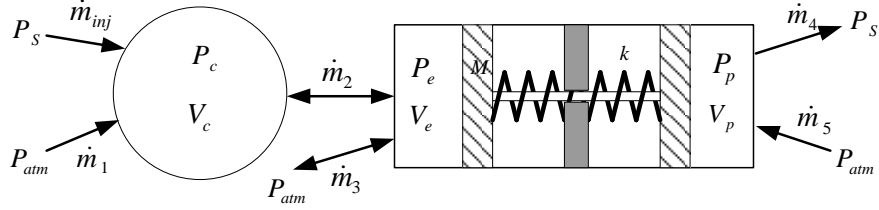
Figure 3.2 Schematic of the lumped-parameter dynamic model of the FLPEC

A power balance equates the energy storage rate to the energy flux rate crossing the CV boundaries. The rate form of the first law of thermodynamics is given as follows:

$$\dot{U}_j = \dot{H}_j + \dot{Q}_j - \dot{W}_j \tag{3.1}$$

where j is a subscript (c, e or p) indicating each of the three CVs, $\dot{U}$ is the rate of change of internal energy, $\dot{H}$ is the net enthalpy flow rate into the CV, $\dot{Q}$ is the net heat flux rate into the CV, and $\dot{W}$ is the rate of work done by the gas in the CV. Expressions for $\dot{H}$, $\dot{W}$ and $\dot{U}$ are given as:

$$\dot{H}_j = \sum \dot{m}_j \left(c_{p_{in/out}} \right)_j \left(T_{in/out} \right)_j \tag{3.2}$$

$$\dot{W}_j = P_j \dot{V}_j \tag{3.3}$$

$$\dot{U}_j = \dot{m}_j \left(c_v \right)_j T_j + m_j \left(c_v \right)_j \dot{T}_j = \frac{1}{\gamma_j - 1} \left(\dot{P}_j V_j + P_j \dot{V}_j \right) \tag{3.4}$$

where $\dot{m}$ is an individual mass flow rate entering (positive sign) or leaving (negative sign) the CV, $c_{p_{in/out}}$ and $T_{in/out}$ are the constant-pressure specific heat and the temperature of the substance entering or leaving the CV, respectively, P, V and T are the pressure,

volume and temperature in the CV, respectively, c_v is the constant-volume specific heat of the substance in the CV, and γ is the ratio of specific heats of the substance in the CV. Combining Equations (3.1-3.4), the following differential equations can be obtained for the pressure and temperature dynamics:

$$\dot{P}_j = \frac{(\gamma_j - 1)\sum \dot{m}_j \left(c_{p_{in/out}}\right)_j \left(T_{in/out}\right)_j + (\gamma_j - 1)\dot{Q}_j - \gamma_j P_j \dot{V}_j}{V_j} \tag{3.5}$$

$$\dot{T}_j = \frac{\sum \dot{m}_j [\left(c_{p_{in/out}}\right)_j \left(T_{in/out}\right)_j - (c_v)_j T_j] - P_j \dot{V}_j + \dot{Q}_j}{m_j (c_v)_j} \tag{3.6}$$

The mass flow rates crossing all six valves depend on the upstream and the downstream pressures where a positive sign convention indicates mass flow into the CV. Upstream and downstream pressure roles will switch for the two two-way mass flow rates shown ($\dot{m}_2$ and $\dot{m}_3$) as the pressures P_c and P_e change dynamically according to Eq. (3.5). The following equations give the mass rate under subsonic and sonic conditions [28]:

$$\dot{m}_j = \psi_j(P_u, P_d) = \begin{cases} C_d a_j C_1 \dfrac{P_u}{\sqrt{T_u}} & \text{if } \dfrac{P_d}{P_u} \le P_{cr} \\[3em] C_d a_j C_2 \dfrac{P_u}{\sqrt{T_u}}\left(\dfrac{P_d}{P_u}\right)^{1/\gamma_u}\sqrt{1-\left(\dfrac{P_d}{P_u}\right)^{\gamma_u - 1/\gamma_u}} & \text{if } \dfrac{P_d}{P_u} > P_{cr} \end{cases} \tag{3.7}$$

where C_d is a nondimensional discharge coefficient of the valve, a is the area of the valve orifice, P_u and P_d are the upstream and downstream pressures, T_u is the upstream temperature, γ_u is the ratio of specific heats of the upstream substance, and C_1, C_2 and P_{cr} are substance-specific constants given by,

$$C_1 = \sqrt{\frac{\gamma_u}{R_u}\left(\frac{2}{\gamma_u+1}\right)^{\gamma_u+1/\gamma_u-1}} \qquad (3.8)$$

$$C_2 = \sqrt{\frac{2\gamma_u}{R_u(\gamma_u-1)}} \qquad (3.9)$$

$$P_{cr} = \left(\frac{2}{\gamma_u+1}\right)^{\gamma_u/\gamma_u-1} \qquad (3.10)$$

where R_u is the gas constant of the upstream substance. The valve orifice areas of the combustion and exhaust valves (a_2 and a_3) are dynamically determined by the inertial dynamics of their respective valve stems.

3.2.1 Modeling of the combustion process

Since the expansion and pumping processes occur very quickly, heat lost during these two processes is neglected. That is $\dot{Q}_e = \dot{Q}_p = 0$. However, the heat flux rate for the pressure and temperature dynamics of the combustion chamber is primarily determined by the heat released during the combustion. The combustion process is coupled to the temperature dynamics in the combustion CV. Given that the *PV* work term in Eq. (3.6) changes on a time-scale of the same order as the combustion process, a model of the heat release rate during combustion must be included. The total energy stored in the air/fuel mixture at the time of the spark can be computed by $E_c = \Delta H_r m_c\big|_{t_{spark}}$, where m_c is the total mass in the combustion chamber, and ΔH_r is computed from the lower heating value for the stoichiometric combustion of propane,

$$\Delta H_r = \frac{46350\,\text{kJ}}{\text{kg fuel}} \times \frac{1\,\text{kg fuel}}{16.63\,\text{kg air/fuel mixture}}$$

$$= 2787\,\frac{\text{kJ}}{\text{kg air/fuel mixture}} \tag{3.11}$$

The rate at which heat is released by combustion in the combustion chamber is given by,

$$\dot{Q}_c = \Delta H_r \dot{m}_{cc} \tag{3.12}$$

where m_{cc} is the mass of the combustion products.

In the combustion research community, the Arrehnius law [29] is often used to compute the reaction rate. Using this method, the following equation is obtained giving the reaction rate of the temperature dependent combustion,

$$\dot{m}_{cc} = K e^{-E_a / R_c T_c} m_{uc} \tag{3.13}$$

where $\dot{m}_{cc}$ is the rate of emergence of combustion products, E_a is the activation energy, and K is the pre-exponential factor. The mass of uncombusted material m_{uc} in the combustion chamber is given by,

$$m_{uc} = m_c - \int_{t_{spark}}^{t} \dot{m}_{cc}\,dt \tag{3.14}$$

In the Laplace domain, Equations (3.12), (3.13) and (3.14) can be more compactly represented by the following,

$$Q_c = \frac{E_c}{\tau s + 1} \tag{3.15}$$

where

$$\tau = \frac{1}{Ke^{-E_a/R_cT_c}} \tag{3.16}$$

The Arrehnius law assumes that the fuel is homogeneously combusted and the temperature is same within all regions of the combustion chamber. However, the combustion is spark-ignited in the FLPEC. Hence, the first order model will not adequately capture the spatial propagation dynamics of the combustion process. Instead, a second-order model is applied to account for the complexities associated with combustion flame propagation and temperature distribution within the chamber. The overall heat release rate is then given as,

$$Q_c = \frac{E_c\tau_c^2}{s^2 + 2\xi\tau_c s + \tau_c^2} \tag{3.17}$$

Given that the reaction is assumed irreversible, the damping ratio must satisfy $\xi \geq 1$. The temperature-dependent rate is still given by the Arrehnius law: $\tau_c = Ke^{-E_a/R_cT_c}$.

$\dot{Q}_c$ is regarded as the ***effective heat release rate*** which "contributes" to pressure and temperature dynamics as shown in Equations (3.5) and (3.6). τ_c can be further simplified as,

$$\tau_c = Ke^{-A/T_c} \tag{3.18}$$

where K and A are empirically obtained constants.

3.2.2 Combustion valve dynamics

Since the combustion valve has dynamic characteristics that influence its flow area, it has to be properly modeled so that Eq. (3.7) can be computed in real-time. Figure 3.3 shows the free-body diagram of this valve.

Applying Newton's second law, the valve dynamics are thus given:

$$m_{c\_v}\ddot{x}_v = P_c A_{c\_v} + F_M - P_e A_{c\_v} \qquad (3.19)$$
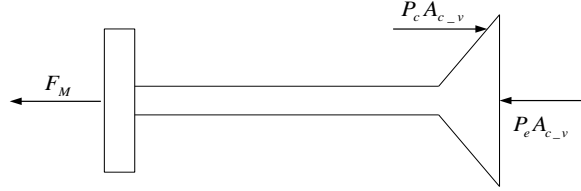
Figure 3.3 Free-body diagram of the combustion valve

where m_{c_v} is the mass of the valve, x_v is the position of the valve, F_M is the magnetic

force generated by the permanent magnet, respectively, and A_{c_v} is the cross-sectional

area of the valve head. Furthermore, the valve flow area $a_2(x_v)$ can be described by the

following:

$$a_2(x_v) = \min\left\{2\pi r_v x_v, \ \pi\left(r_v^2 - r_{v\_stem}^2\right)\right\} \qquad (3.20)$$

where r_v and r_{v_stem} are the radii of the valve head and valve stem, respectively.

3.2.3   Exhaust valve dynamics

The dynamics of the exhaust valve, as shown in Figure 3.4, are given similarly to

the combustion valve as follows,

$$m_{e\_v}\ddot{x}_{e\_v} = (P_{atm} - P_e)A_{e\_v}^2 - k_{e\_v}(x_{e\_v} + x_{e\_v0}) - b_{e\_v}\dot{x}_{e\_v} + F_{solenoid} \qquad (3.21)$$

where x_{e_v} is the displacement of the exhaust valve into the expansion chamber side,

A_{e_v} is the cross-sectional area of the exhaust valve, b_{e_v} is the effective viscous friction,

x_{e_v0} is the pre-compressed spring force giving the valve returning force, and $F_{solenoid}$ is

the force exerted on the exhaust valve by the solenoid valve controller.

Figure 3.4 Free-body diagram of the exhaust valve
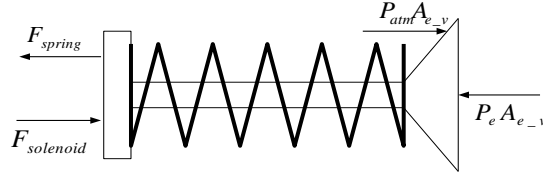
Similarly, the valve flow area $a_3(x_{ex})$ can be described by the following:

$$a_3(x_{ex}) = \min\left\{2\pi r_{ex} x_{ex},\ \pi\left(r_{ex}^{\,2} - r_{ex\_stem}^2\right)\right\}$$
(3.22)

where r_{ex} and r_{ex_stem} are the radii of the exhaust valve head and stem, respectively.

3.2.4 Free-piston inertial dynamics

The liquid slug trapped between the elastomeric diaphragms essentially constitutes a mass-spring-damper system, where the fluid mass M and diaphragms' stiffness k can be selected for a desired resonant frequency. The dynamics given by the liquid piston are modeled by the following differential equation:

$$\ddot{V}_e = \frac{1}{M}\left[\left(P_e - P_p\right)A^2 - kV_e - b\dot{V}_e + kV_{e\_rlx}\right]$$
(3.23)

where V_e is the volume in the expansion side, A is the cross-sectional area of the liquid-piston, b is the effective viscous friction assumed for a 50% overshoot, and V_{e_rlx} is the "relaxed" volume in the expansion chamber when the diaphragms are unstretched.

3.3 Simulation results and validation

This section shows experimental model validation of three processes inside the combustion chamber: 1) pressure dynamics inside the chamber during the injection of the air/fuel mix, 2) the dynamics of heat release during combustion and the resulting influence on pressure, and 3) the opening of the combustion valve and its effects on the

pressure.

Figure 3.5 shows the simulated and experimentally measured pressure and displacement of the combustion valve in the combustion chamber during the injection of the air/fuel mixture. The engine dynamics, when combusted under different injection pressures of 80 *psig*, 62 *psig* and 45 *psig* respectively, are shown in Figure 3.5. The model is given by Equations (3.5) and (3.7). The only parameter empirically determined was the coefficient of discharge C_d in Eq. (3.7). Since the temperature during the combustion is difficult to measure on the real device, only the pressure dynamics can be compared between simulated and experimental data. As introduced in chapter 2, the system-level controller is based on pressure dynamics. Therefore, it is important to validate the pressure dynamics in all three CVs, especially in the combustion chamber given that it provides all of the driving power to the remainder of the system. The device was tested as an open system, where the expansion chamber was not attached to the combustion chamber; that is, the combustion valve was exposed to the atmosphere. The results show the pressure in the combustion chamber immediately after the spark. The dynamics of heat release during combustion cause a rapid rise in pressure, and the opening of the combustion valve causes the pressure drop. The two constants K and A in Eq. (3.18), and the magnitude of F_M in Eq. (3.19) were empirically adjusted to fit the overall combustion chamber pressure dynamics to the experimental results of the combustion pressure. The electromagnetic force F_{EM} in Eq. (3.19) was set to zero as this electromagnet was not utilized in this experiment.
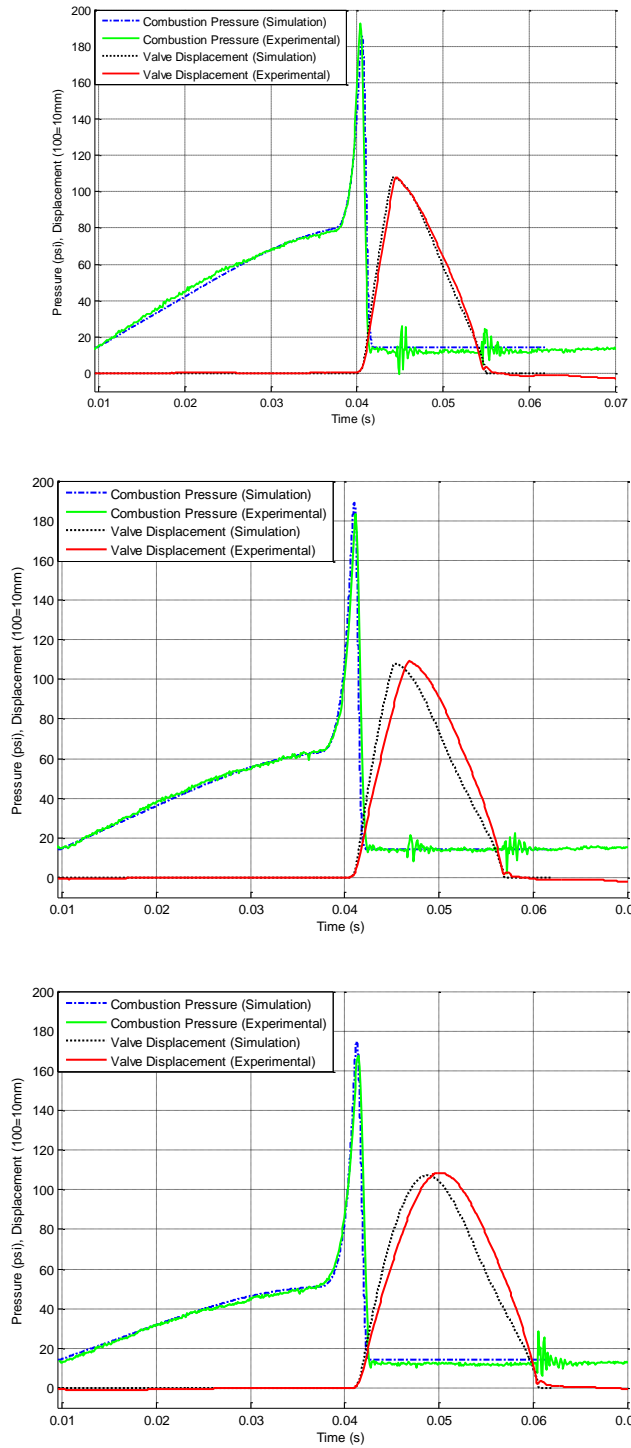
Figure 3.5 Simulation results and experimental data of the combustion pressure dynamics and the displacement of the combustion valve in the combustion chamber.
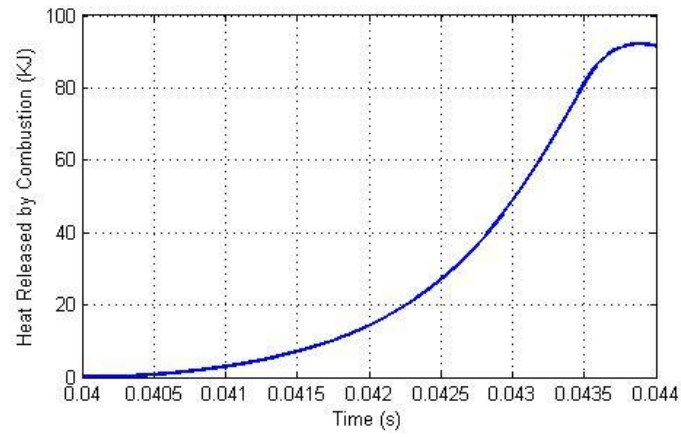
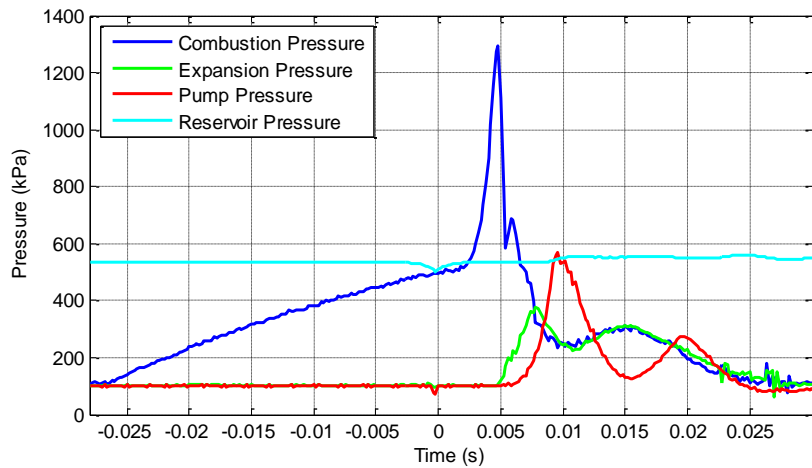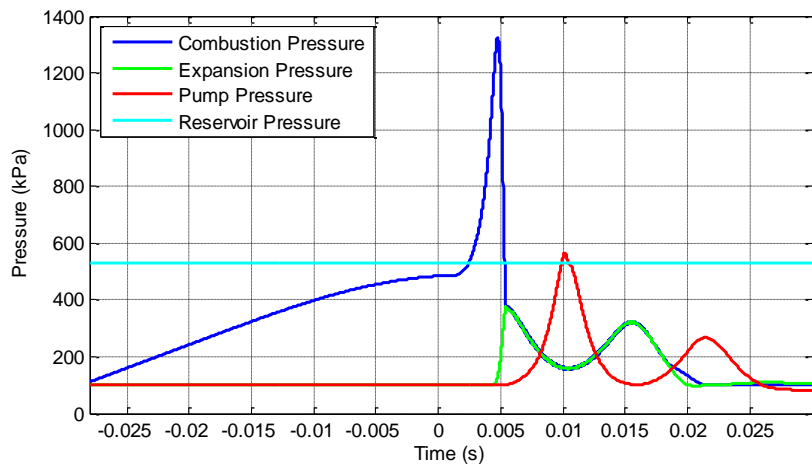Figure 3.6 Heat release during the combustion (simulated)

Figure 3.7 Validation of the overall system dynamics for FLPEC

51

Figure 3.6 shows the total heat released by combustion as described by Eq. (3.17). The total heat E_c stored in the air/fuel mixture is 130.2 *kJ* for this combustion event. However, in matching the simulated pressure dynamics to the experimentally obtained data, the values of *K* and *A* yield an effective heat release E_c of 93.8 *kJ*, which means that the experimental combustion lost 36.4 *kJ* to some combination of incomplete combustion and heat losses through the combustion chamber walls.

Figure 3.7 shows the overall system dynamics validation. Pressures in four CVs are shown, which are combustion pressure, expansion pressure, pump pressure and reservoir pressure respectively. It can be seen that the simulated pressure dynamics in these CVs have a very good correlation to the experimental data.

3.4   Conclusions

This chapter presented the modeling and simulation of an experimental prototype of a free liquid-piston engine compressor. The combustion process was modeled as a second order dynamic with the heat release rate governed by the Arrhenius law. The dynamics of three control volumes, the combustion chamber, the expansion chamber and the pump chamber respectively, were modeled. The mass flows in/out of these control volumes were also modeled. The simulation results for the pressures in the combustion chamber show good agreement with the experimentally measured pressure. Therefore, the simulation models of the FLPEC provide an accurate platform for testing the control algorithm.

Chapter IV

SIMULATION RESUTLS BASED ON VIRTURAL CAM CONTROL

The mathematical model and simulation of the FLPEC prototype exhibit a close correlation with experimental data. Hence, the validity of the proposed virtual-cam based control structure is ready to be tested in simulation.

4.1   Control objective

The control objective is to drive the system in an efficient manner by extracting the maximum possible amount of PV work from the combustion products. The controller should be able to dynamically adjust the control variables, i.e., the fuel injection duration and valve timings. For instance, the pressure in the reservoir can be increased by continuous pumping, or decreased by supplying air to the end application. This results in varying fuel injections and loads, since the pressures in the reservoir are different. The duration of air/fuel injection must be adaptively controlled so that optimal efficiency can be achieved and the compressor can be kept running in a desired way under varying operating conditions. Furthermore, proper timing of all of the valves is critical in achieving the best performance of the FLPEC. Like in most other free-piston applications, the period from cycle to cycle could be changed for the device. Hence, the controller should also be able to achieve operational frequency control.

Figure 3.7 shows the simulated dynamics of the combustion pressure, expansion pressure, compression pressure and reservoir pressure. It can be seen that the combustion pressure rises rapidly upon the ignition of the air/fuel mixture. The free-liquid piston is

then pushed by high pressure on the expansion chamber side, which results in pumping. Successful pumping is manifested by a slightly higher compression chamber pressure P_p than the reservoir pressure P_s. The pumping process begins at the time when P_p is increasing and becomes greater than P_s. It is imperative that the duration of the air/fuel injection is long enough to achieve desired stroke length and full pump under a certain load. However, excessive air/fuel injected into the combustion chamber may result in unutilized energy, which consequently decreases the FLPEC's efficiency. In order to compress the air in the compression chamber to a certain pressure, the piston needs to travel certain stroke length. Therefore, the stroke length controlled by the air/fuel mass injection is critical for successful pumping. By putting the control in the virtual cam context, the virtual cam and camshaft are created in the first cycle and adaptively adjusted in the following cycles.

4.2   Virtual cam construction

There are three virtual cams corresponding to three valves: 1) Air/fuel valve cam; 2) Exhaust valve cam of the expansion chamber; 3) Spark ignition cam. As previously mentioned, each control command sent by a given virtual cam will result as a duplex of $\{\theta_s, \theta_e\}$, which defines the timings for opening and closing a given valve. This structure results in five control variables being controlled by three virtual cams. Three pairs of parameters for three virtual cams can be written as $Cam_{inj} = \{\theta_{inj\_b}, \theta_{inj\_e}\}$ (injection valve control), $Cam_{ex} = \{\theta_{ex\_b}, \theta_{ex\_e}\}$ (exhaust valve control) and $Cam_{sp} = \{\theta_{sp\_b}, \theta_{sp\_e}\}$ (spark control). The values of these pairs influence five control variables: 1) The amount of

air/fuel mixture injected for each cycle, or the time duration of the air/fuel injection procedure; 2) The initiating time of air/fuel injection; 3) The timing of the spark; 4) The time at which the exhaust valve opens; 5) The duration for which the exhaust valve is open.

The commands for a sample engine cycle are shown in Figure 4.1. The corresponding virtual cams on the wheel are built based on these commands, as shown in the left figure of Figure 4.2, an equivalent virtual cam lobes sketch is shown on the right. By changing the angular velocity of the wheel, the period or the engine operational frequency can be adjusted as needed. When the frequency is changed, the stored cam parameters need to be accordingly changed so that the timings in the time domain remain unchanged. Assuming the original frequency is f_1 and the new frequency is f_2, a new cam parameter can be found by scaling the old parameter by $\theta_2 = f_2\theta_1/f_1$. If any of these parameters exceed 2π, i.e. some timings can not be carried out within one cycle, then the desired frequency is too high to be implemented and a lower frequency should be considered.
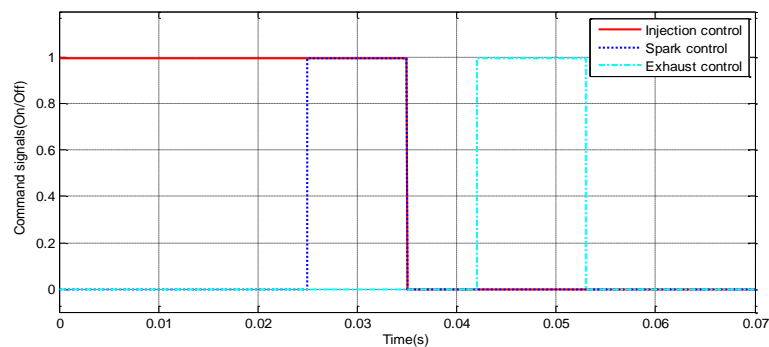
Figure 4.1 Command signals in Simulation
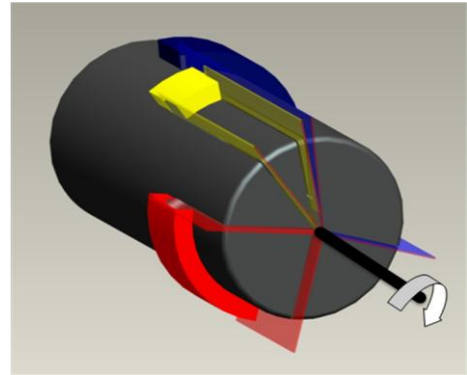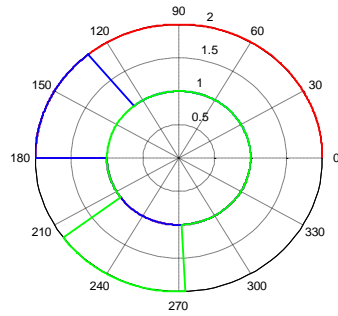
Figure 4.2 Virtual cams constructed by command signals
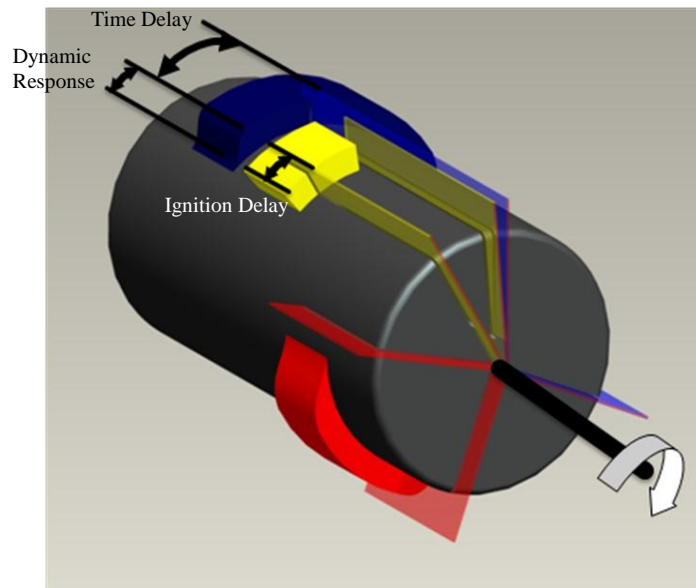
Figure 4.3 The 'kinematic equivalent' virtual cam lobes

With delay and valve dynamics, the actual system behavior will be different from that shown in Figure 4.1. Comparing Figure 4.3 with the original command lobe edges in the right figure of Figure 4.2, now valve timings are shifted and are not the same as those dictated by high level control. Hence, the low-level cam construction function should be able to compensate for these delays and valve response dynamics. These system delays

and dynamic response can be either experimentally measured or modeled using empirical data. The specific method of addressing these topics is not the focus of this work. Figure 4.3 shows the 'kinematic equivalent' virtual cam lobes which illustrate the effect of including delays and valve dynamics.

4.3   Integrated virtual cam control

In simulation test, an engine operational frequency of 20Hz is chosen, i.e. angular velocity of the virtual camshaft is $\omega = 40\pi$.The cycle-to-cycle based dynamic control requires information obtained in the previous cycles to adaptively adjust the virtual cam parameters. However, for the very first cycle, there is no prior information to use, and hence, preselected initial virtual cams are used,

$$Cam_{inj}[0] = \left\{0, \frac{3\pi}{5}\right\}$$ (4.1)

$$Cam_{ex}[0] = \left\{\frac{4\pi}{5}, \frac{8\pi}{5}\right\}$$ (4.2)

$$Cam_{spark}[0] = \left\{\frac{\pi}{5}, \frac{3\pi}{5}\right\}$$ (4.3)

By applying the above initial virtual cams to the target engine controller, the following cycles will always use the proposed control laws to adaptively adjust the cam parameters. For the injection cam, Cam_{inj}, injection of air/fuel mixture always starts as soon as a new cycle is initialized, which is $\theta_{inj\_b}(k+1) = \theta_{inj\_b}(k) = 0$. The duration of the next injection is calculated based on by Eq. (2.29) and the exhaust valve timing control is given by Equations (2.30) and (2.31). The pressure-based control approach is used in the simulation. As previously introduced in chapter 2, TDC and BDC measurement can be

conducted using pressure dynamics in the combustion chamber or compression chamber. However, since the combustion pressure sensor is costly and the pressure measurement is normally associated with some problems like drifting and noise, in the simulations and future experimental tests only pump side pressure will be used for both injection duration control and exhaust control. Next, the exhaust valve control will be first discussed by only using the compression pressure dynamics.
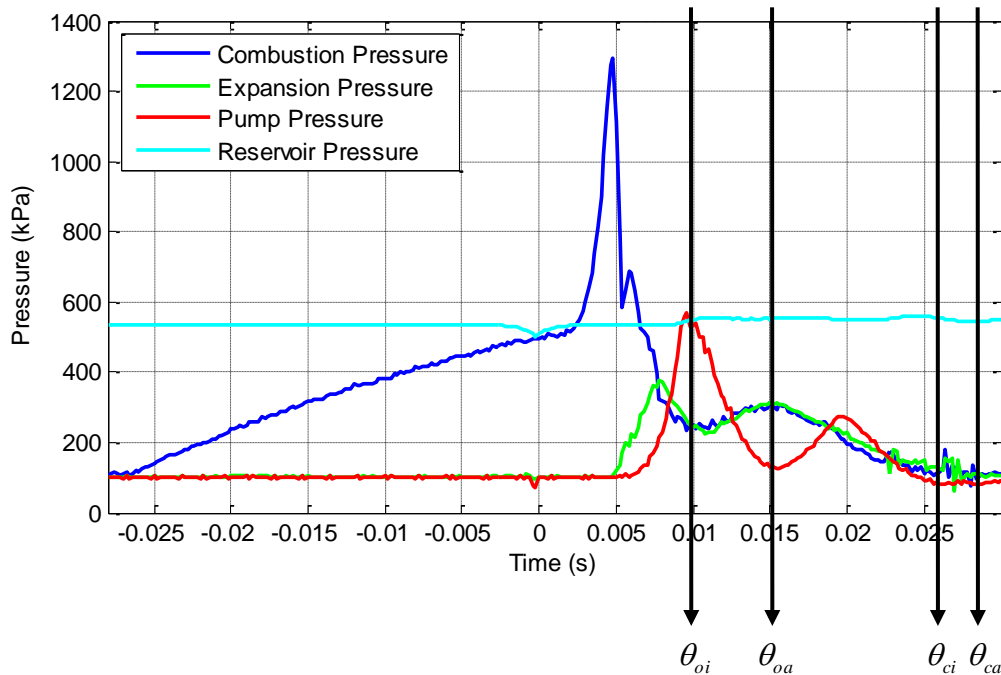

Figure 4.4 States in the exhaust valve control

The ideal time to open the valve is when the piston reaches BDC and the ideal time to close the exhaust valve thus is when the piston reaches TDC. TDC/BDC can be obtained by measuring the compression chamber pressure P_P and the reservoir pressure

P_s: 1) BDC is where compression chamber pressure $\dot{P}_P = 0$ and $P_P > P_s$, which refers to the instant at which the pump pressure begins to drop and will go below the reservoir pressure). 2) TDC is where pump pressure and expansion pressure both drop down to atmospheric pressure and $\dot{P}_P = 0$.

The exhaust control timings cannot be implemented in time due to the delays mentioned before, so the control law described by Equations (2.30-2.31) is used here. The required variables for the exhaust control are illustrated in Figure 4.4: ideal cam position to open exhaust valve is denoted as θ_{oi}, that is when piston reaches BDC; ideal cam position to close exhaust valve is denoted as θ_{oc}, that is when piston returns to TDC. The actual time when the exhaust valve is opened is denoted as θ_{oa} and the actual close time is denoted as θ_{ca}. At the end of the kth cycle, the errors between actual timings and ideal timings are calculated by $(\theta_{oi}[k] - \theta_{oa}[k])$ and $(\theta_{ci}[k] - \theta_{ca}[k])$. By the control algorithm described by Equations (2.30-2.31), the valve timings for the next cycle, $\theta_o[k+1]$ and $\theta_c[k+1]$, are controlled to approach the ideal timings in the current cycle, $\theta_{oi}[k]$ and $\theta_{ci}[k]$.

The fuel injection control essentially is to optimize the energy input for specific load and to achieve stroke length so that the optimal engine efficiency can be achieved. The original amount of chemically stored energy in the injected mass of the air/fuel mixture is given by,

$$E_{in} = \eta_c m_{c0} e \tag{4.4}$$

where m_{c0} is the mass of the fuel injected into the combustion chamber, η_c is the

combustion efficiency and e is computed from the lower heating value of the stoichiometric combustion of propane. The duration of the air/fuel injection is proportional to the mass of the fuel, given by Eq. (4.5),

$$E_{in} = e \int_0^{t_{inj}} \dot{m}_{fuel} dt \qquad (4.5)$$

Therefore, the input energy for each cycle is controlled by regulating the air/fuel injection duration. To do so, the virtual cam responsible for the air/fuel injection valve is built to 1) maximize the pump energy; Specifically for the FLPEC, this means maximizing the power stroke length to the physical limit of the engine (volume of the compression chamber is ideally zero at the end of pumping); 2) adjust the mass of the fuel injected according to the load variations. The load of the free-piston engine air compressor is the reservoir pressure. Air in the compression chamber can be pumped into the reservoir only if the pump pressure becomes higher than the reservoir pressure. Thus, a higher reservoir pressure upon pumping is considered as a higher load in a given cycle. The adjustment of the fuel injection parameters is described by Eq. (2.29). The stroke length control is carried out by $E_x(x_d - x_{stroke}[k])$, where x_d is the desired stroke length. The term of $E_L(L[k+1] - L[k])$ adjusts the fuel mass according to the load variation from the kth cycle to the next cycle.

With the discussions above, the following diagram illustrates the virtual cam based control structure. In the simulation, noises are added to the combustion pressure and the compression pressure. Therefore, a filter is used and intended to cause some delays as in real experimental measurements.
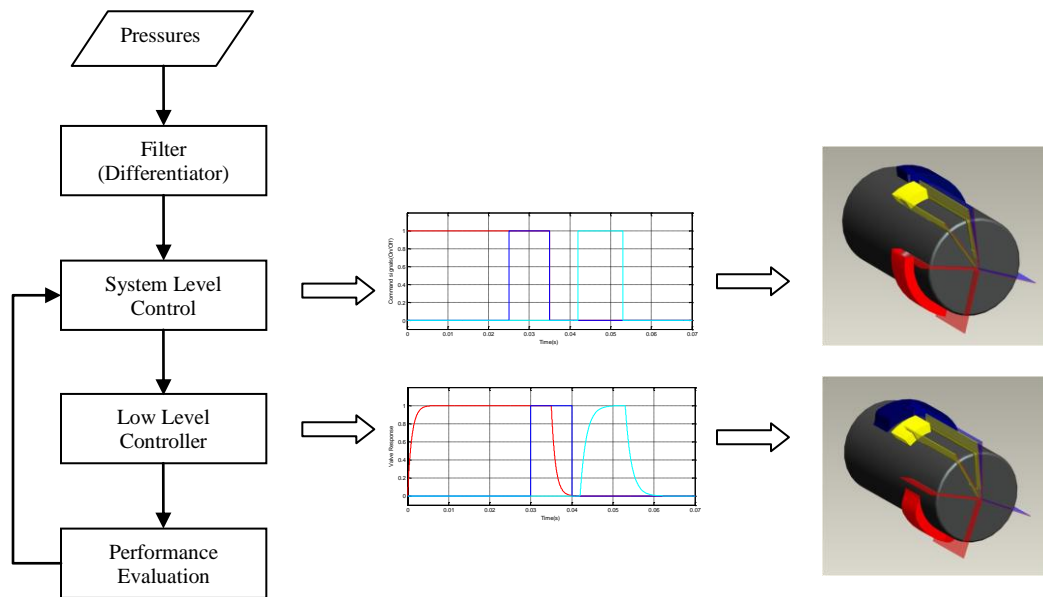
Figure 4.5 Diagram of the proposed control structure using virtual cams

4.4   Simulation results

The initial pressures and temperatures in the three chambers (combustion, expansion and reservoir) were all set to atmospheric pressure and ambient temperature, the free piston started at its "relaxed" position, and all the valves were set to be initially closed. Figure 4.6 shows the simulation results of the exhaust valve control for three cycles under the control signals (voltages for electronic exhaust valve, shown in Figure 4.7). In the first cycle, virtual cam parameters are given as Eq. (4.1-4.3). At the end of the first cycle, new reference exhaust commands are generated based on the observed system dynamics in this cycle. Since there is no prior data, the initial commands are very different from preferred reference ones. As a result, the expansion energy of the expansion chamber is low, indicated by the low peak expansion pressure. Using cycle-to-cycle adjustment, actual commands begin to get close to reference commands on the second cycle. The third cycle has a strong pump (large amount of compression energy in

the compression chamber) due to the close-to-ideal timings of the exhaust valve, which increases the compression ratio for the next cycle. This simulation shows the controller is capable of optimizing the exhaust valve timings in only few cycles. Thus, the simulation results indicate that the controller can adjust virtual cam parameters to optimal references quickly.
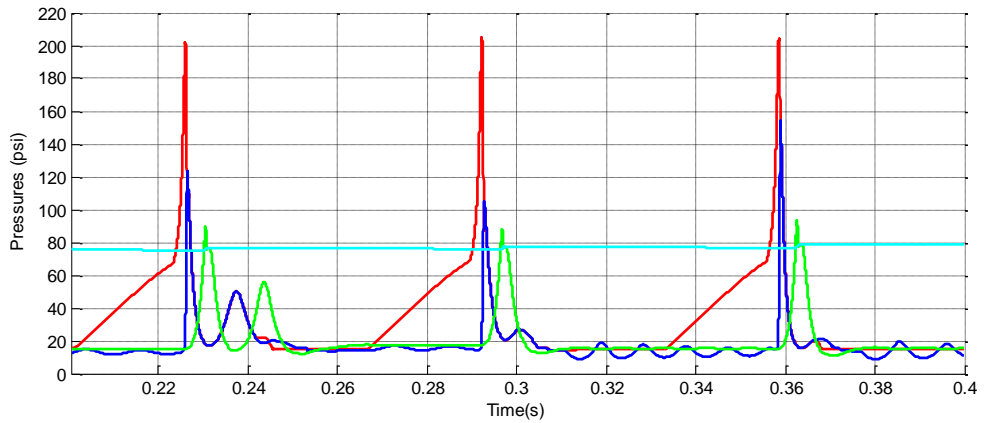

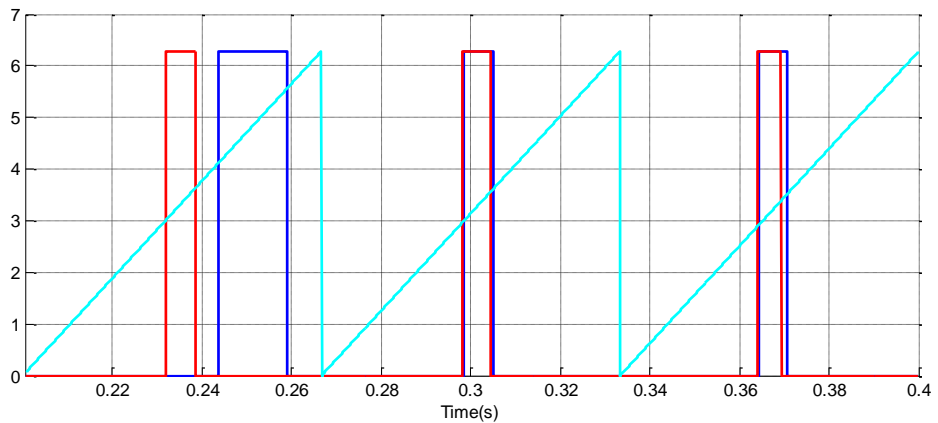Figure 4.6 Simulation results for FLPEC in three cycles

Figure 4.7 Virtual cam commands and their reference commands

Figure 4.8 shows the overall system performance. Since the initial conditions for

exhaust valve timings and injection duration are preset (not optimal), non-optimal compression ratio results in poor pumping performance in the few cycles at the very beginning. Once the virtual cams parameters converge to those optimal values, the system runs well and the reservoir pressure increased quickly from strong pumps.

For the FLPEC, the ideal BDC is where the pump volume is zero. That is, all the air in the compression chamber is pumped into the reservoir. However, this is not practically achievable due to the limitation of check valve dynamics and the piston inertance. It is because the check valve can not provide a large enough opening for long enough to allow the fast moving piston to push all of the air in the compression chamber into the reservoir. Therefore, in the simulations, desired BDC is set to be a small volume of $2.5 \times 10^{-5} m^3$. As shown in Figure 4.9, the volume of the compression chamber reaches its physically limited maximum TDC and approaches the desired BDC in few cycles.
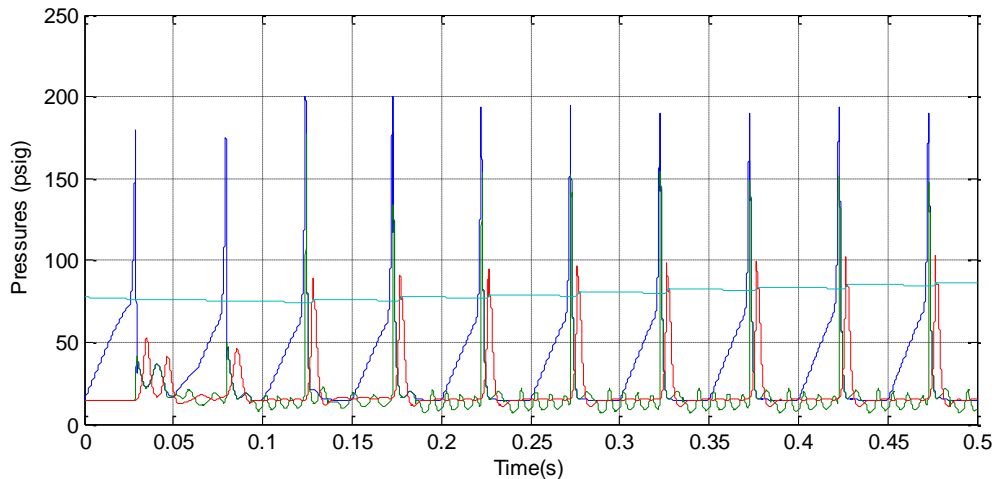

Figure 4.8 Overall system dynamics in Simulations
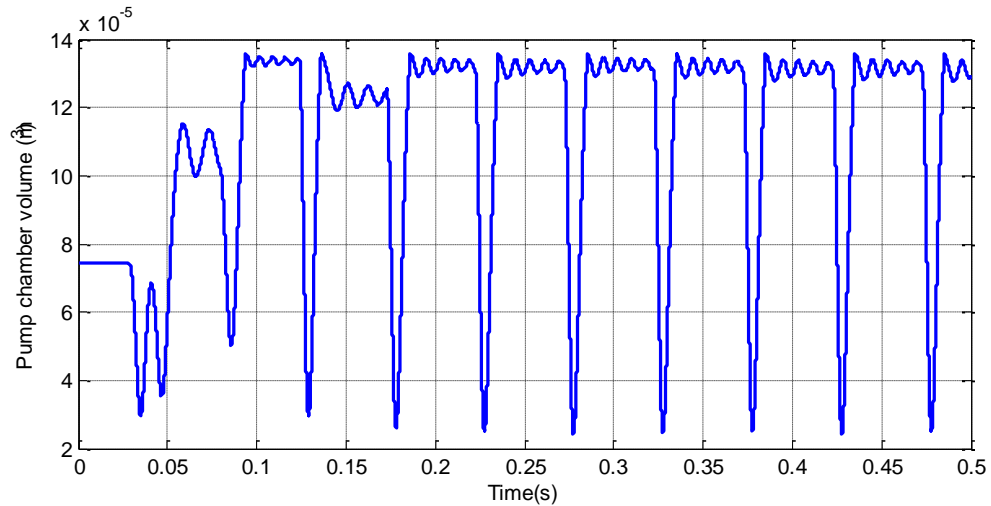
Figure 4.9 Simulated volume of the compression chamber

The reservoir pressure dynamics are shown in Figure 4.10. It can be seen that the reservoir loses its pressure because it outputs air for the injection without receiving air from pumping during the first two cycles. Figure 4.11 shows the injection control input. The injection duration is increased for the second cycle because the compression ratio in the compression chamber is small in the first cycle, requiring more fuel to be injected. Once successful pumping is maintained and the compression ratio approaches the desired value, the injection duration only increases slowly along with the increased reservoir pressure (load for pumping). The engine efficiency approaches its theoretical optimum value as the control parameters are adjusted over time, as shown in Figure 4.12.
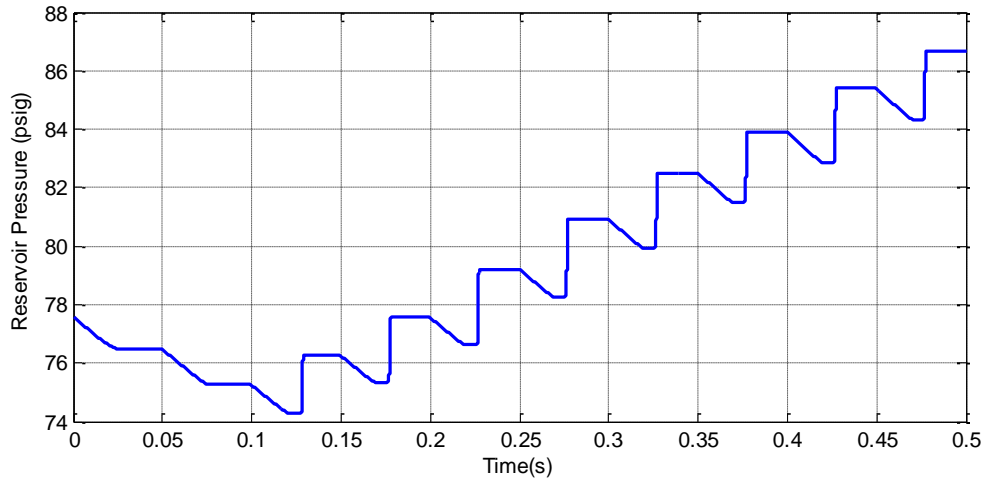
Figure 4.10 Simulated reservoir pressure dynamics
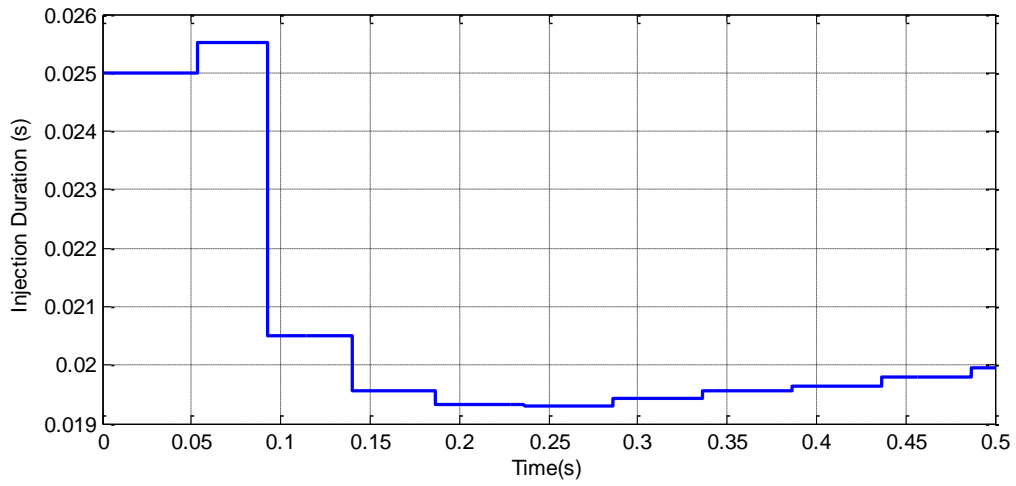
Figure 4.11 Simulated injection durations convergence
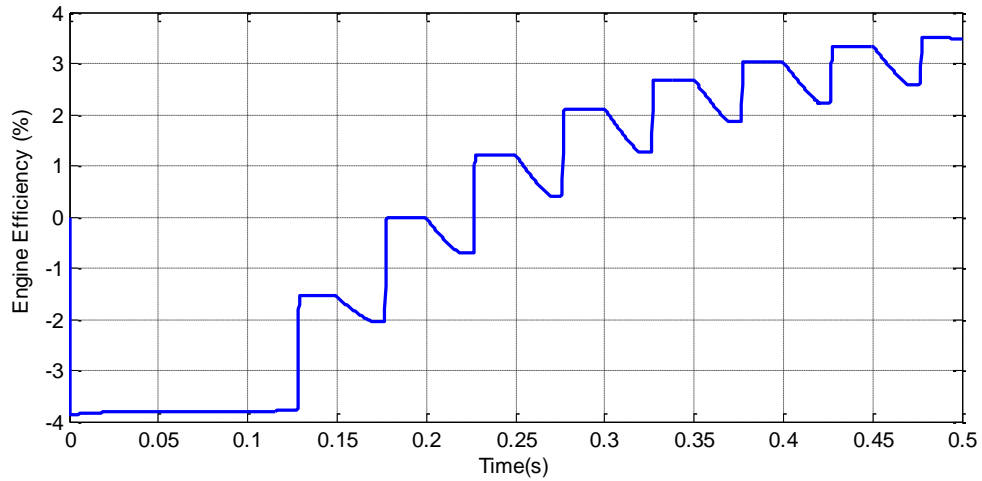
Figure 4.12 Simulated engine efficiencies
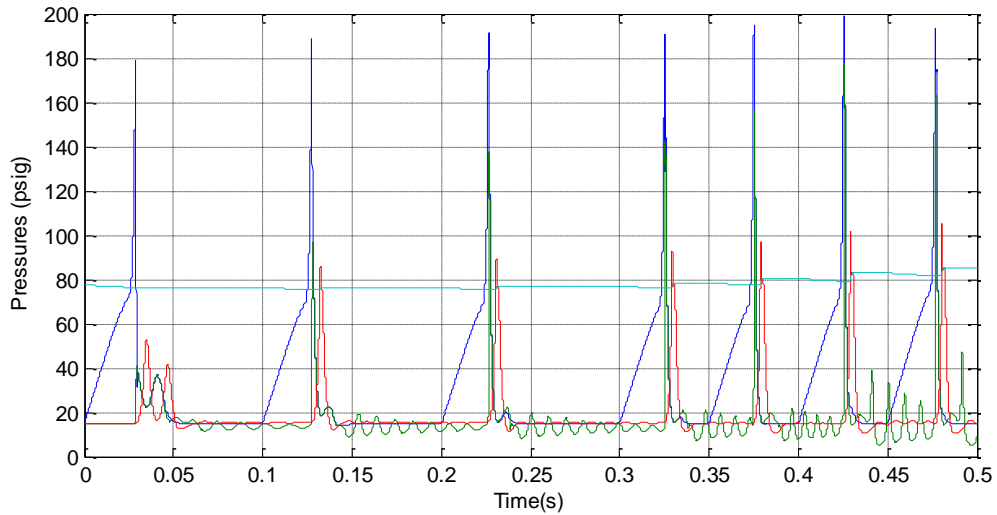
Figure 4.13 Frequency control in the simulations

Frequency control is achieved by changing the angular velocity ω of the self-spinning virtual camshaft at the end of a given cycle. Figure 4.13 shows frequency control results in simulation. The free-piston engine was operated at 10Hz for three cycles, after which the frequency was changed to 20 Hz. When the angular velocity ω is changed from $f_1 = 10\text{Hz}$ to $f_2 = 20\text{Hz}$, the virtual cam position needs to be

correspondingly adjusted by $\theta_2 = f_2\theta_1/f_1 = 2\theta_1$. For instance, if the injection duration was $\{0,0.5\pi\}$ with 10Hz frequency, it will be adjusted to $\{0,\pi\}$ with 20Hz frequency. Thus, the timings are kept constant in the time domain.

The injection and exhaust controls are based on a cycle-to-cycle adjustment method. They are not affected by the operating frequency. The adjustment of the engine efficiency and the compression ratio are achieved along with frequency control, as shown by Figure 4.14 and Figure 4.15.
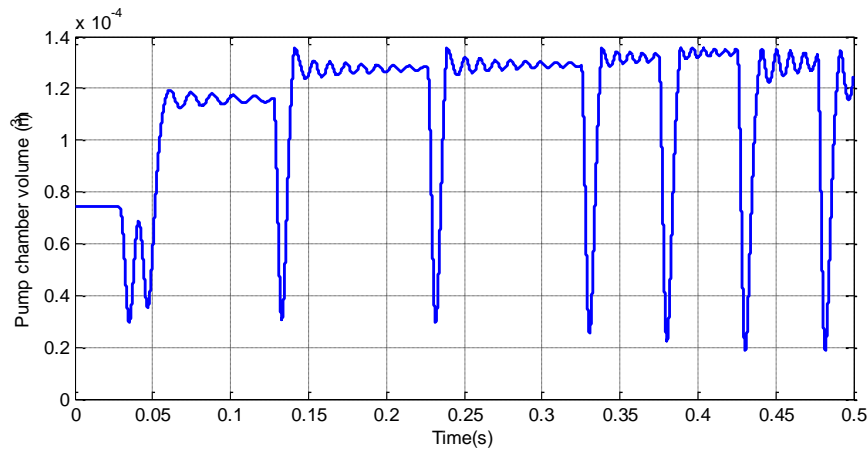
Figure 4.14 Simulated volume of the compression chamber during the frequency control
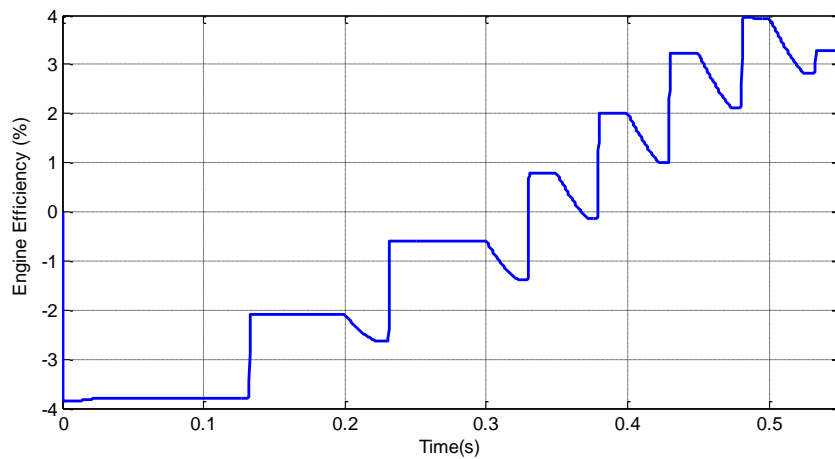
Figure 4.15 Simulated engine efficiencies during the frequency control

4.5　Conclusions

In this chapter, the virtual-cam based control method was tested in the simulation of the FLPEC. The pressure-based control scheme for this device was developed to control 1) The duration of the air/fuel injection for each cycle; 2) The timing of the air/fuel injection; 3) The spark timing; 4) The timing and duration of the exhaust valve. Simulation results showed a good dynamic performance of the engine. Therefore, the next step is to implement the proposed control scheme on the real device and test its performance.

Chapter V

A HIGH INERTANCE FREE LIQUID PISTON COMPRESSOR

In the previous chapter, simulation results have shown the validity of the proposed control methodology. However, prototype one (FLPEC) presents some difficulties for implementing the controller. That is, the separated combustion chamber design causes scavenging problem resulting in intermittent firing and incomplete combustion. The second prototype, a high inertance free liquid piston compressor (HIFLPC), was designed and fabricated by Andy Willhite and then experimentally tested by myself and Andy Willhite [34-35]. Therefore, the proposed control method was implemented on this device and experimentally tested for the performance assessment.

5.1   Introduction

The work of Riofrio, et al. [2-3] presented a unique design of a free liquid-piston engine compressor (FLPEC). By utilizing the free liquid piston, the FLPEC demonstrated a solution for an efficient, compact conversion of fuel to pneumatic potential. Performance of the FLPEC was characterized in [3], with a measured efficiency of 2.01%, corresponding to 931 kJ of cool gas pneumatic potential per kilogram of fuel.

The FLPEC has a unique design of a separated combustion chamber, which is sealed by a combustion valve from the expansion chamber. Upon combustion, the high-pressure combustion products force open the combustion valve so that high pressure combustion products vent into the expansion chamber and expand the expansion chamber. Since the combustion chamber is separated and sealed by the combustion valve, it can hold the high-pressure air/fuel mixture in the combustion chamber before

combustion occurs. This design eliminated the intake and compression strokes in conventional IC engines by directly injecting high-pressure air/fuel mixture into the combustion chamber. However, it presented a problem for scavenging the combustion products from the separated combustion chamber, leading to intermittent firing. Andy Willhite [34] also pointed out some other problems associated with this design. They include flow losses around the combustion valve, incomplete combustion and so on.

All of these problems were associated with either the separated combustion chamber apparatus on the engine side or the pump check valve on the compressor side. The pump stroke of the FLPEC was too "fast" – leading to the necessity of the separated combustion chamber in the engine section. For instance, without the separated combustion chamber, direct injection of air/fuel mixture into a combined combustion and expansion chamber will result in pushing the diaphragm significantly during injection. If the piston is too "fast" or too light, the initial combustion chamber volume upon combustion will be very large, resulting in poor expansion ratio.
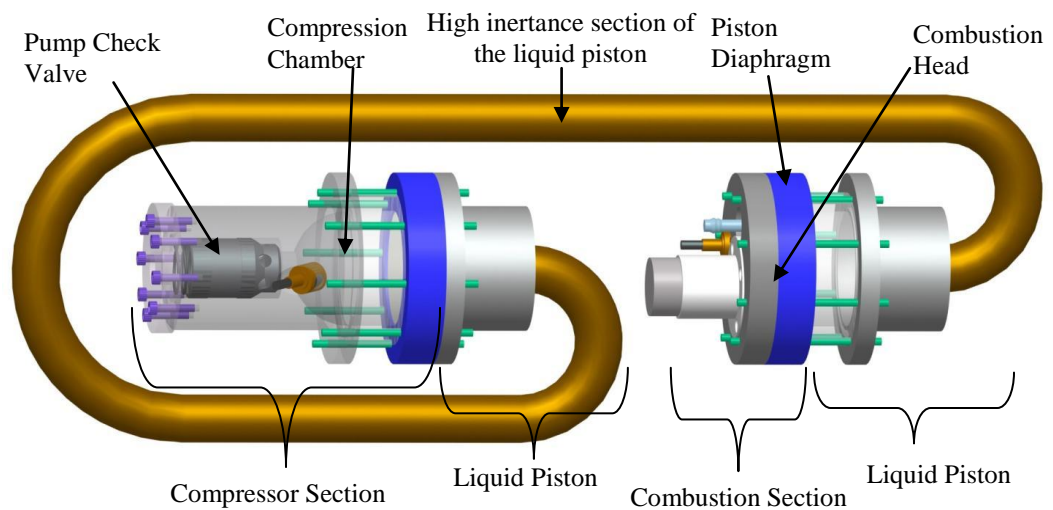
Figure 5.1 Schematic of the High Inertance Free Liquid Piston Compressor (HIFLPC)
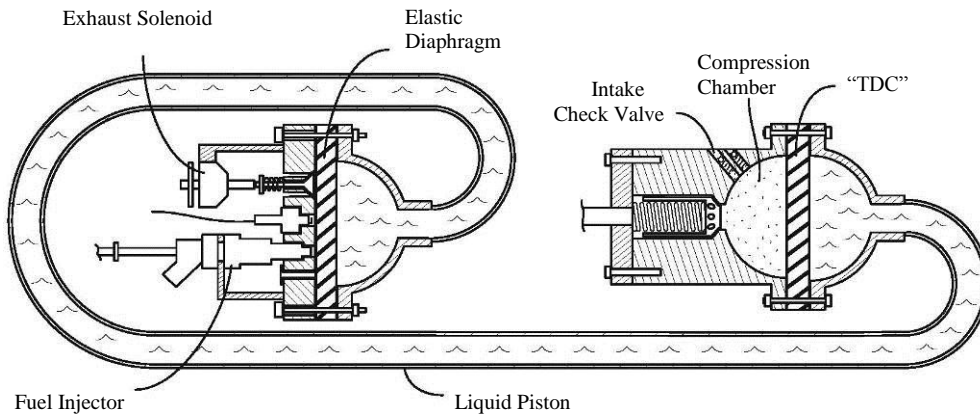
(a). Schematic of HIFLPC at effective TDC
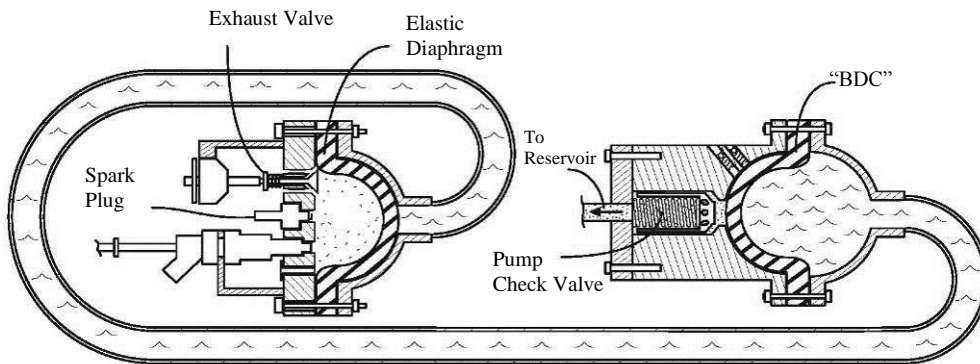
(b). Schematic of HIFLPC at effective BDC

Figure 5.2 Schematic of HIFLPC

Since the FLPEC utilized a liquid piston, the property of liquid inertance could increase the system's effective inertia by exploiting the liquid piston's geometry. The dynamics of the system could be made slower without necessarily adding mass to the system. With a high enough inertance, the dynamic load of the piston could be sufficient to eliminate the need of the FLPEC's separated combustion chamber altogether by

dynamically holding the air/fuel pressure high enough during injection to maintain a high pre-combustion pressure. Also, slower flow rate of air during the pump stroke allows for a smaller check valve that is faster relative to the power stroke duration that can mitigate backflow while not causing unacceptable flow losses. Andy Willhite et al. [34-35] presented a design which exploits these high-inertance effects, the High Inertance Free Liquid Piston Compressor (HIFLPC), as shown schematically in Figure 5.1.

5.2 Basic operation of the HIFLPC

The schematic configurations of the high inertance free liquid piston compressor (HIFLPC) are illustrated in Figure 5.2 at effective TDC (a) and BDC (b), respectively. Before an engine cycle is started, the diaphragms are at their "relaxed" positions where the diaphragm on combustion side fully contacts with the combustion head, leaving nearly (or ideally) zero volume in combustion chamber. This is analogous to TDC in conventional engines. On the pump side, the compression chamber is at atmospheric pressure while the intake check valve (from outside to the compression chamber) and pump check valve (from the compression chamber to the reservoir) are both shut. The power stroke starts with the injection of air and fuel for a short duration. The air/fuel injection scheme will be discussed later. During the air/fuel injection, the diaphragms are pushed toward the pump side, resulting in an increase of the combustion chamber volume. By utilizing the high-inertance liquid piston, the diaphragms are expanded very little during injection such that the combustion chamber can dynamically hold the high-pressure air/fuel mixture until combustion occurs. Combustion of the air/fuel mixture converts the stored chemical energy into kinetic energy of the liquid-piston through

expansion work. Therefore, the piston rapidly moves toward the pump side and compresses the air in the compression chamber. Once the compression pressure exceeds the reservoir pressure, the pump check valve opens and mass flow into the reservoir occurs. At the end of pumping, once the piston begins to retract, the compression pressure drops to where it is equal to the reservoir pressure. The piston position at this moment is analogous to BDC in conventional engines, as illustrated by Figure 5.2(b). At this position, the combustion exhaust valve is opened and the piston begins to move back toward the combustion side by releasing the energy stored in the diaphragms during the power cycle. Once the piston has returned to its original TDC position, one engine cycle is over as soon after the combustion exhaust valve is closed.

The lack of a compression stroke allows the engine compressor to "fire on demand"- that is, there is no need to have a starting routine or maintain an idle cycle. This allows the HIFLPC to operate at varying frequencies by controlling the delay between TDC and the command for air/fuel injection.

5.3   Prototype fabrications and experimental setup of the HIFLPC

An experimental prototype of the HIFLPC device, shown in Figure 5.3, was fabricated for performance evaluation and control testing. The device as configured for testing has an approximate weight of 2.6 kg, with a footprint of around 18" by 18" with the liquid piston configuration shown.
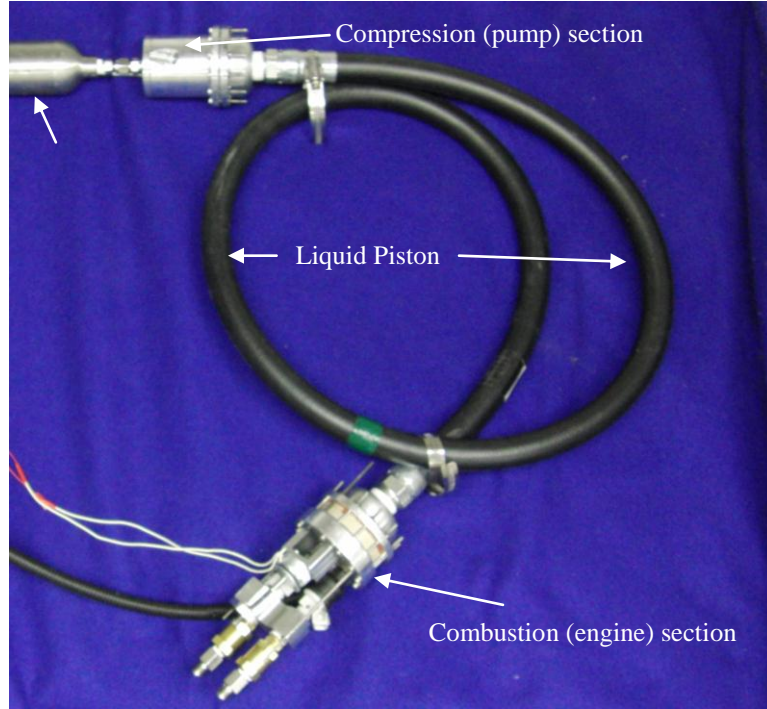
Figure 5.3   Assembled HIFLPC prototype

5.3.1   Critical physical parameters of prototype

Table 5.1: Physical parameter overview of HIFLPC prototype:

Parameter	Value	Description
A_1, A_3	2026.8	Cross-sectional area of hemispherical liquid piston region that mates to combustion chamber with diaphragm.
A_2	285.02	Cross-sectional area of high-inertance tube of liquid piston
L_2	1828.8	Length of high-inertance tube of liquid piston
I	$6.40 \times 10^6\, kg/mm^4$	Calculated inertance of liquid piston
$D_{diaphragm}$	50.8 mm	Diaphragm working diameter
D_{comb}	50.8 mm	Combustion chamber inner diameter
D_{comp}	50.8 mm	Compressor chamber diameter
V_{comp}	$5.40 \times 10^4\, mm^3$	Compressor chamber initial volume
V_{res}	$5.17 \times 10^5\, mm^3$	Volume of reservoir

Table 5.1 lists critical physical parameters of prototype components. The liquid piston dimensions were sized based on an optimization discussed in Andy Willhite [35].

5.3.2 Injection circuit and control

In the application of a free-piston engine compressor, high-pressure air is always on hand. Such a system presents the opportunity of combining the high-pressure injection of fuel with high-pressure air. Such a scheme allows an engine to bypass the conventional intake and compression strokes; the simultaneous introduction of high-pressure air and fuel presents a high-pressure mixture directly before combustion that is equivalent to the end of a conventional compression stroke. Utilizing high pressure for the air/fuel injection is proposed here for small scale free-piston engine compressors.

Conventional air/fuel ratio control for internal combustion engines commonly includes an inner-loop controller based on the deviation of the estimated three-way catalyst stored oxygen state [36-37]. In contrast, the proposed system directly injects a high-pressure air and fuel to the combustion chamber through separate air and fuel lines, assisted by high upstream driving pressures. Fuel is firstly injected into the combustion chamber. As soon as the fuel injection is finished, air is then injected into the combustion chamber. Therefore, part of the control strategy is to command the air and fuel injection durations to achieve a certain air/fuel ratio.

The proposed system consists of two supply lines: the air line and the fuel line. Figure 5.4 shows the injection scheme of the proposed design. The air used for the mixture injection comes from the HIFLPC's air reservoir. On the other line, the fuel

source is a 0.5kg bottle of propane, which at room temperature has a vapor pressure of about 1 MPa (154 *psia*). Note that there is a fuel buffer cylinder between the fuel valve and the fuel injector, as shown in Figure 5.4. Its function will be discussed in the control section.
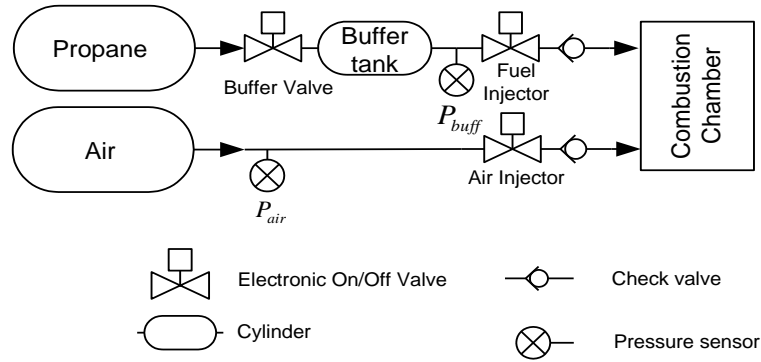
Figure 5.4 Air and fuel injection circuit

The mass flow rates through all valves or any flow restricted areas depend on the upstream and the downstream pressures. The following equations give the mass rate $\dot{m}$ under subsonic and sonic conditions [28]:

$$\dot{m}_j = a\psi_j(P_u, P_d)$$

$$= \begin{cases} C_d C_1 \dfrac{P_u}{\sqrt{T_u}} & \text{if} \quad \dfrac{P_d}{P_u} \le P_{cr} \\[4mm] C_d C_2 \dfrac{P_u}{\sqrt{T_u}} \left(\dfrac{P_d}{P_u}\right)^{1/\gamma_u} \sqrt{1 - \left(\dfrac{P_d}{P_u}\right)^{\gamma_u - 1/\gamma_u}} & \text{if} \quad \dfrac{P_d}{P_u} > P_{cr} \end{cases} \tag{5.1}$$

where C_d is a nondimensional discharge coefficient of the valve, a is the area of the valve orifice, P_u and P_d are the upstream and downstream pressures, T_u is the upstream

temperature, γ_u is the ratio of specific heats of the upstream substance, and C_1, C_2 and P_{cr} are substance-specific constants given by

$$C_1 = \sqrt{\frac{\gamma_u}{R_u}\left(\frac{2}{\gamma_u+1}\right)^{\gamma_u+1/\gamma_u-1}}$$

(5.2)

$$C_2 = \sqrt{\frac{2\gamma_u}{R_u(\gamma_u-1)}}$$

(5.3)

$$P_{cr} = \left(\frac{2}{\gamma_u+1}\right)^{\gamma_u/\gamma_u-1}$$

(5.4)

where R_u is the gas constant of the upstream substance. The specific heat ratio of the air is $\gamma_a = 1.4$ and the specific heat ratio of the propane is $\gamma_f = 1.12$. Given the orifice areas of the air and fuel injectors (a_a and a_f) and assuming injectors are opened and closed instantaneously, injected air and fuel mass are given as,

$$m_a = \int_{t_{a0}}^{t_{a1}} a_a \psi_a (P_a, P_{ad})$$

(5.5)

$$m_f = \int_{t_{f0}}^{t_{f1}} a_f \psi_f (P_f, P_{fd})$$

(5.6)

where P_a is the air upstream pressure, P_f is the fuel upstream pressure and P_{ad} and P_{fd} are the downstream pressures for air injection and fuel injection respectively. In Figure 5.4, P_a is the air pressure in the reservoir; P_f is the fuel pressure in the buffer tank; the air/fuel mixture ratio is given by,

$$\lambda_{af} = \frac{m_a}{m_f} = \frac{\int_{t_{a0}}^{t_{a1}} a_a \psi_a (P_a, P_{ad})}{\int_{t_{f0}}^{t_{f1}} a_f \psi_f (P_f, P_{fd})}$$

(5.7)

where t_{f0} to t_{f1} is the injection duration of fuel, t_{a0} to t_{a1} is the injection duration of air, and $t_{f1} = t_{a0}$. For the HIFLPC air and fuel injection valves, the *Bosch 0 280 150 846 CNG* fuel injector (see Figure 5.5) was chosen due to its fast response time (less than 5*ms*), adequate full-open flow rate, and specific design for gaseous fuel (as opposed to standard automobile liquid fuel injectors).
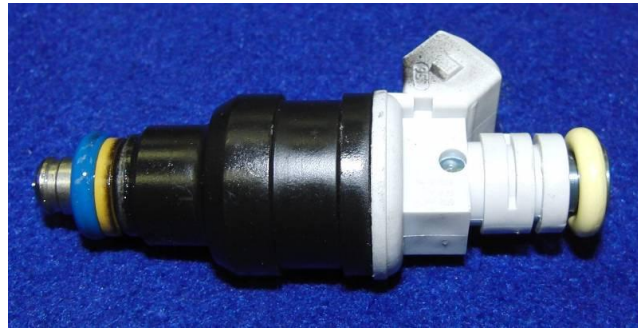

Figure 5.5 Bosch 0 280 150 846 CNG fuel injector

Propane is supplied to the fuel injector via the injection circuit, as shown in Figure 5.6. The propane source is a standard 16.4 oz. propane tank for small outdoor stoves (*Coleman model #5103B164T.*) An intermediate "buffer tank" is used for the propane supply upstream of the injector. This buffer tank has a volume of 75cc that is small enough to give a good resolution of pressure drop (for fuel consumption measurement) in a typical injection cycle and is big enough to avoid pressure fluctuation (a fairly constant upstream fuel pressure) during the fuel injection. A 2-way solenoid valve (*Parker Series 9*), driven by a simple on/off controller, regulates the buffer tank propane pressure (measured by a *Festo SDE-16-10V* sensor.)
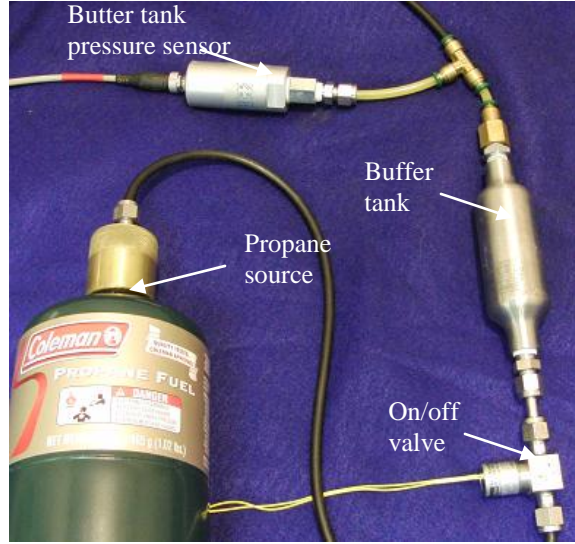
Figure 5.6 Fuel pressure control circuit

The reservoir tank not only receives pressurized air from the compressor, it also routes a portion of that air back to the air injector on the engine to be mixed with fuel. Since both air and fuel use the same Bosch injectors, the effective cross-sectional area of the air and fuel injector is taken to be $a_{A/F} = a_a = a_f = 1.82mm^2$. Therefore, the controllable variables in this setup are the injection durations and the upstream pressures on the air and fuel lines. A simple control method is used to achieve a certain air/fuel ratio and quantity of the mixture of each injection. Fuel is first injected from t_{f0} to t_{f1} at a controllable upstream fuel pressure, followed by the air injection over t_{a0} to t_{a1}, see Figure 5.8. The minimum response time of the injector is a little less than 5ms. Hence, the fuel injection duration is controlled to last for $t_{f1} - t_{f0} = 5ms$. If the fuel is directly injected from the propane tank that has a vapor pressure around 154 $psia$ for 5ms, the engine will receive much more fuel investment than required for its configuration (size of combustion chamber, power output and so on). As a result, upstream pressure of the fuel

needs to be relatively low in order to avoid excessive fuel injection for such a small engine. As shown in Figure 5.6, a fuel buffer tank is added on the fuel injection line so that the buffer tank pressure can be controlled to be much lower than the vapor pressure out of propane bottle. Moreover, it is convenient to measure the pressure drop in the buffer tank to calculate the fuel investment for the efficiency assessment.

By reading the buffer tank pressure P_{buff}, the electronic on/off valve only opens when $P_{buff} < P_{desired}$, i.e. the propane pressure P_{buff} is lower than the desired pressure. The control law for the electronic fuel valve is described as,

$$Fuel = \begin{cases} On & P_{buff} < P_{desired} \\ Off & otherwise \end{cases} \qquad (5.8)$$

The air injection duration is much longer than the fuel injection duration because the stoichiometric ratio for propane is about 16.3:1. Therefore, the injection duration in the next sections refers to the air injection duration. Moreover, the fuel injection duration is set to be fixed at 5 ms and the fuel amount is governed by setting the buffer tank pressure P_{buff}. Given the air injection duration, in order to achieve a certain ratio, the fuel mass can be controlled by regulating the fuel upstream pressure (the buffer tank pressure P_{buff}) to a desired pressure $P_{desired}$. Corresponding desired fuel upstream pressures, $P_{desired}$, for certain air injection durations and pressures are experimentally examined. Given a reservoir pressure of 60 *psig* and injection duration of 15 *ms*, the buffer tank pressure of propane is 16 *psig* for a lean combustion. It is experimentally obtained by lowering the propane pressure, under a constant reservoir pressure 60 *psig*, to where consistent combustion is still achievable. However, if the air upstream pressure

rises to 80 *psig*, the buffer tank pressure should be adjusted to 18 *psig* for 15*ms* injection duration because more air is injected under higher air upstream pressure. As a result, the injection controller adjusts the buffer tank pressure as a function of the pressure change in the reservoir. The simple control strategy is given by,

$$P_{desired} = P_{prop\_r} + K_p (P_{res\_r} - P_{res})$$ (5.9)

where P_{prop_r} is the reference buffer tank pressure, 16 *psig*; P_{res_r} is the reference reservoir pressure, 60 *psig*; $P_{desired}$ is the desired propane buffer tank pressure, which is achieved by controlling the electronic on/off fuel valve, as described in Eq. (5.8); P_{res} is the reservoir pressure measured in real-time; finally, K_p is a constant gain for adjusting propane buffer tank pressure.
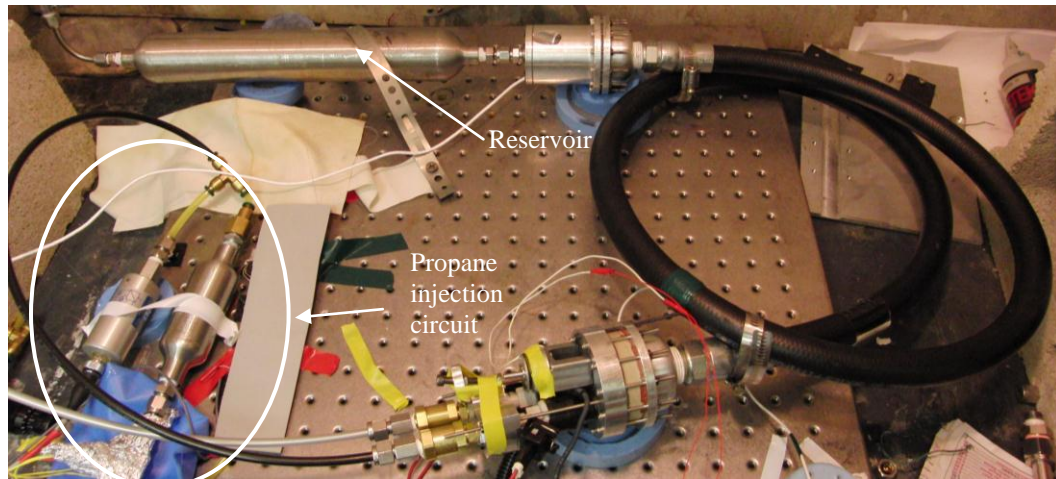
5.3.3 Experimental test set-up

Figure 5.7 HIFLPC test configuration.

The HIFLPC system was assembled with reservoir and air/fuel injection circuit as shown in Figure 5.7. Three pressures are used for measuring the engine dynamics: 1) the combustion pressure is measured by an *Optrand AutoPSI* pressure sensor (model

C22294-Q) installed in the combustion chamber; 2) the compression pressure is measured by a *Kulite XTL190-300A* pressure sensor installed in the compression chamber; 3) the reservoir pressure is measured by a *Festo SDE-16-10V* sensor. Appropriate conditioning circuits were built to connect sensors and valve actuators to the data acquisition card mounted on a PC. MATLAB/Simulink's Real-Time Workshop was used to send control signals to the drivers of the active valves and spark ignition and to acquire the pressure data (sampled at 10 kHz).

Figure 5.8 is a representation of the signal timing used for data collection, tuned for consistent cycle-to-cycle operation of the HIFLPC at the tested reservoir loads. The vertical axis only indicates on/off with slight offsets to distinguish the signals. In order to obtain the most power out of the engine, the operational frequency was tuned to 4 Hz. The ignition coil ignites the spark plug 9 *ms* later after the spark command is sent out. Therefore, the time to ignite the spark plug is advanced to compensate for this delay.
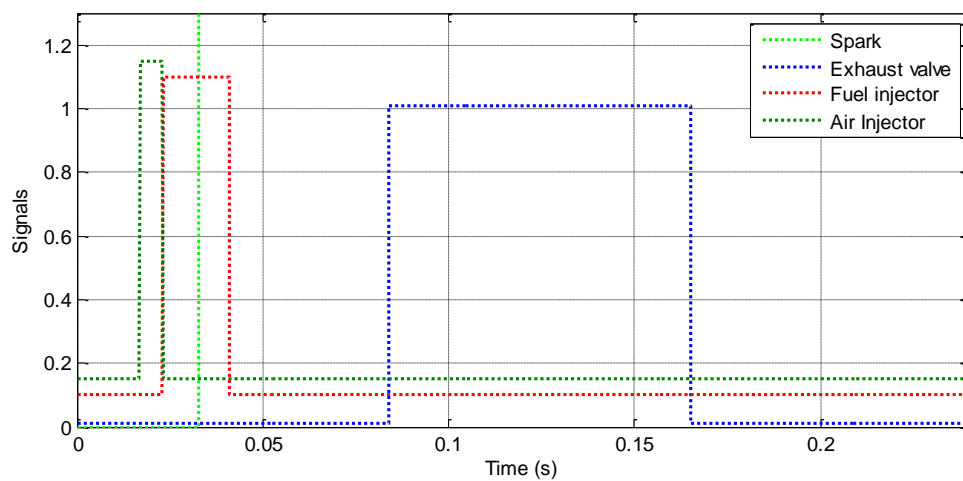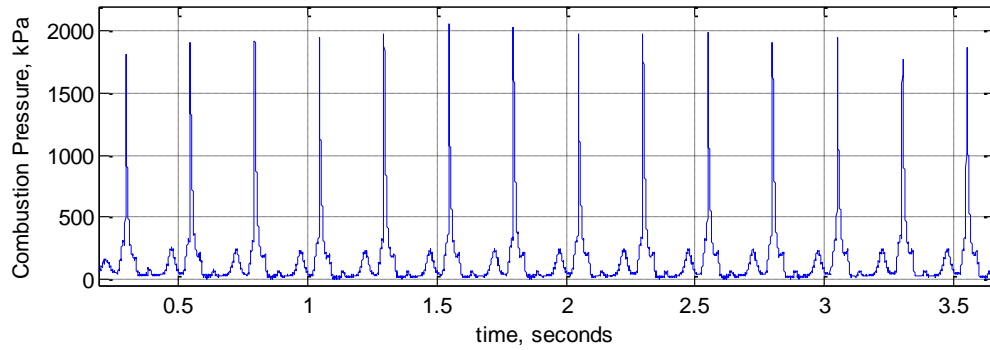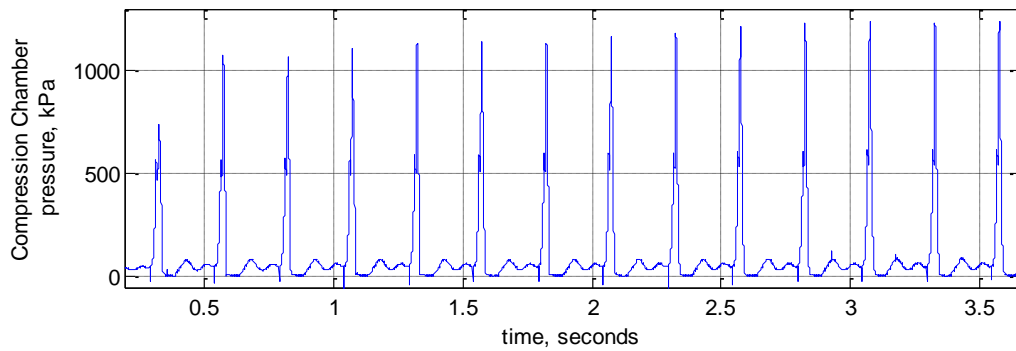

Figure 5.8 Signal timings for the prototype operation

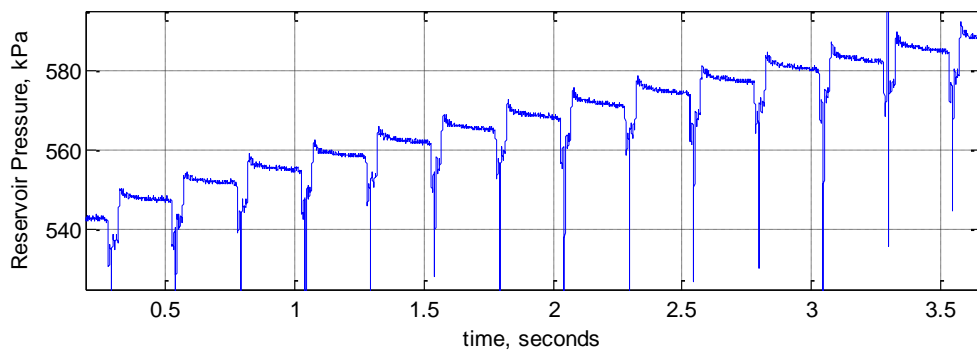## 5.4 Experimental results with fixed timings

5.4.1 Experimental results

(a) Combustion pressure

(b) Compression pressure

(c) Reservoir pressure

Figure 5.9 Measured pressures for HIFLPC operation at 4 Hz

Comprehensive testing of the HIFLPC was conducted by Willhite [35] and the data was used to show the engine dynamics and to calculate the efficiency as shown below. First, pressure dynamics in three control volumes are shown in Figure 5.9: (a) the combustion chamber, (b) compression chamber, and (c) reservoir. The data reflect consistent cycle-to-cycle combustion events, resulting in a reservoir pressure increase from 542 to 589 kPa (about 64 to 71 $psig$) over a period of 3.5 seconds. The measured efficiency and power by the manually tuned timings will be used to compare to the closed-loop control results in the next chapter.

5.4.2 Efficiency and power calculations

As in [35], the efficiency of the HIFLPC can be calculated on a per cycle basis by,

$$\eta_{cycle} = \frac{E_{out}}{E_{in}} = \frac{(E_{res,f} - E_{res,i})}{E_{propane}} \tag{5.10}$$

where $E_{res,i}$ and $E_{res,f}$ are the reservoir pneumatic potential energies before and after the cycle, respectively, $E_{propane}$ is the amount of petrochemical potential of the mass of propane injected for combustion (the lower heating value). The pneumatic potential of the reservoir is considered to be the amount of work that can be done by fully expanding a pressurized ideal gas,

$$E_{res} = W_{exp} = \int_{V_{res}}^{V_{atm}} PdV \tag{5.11}$$

Whether the expansion of the reservoir air should be considered adiabatic or thermal (or somewhere between) depends on the size and the motion characteristics of the pneumatic actuators that would be the end users of the pneumatic supply delivered by

the HIFLPC. Therefore, two efficiencies were calculated for the device in [34], one based

on adiabatic reservoir potential, $E_{res,adb}$, and one based on isothermal potential, $E_{res,iso}$.

Assuming adiabatic behavior,

$$PV^{\gamma} = \text{constant} \tag{5.12}$$

Eq. (5.11) can be written as,

$$E_{res,adb} = \frac{P_{res} V_{res}}{1 - \gamma_{air}} \left[\left(\frac{P_{res}}{P_{atm}} \right)^{\frac{1 - \gamma_{air}}{\gamma_{air}}} - 1 \right] \tag{5.13}$$

Given that, for isothermal expansions,

$$PV = \text{constant} \tag{5.14}$$

the isothermal reservoir potential can be written as,

$$E_{res,iso} = P_{res} V_{res} \ln \left(\frac{P_{res}}{P_{atm}} \right) \tag{5.15}$$

Figure 5.10 shows reservoir pressure data for one cycle of the device operation as

seen in Figure 5.9. This cycle will be used in the following example for calculating the

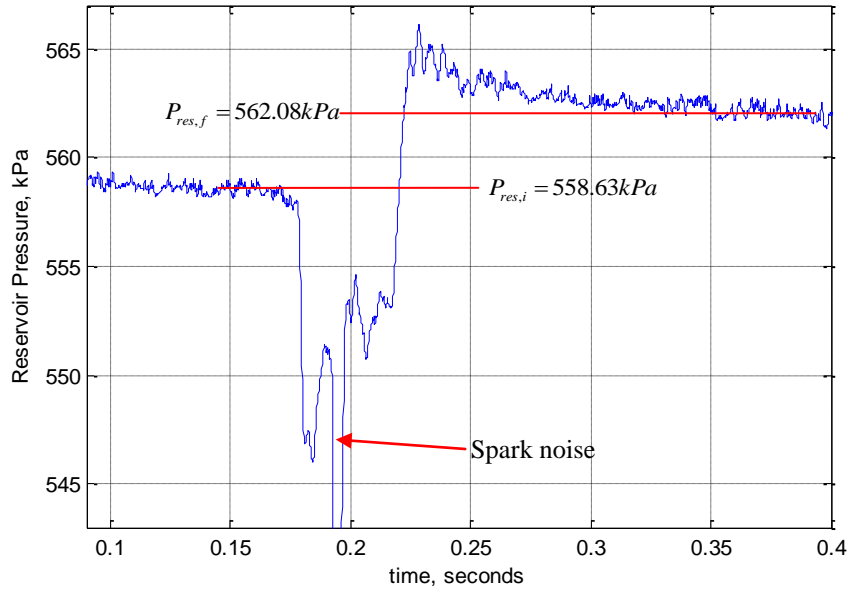adiabatic and isothermal HIFLPC efficiencies.

Figure 5.10 Single cycle reservoir pressure gain

Using the initial and final pressures noted in Figure 5.10, whereby the final pressure is obtained after thermal losses, the adiabatically determined net energy gain in the reservoir for the pump cycle shown is calculated as follows,

$$E_{res,adb,i} = \frac{(558.63kPa)(5.17 \times 10^6 \, mm^3)}{1 - \gamma_{air}} \left[\left(\frac{(558.63kPa)}{(P_{atm})} \right)^{\frac{1-\gamma_{air}}{\gamma_{air}}} - 1 \right] = 279.2 \text{ Joules} \quad (5.16)$$

$$E_{res,adb,f} = \frac{(562.08kPa)(5.17 \times 10^6 \, mm^3)}{1 - \gamma_{air}} \left[\left(\frac{(562.08kPa)}{(P_{atm})} \right)^{\frac{1-\gamma_{air}}{\gamma_{air}}} - 1 \right] = 281.7 \text{ Joules} \quad (5.17)$$

$$E_{out,adb} = E_{res,adb,f} - E_{res,adb,i} \approx 2.4 \text{ J} \quad (5.18)$$

The calculation of the isothermally determined net energy gain can be conducted as follows,

$$E_{res,iso,i} = (558.63kPa)(5.17 \times 10^6 mm^3) \ln\left(\frac{(558.63kPa)}{P_{atm}}\right) = 493.0 \text{ Joules} \qquad (5.19)$$

$$E_{res,iso,f} = (562.08kPa)(5.17 \times 10^6 mm^3) \ln\left(\frac{(562.08kPa)}{P_{atm}}\right) = 497.8 \text{ Joules} \qquad (5.20)$$

$$E_{out,iso} = E_{res,iso,f} - E_{res,iso,i} \approx 4.8 \text{ J} \qquad (5.21)$$

During the fuel injection, the electronic regulating valve for the buffer tank is turned off by the injection controller. Therefore, the mass of propane injected can be determined by measuring the pressure drop (before and after fuel injection occurs) in the fixed-volume propane buffer tank (once again assuming ideal gas):

$$m_{propane} = \frac{(P_{propane,i} - P_{propane,f})V_{buffer}}{R_{propane}T_{propane}} \qquad (5.22)$$

The propane buffer tank pressures before and after injection are presented in Figure 5.11. From this data, the mass of propane for this cycle is calculated to be:

$$m_{propane} = 1.562 \times 10^{-6} \text{ kg} \qquad (5.23)$$

Therefore, the potential of the fuel can then be calculated as:

$$E_{propane} = m_{propane}e = 72.4 \text{ J} \qquad (5.24)$$

where e is the specific energy density of propane (46,350 kJ/kg), calculated from the lower heating value of the fuel.
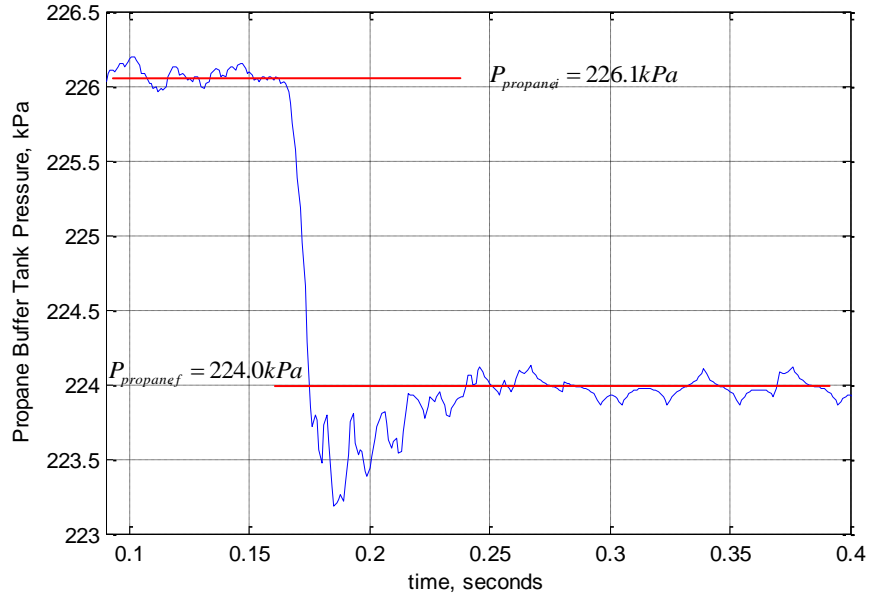
Figure 5.11 Fuel circuit buffer tank pressure for one cycle

Using Eq. (5.10), the adiabatic efficiency and isothermal efficiency for this cycle are calculated as,

$$\eta_{cycle,adb} \approx \frac{2.4J}{72.4J} = 3.45\% \tag{5.25}$$

$$\eta_{cycle,iso} \approx \frac{4.8J}{72.4J} = 6.63\% \tag{5.26}$$

Applying the above calculation procedure to ten cycles of the selected data, average adiabatic and isothermal efficiencies were calculated,

$$\eta_{avg,adb} = 3.35\% , \quad \text{and} \quad \eta_{avg,iso} = 6.26\% \tag{5.27}$$

Average power output was also calculated for the same ten cycles, given 4 Hz operating frequency:

$$P_{avg,adb} = 9.6\,\text{W}, \quad \text{and} \quad P_{avg,iso} = 17.9\,\text{W} \tag{5.28}$$

5.5   Discussion of the experimental results with best-tuned parameters

The experimental results above were achieved with the best-tuned fixed timings, which include: 1) air/fuel injection duration; 2) exhausting timings; 3) operational frequency; 4) ignition timings. The term "best-tuned" results from the highest engine efficiency achieved. An operating frequency of 4 Hz was used in the test.

The air/fuel injection duration primarily influences the engine efficiency because it determines the energy input in each cycle. Insufficient injection may not provide enough energy for a positive gain in the reservoir (i.e. negative efficiency), whereas excessive injection results in a waste of the fuel investment. Injection duration is determined by multiple factors such as the air upstream pressure during the injection, loads on the pump side during pumping and the desired stroke length. Therefore, optimal injection durations vary while all these factors change. That is, a certain and fixed injection duration might only be optimal for a narrow neighborhood of a particular reservoir pressure.

Exhaust timings not only affect engine efficiency, but also greatly influence the combustion performance. As mentioned in the previous chapters, the exhaust valve needs to be opened as soon after the piston reaches BDC, where the pumping is finished and the piston starts to return back to the TDC position. Earlier opening of the exhaust valve reduces the pumping duration and, as a result, less gain in the reservoir; On the other hand, late opening of the exhaust valve leads to compression of the combustion products while the combustion chamber is still sealed. The return stroke length and duration will be shortened in an undesired way. Closing timing of the exhaust valve is critical for

successful combustion in the next cycle. For HIFLPC, the exhaust valve is desired to be closed right at TDC where the diaphragm completely contacts the combustion head so that 1) all the combustion products are exhausted; 2) initial volume of the combustion chamber is near zero for the next cycle. Early closing of the exhaust valve causes some combustion products to remain in the combustion chamber affecting the air/fuel ratio in the next cycle and may cause poor combustion or misfiring. Late closing of the exhaust valve gives a non-zero initial volume of the combustion chamber for the next cycle due to piston rebound. Engine efficiency is affected due to the fact that the effective compression ratio (the pre-combustion pressure) is strongly determined by the initial volume of the combustion chamber. The air/fuel ratio is also affected because extra air (non-zero initial combustion volume) is in the combustion chamber before the injection occurs.

Based on the discussion above, an open-loop fixed timing controller is not sufficient to deal with variations such as reservoir pressure, loads on the pump side, initial piston positions and other variations. Therefore, the virtual-cam control methodology is implemented on the HIFLPC to achieve the following goals: 1) better efficiency than the manually tuned results; 2) wider operating range in term of the reservoir pressure; 3) more consistent combustion; 4) frequency control. Implementation of the controller and the experimental results are presented in the next chapter.

Chapter VI

Experimental Results of the Virtual-Cam Based Control Methodology

In conventional internal combustion engines, valves are opened and closed using a cam surface. The cam is kinematically related to the piston positions through the crankshaft and timing belt. In contrast, there is no crankshaft or kinematic cam surface in a free-piston engine to physically realize this mechanism. As a consequence, a free-piston engine has variable stroke lengths, which presents a challenge for active piston motion and precise stroke length control. For instance, the free-piston engine configuration is well suited for HCCI engines because the requirements for accurate ignition timing control are very flexible due to the fact that the piston motion is not restricted by crank-rod mechanism. However, accurate piston motion control is a challenge for HCCI free-piston engines [4]. This chapter presents a virtual-cam based approach to relate free-piston motion to actuated engine valve control within a clear and familiar intuitive physical context. The primary functionality of the virtual cam control framework is to create a repetitive index, which can be modified from cycle to cycle, for the exhaust/injection valves and spark timing similar to the function of physical cams in conventional engines. Since the cam is virtually created, it can be dynamically rebuilt to comply with cycle-to-cycle variations such as amount of the air/fuel supply, engine load and stroke length. This index rebuilding process is based on a cycle-to-cycle adaptive control method that uses the knowledge obtained from previous cycles to adjust the cam parameters. Experimental results are presented for a novel liquid-piston free-piston

engine intended as a compact and efficient energy source for untethered power dense pneumatic systems such as untethered robots.

6.1 Modifications of the general control laws

The proposed control methodology is designed for general free-piston engines. The injection and exhaust control laws, Eq. (2.29) and Eq. (2.30-2.31) respectively, are derived from a generalized free-piston engine configuration. In order to implement them on a specific engine, these general control laws need to be slightly modified to fit the engine application, i.e. HIPLPC in our work. Therefore, the modifications of the proposed control laws are firstly introduced in the next section.

6.1.1 Modifications of the injection control law

First, recall the injection control law, given by Eq. (2.29),

$$m_f[k+1] = m_f[k] + E_x(x_d - x_{stroke}[k]) + E_L(L[k+1] - L[k]) \tag{6.1}$$

Following variables are required for the injection control: 1) $m_f[k]$, mass of air/fuel mixture injected in the kth cycle; 2) $x_{stroke}[k]$, the stroke length in the kth cycle; 3) $L[k]$ and $L[k+1]$, loads in the kth and $k+1^{th}$ respectively.

According to Equations (4.4-4.5), the injection duration is proportional to the mass of the air/fuel mixture injected. Thus, mass of the air/fuel mixture can be represented by the injection duration, denoted by $D_{inj}[k]$ as in the kth cycle. As introduced in the injection control section, a unique air/fuel injection system is used in HIFLPC. The injection duration used in the control refers to the air injection duration while the fuel injection duration is fixed to 5ms. In order to achieve a certain ratio of air to fuel, given the air injection duration and air upstream pressure (reservoir pressure in

this case), the propane buffer tank pressure is accordingly regulated to adjust the fuel mass injected.

The load for an air compressor is the reservoir pressure during the power stroke. In this application, the injection procedure uses the reservoir as the air source. The reservoir provides air for combustion and pneumatic actuation or load. As a result, the reservoir pressure drops by supplying air for injection and also for pneumatic actuators anytime even during the power stroke. Therefore, it is impractical to predict the load, or reservoir pressure, when the pump occurs. Higher pressure in the reservoir (load for the compressor) needs more energy input according to the control law described by Eq. (6.1). For the air/fuel injection, higher pressure in the reservoir means higher upstream air pressure and it needs shorter injection duration for a certain amount of air. These two facts conflict in the injection duration control. In the HIFLPC simulations [34][35], it has been shown that the air injection duration needs to be shorter as the reservoir pressure goes up. In other words, the simulation results showed that the reservoir pressure effects the injection duration requirement more than the load does. Hence in the experimental tests, the load part in the control law, i.e. $E_L (L[k+1] - L[k])$, is not considered, and only the stroke length part, i.e. $x_d - x_{stroke}[k]$, is considered.

In general, the injection control law also requires measuring the piston position to obtain TDC and BDC positions. It is difficult/impractical to measure the position of the liquid piston on this device because the piston is not rigid and it does not have a linear position displacement along its motion. In this work, a pressure-based stroke length measurement is proposed for injection duration control. Upon successful pumping, air in

the compression chamber is pumped into the reservoir. During the return stroke, the "missing" air is refilled by a breathe-in process through the check valve on the compression chamber side. During the return stroke, the breathe-in duration is proportional to the length of the return stroke, which is essentially the pump stroke length. The pump stroke length, i.e. expansion of the combustion chamber, determines the amount of the air pumped under a certain reservoir pressure. Therefore, the breathe-in duration is now related by a proportional relationship to the amount of the air pumped, i.e. the pressure increase in the reservoir.

Figure 6.1 shows an example of the relationship between the breathe-in duration during the piston return and the reservoir pressure gains. It can be seen that longer breathe-in duration indicates more air is pumped into the reservoir cylinder. By setting different injection durations (different amount of energy input in each cycle under a certain reservoir pressure), breathe-in durations and reservoir pressure dynamics were experimentally measured. Figure 6.2 shows the correlation between the reservoir pressure increase (all from 60 *psig*) for a single engine pump and the breathe-in duration. Since the breathe-in process cools the pump side by replenishing the compression chamber, temperature of the compression chamber always stays close to ambient temperature. Therefore, the proportional relationship is not appreciably affected by the temperature fluctuations.

The amount of air pumped into the reservoir determined by TDC and BDC together, i.e. expansion ratio of the combustion chamber. Hence, the TDC and BDC position measurement or the stroke length $x_{stroke}[k]$ is replaced by the breathe-in duration

$D_{breathe}[k]$ in Eq. (6.1) and the desired stroke length x_d is replaced by a desired breathe-in

duration $D_{desired}$.
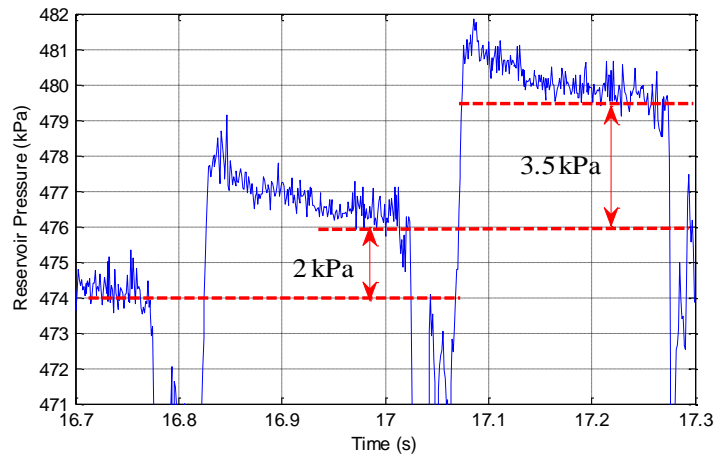
(a) Reservoir pressure
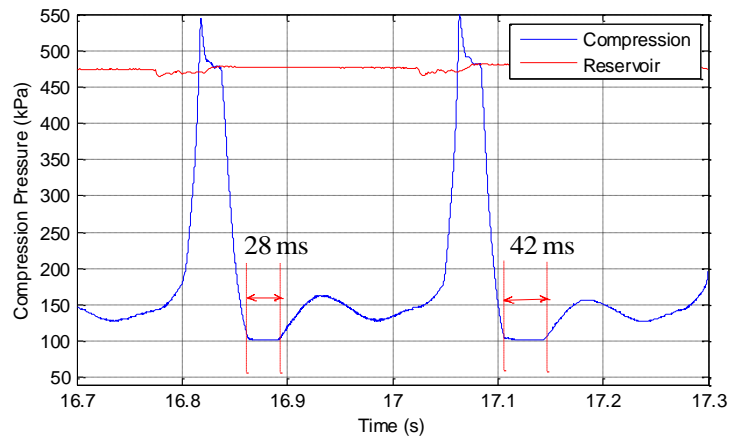
(b) Breathe-in durations

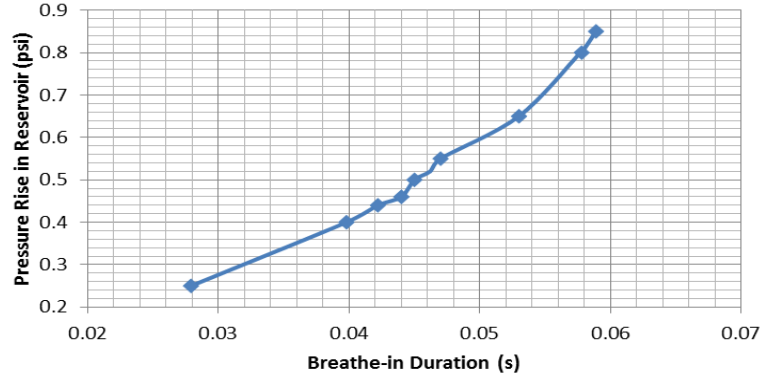Figure 6.1 Reservoir pressure and breathe-in durations

Figure 6.2 Breathe-in duration vs. pressure gain in reservoir

With all the modifications discussed above, the injection control law now reads as,

$$D_{inj}[k+1] = D_{inj}[k] + K_d(D_{desired} - D_{breathe}[k]) \qquad (6.2)$$

where $D_{inj}[k]$ is the injection duration used in the kth cycle and $D_{inj}[k+1]$ is the injection duration will be used in the $k+1^{th}$ cycle; $D_{breathe}[k]$ is the breathe-in duration measured in the kth cycle; $D_{desired}$ is the desired breathe-in duration as a constant; K_d is a constant to weight the adjustment of the injection duration.

6.1.2 Modifications of the exhaust control laws

Recall the exhaust control laws previously derived, given by Eq. (2.30-2.31) respectively,

$$\theta_{oa}[k+1] = \theta_{oa}[k] + \beta_o(\theta_{oi}[k] - \theta_{oa}[k]) \qquad (6.3)$$

$$\theta_{ca}[k+1] = \theta_{ca}[k] + \beta_c(\theta_{ci}[k] - \theta_{ca}[k]) \qquad (6.4)$$
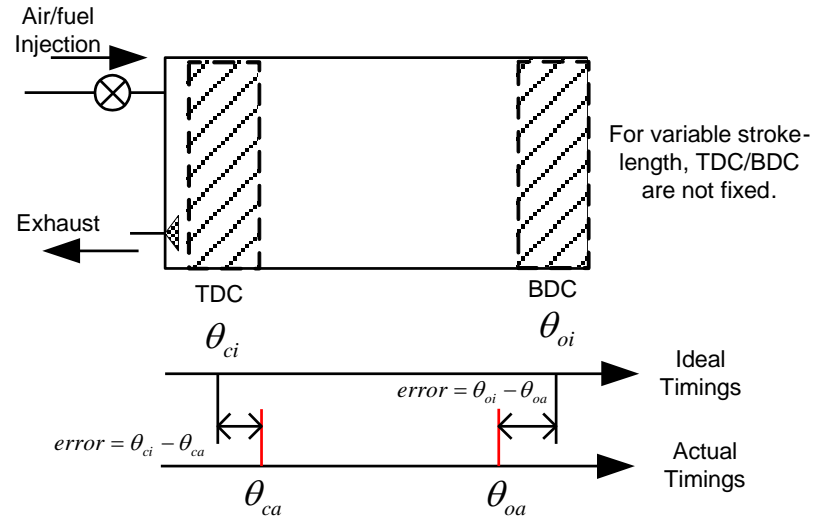
Figure 6.3 Exhaust control scheme for HIFLPC

Figure 6.3 illustrates the working principle of the exhaust control law. At the end

of the kth cycle, the ideal times to open/close exhaust valve are denoted by $\{\theta_{oi}, \theta_{ci}\}_{ex}$,

which are times when the piston reaches BDC/TDC positions. The actual times that

open/close the valve in this cycle are recorded as $\{\theta_{oa}, \theta_{ca}\}_{ex}$. The exhaust controller

simply reduces the errors between actual timings and ideals timings by Eq. (6.3-6.4).

Considering the cycle-to-cycle variations, directly applying the ideal timings in one cycle

to the next one is not practical. Therefore, the controller adjusts the timings to move

toward the currently calculated ideal timings in a first order manner.

As mentioned before, piston position is not available in the application of

HIFLPC due to the use of a liquid-piston. To replace the piston position measurement, a

pressure-based approach was proposed in chapter 2. TDC/BDC times can be obtained by

measuring the compression chamber pressure. BDC is where the piston moves to its

maximum distance towards the compression chamber side, which refers to the instant at

which the compression pressure begins to drop and will go below the reservoir pressure. During the return stroke, the breathe-in stage will end as soon as the piston reaches TDC where the compression pressure will exceed the atmospheric pressure. As shown by Figure 6.4, TDC and BDC can be captured by only the compression pressure dynamics. The ideal timings for open/close exhaust valve, i.e. $\{\theta_{oi}, \theta_{ci}\}_{ex}$, can be measured at TDC/BDC positions. At the end of one engine cycle, the error between actual timings and ideal timings are calculated by the control algorithm described by Equations (6.2-6.3), the valve timings in the next cycle, $\theta_o[k+1]$ and $\theta_c[k+1]$, are controlled to approach the ideal timings in the current cycle $\{\theta_{oi}, \theta_{ci}\}$. In cases of misfiring and no pump occurs, the controller just simply ignores the no-pump cycle and does not apply any changes to any timings. More details of this strategy will be discussed in the next section.
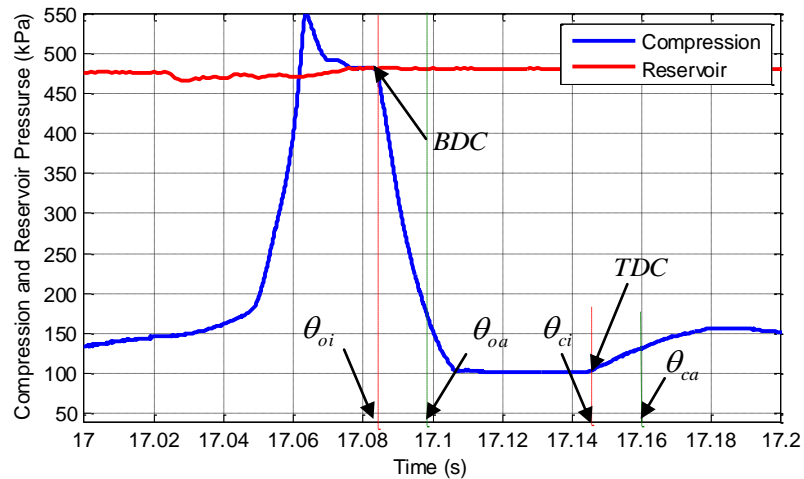

Figure 6.4 Compression and reservoir pressure dynamics

6.2   Virtual-cam based control structure

In the previous sections, the control laws for injection and exhaust have been modified specifically for the HILFPC application. Full engine control should also be able

to carry out frequency control, spark timings control and valve actuations. The full control structure based on the virtual-cam framework is similar to the one presented in Figure 4.2. There are three virtual cams corresponding to three valves: 1) Air/fuel injection valves; 2) Exhaust valve on the combustion chamber; 3) Spark ignition cam.

6.2.1 Control structure

Figure 6.5 illustrates the working principles of the virtual-cam based controller. First, operational frequency of the engine is set, 4 Hz in this case. Control commands are sent to the engine in the following order: 1) Charge the spark coil at θ_{cs}; 2) Inject propane for 5 *ms* started from θ_{ps}; 3) As soon as the propane injection is finished, start to inject air for a duration of $D_{inj}[k]$; 4) Ignite the spark plug before the injection is done to compensate for the ignition delay; 5) Open the exhaust valve at θ_{oa}; 6) Close the exhaust valve at θ_{ca}; 6) Reset time back to 0 when one cycle is over.
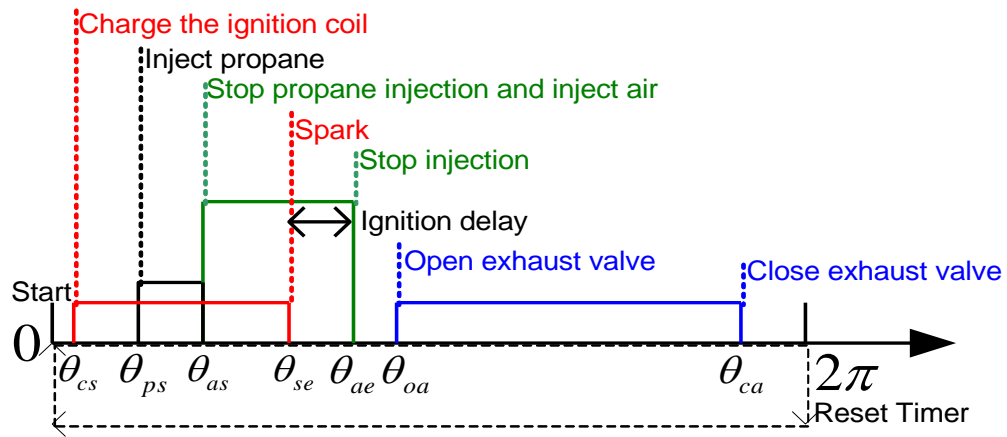

Figure 6.5 Control commands for the HIFLPC

Among these timings, times to charge the ignition coil and to ignite the spark plug are fixed. There is a delay between when spark command signal is sent out and when the

spark plug is actually ignited. By advancing the timings for the spark relative to the end of injection, the air/fuel mixture can be ignited right at the end of injection and times to start the air and propane injection are adjusted to achieve a certain injection duration, i.e. θ_{ps} and θ_{as} respectively. Times to open and close the exhaust valve are those sent from the computer. They are not the actual times that the valve opens and closes due to the dynamics of the solenoid valve used in this application. Delay caused by valve actuator dynamics was experimentally measured by comparing the time difference between the time of the command sent out and that of the valve opened (indicated by sudden drop of the combustion pressure).

Frequency control is one of the control goals of this work. Operational frequency can be simply changed by changing the wait time between the end of the return stroke and the start of next injection. As shown in Figure 6.4, exhaust valve closes when piston diaphragms return to TDC at θ_{ca}. One engine cycle is over when $\theta = 2\pi$. In time domain, different operational frequencies strongly determine the margin between θ_{ca} and $\theta = 2\pi$, for the all events before closing exhaust valve will not be significantly changed.

6.2.2 Dynamic adjustment of repeating indices

The primary purpose of the virtual-cam based control is to create repeating indexes for timing control and dynamically adjust these indexes from cycle to cycle based on the evaluation of the engine performance. To do so, reservoir pressure and compression chamber pressure are measured to obtain breathe-in duration, ideal exhaust open and close times. Since the pressure measurement on the combustion side always

associated with problems such as noise and drifting, the combustion pressure dynamics is only measured to evaluate the engine thermodynamic performance instead of for control purpose.

It is worth noting that injection duration, exhaust timings and operational frequency are adjusted only when the air/fuel mixture successfully combusts and a pumping event occurs. The thermodynamics of the engine is very different while misfiring occurs from that of the engine while successful combustion and pumping occur. Therefore, the controller examines the combustion event first before it executes the control laws. This can be done by measuring the compression and reservoir pressure dynamics. Since the air for combustion is from the reservoir, the compression pressure will not be able to rise above the reservoir pressure when misfiring occurs. The combustion event and pump event is simply indicated by detecting that the compression pressure exceeds the reservoir pressure.

Initial values for injection duration $D_{inj}[0]$, exhausting timings $\{\theta_{oa}, \theta_{ca}\}_{ex}$ and frequency f_{engine} are pre-set before starting the engine, and they are used in the first cycle. At the end of each cycle, injection duration, exhausting timings and frequency are updated by their respective control laws only if successful combustion occurred in the current cycle.

6.3   Exhaust and injection control results

Before the overall engine performance test, the exhaust and injection control were individually tested. Exhaust control was firstly tested because it is required in the

injection control, whereas the injection duration can be set to a constant in the exhaust control test.

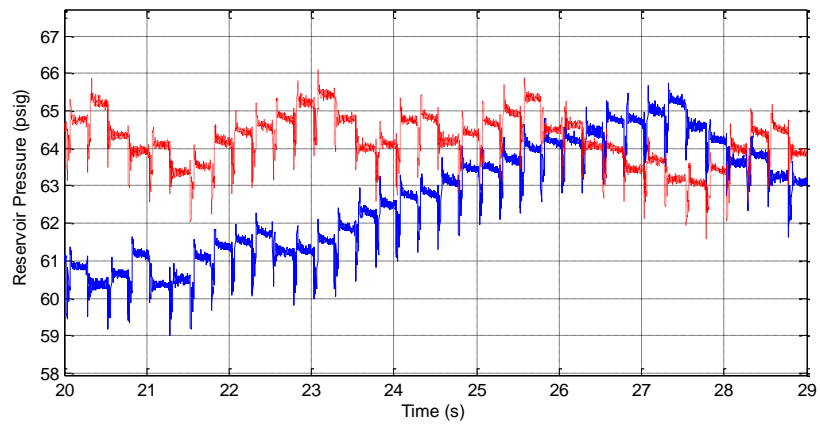### 6.3.1 Exhaust control results

To test the exhaust timing control law, the initial open and close times of the exhaust valve were set to be very early and late in two separate runs. Both open and close timings are adjusted over cycles to approach to the neighbour of ideal timings (the end of pumping and the end of breathe-in), as shown in Figure 6.6. As a result, the exhaust duration converges to the neighbourhood of 55.4 *ms* with the exhaust open time and exhaust closing time converging to the same values as approached from either above or below. Figure 6.6(c) shows the reservoir dynamics during the last 10 seconds of exhaust control. Reservoir pressures in two runs are getting close in this duration. With the same fixed injection durations in these two runs, TDC/BDC timings should be similar when reservoir pressures are close. In Figure 6.6 (a-b), both open and close times verify the validity of the control approach by showing similar exhaust timings in different runs. Although intermittent combustions occurred in both runs, the controller shows its robustness by ignoring the misfiring cycles.
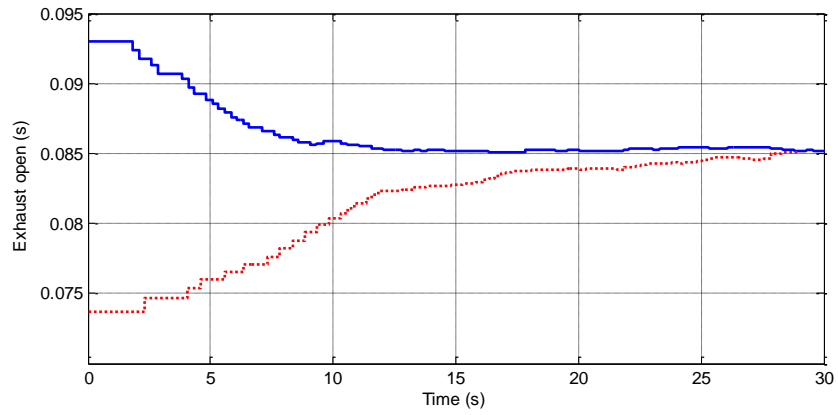
(a) Exhaust open timings
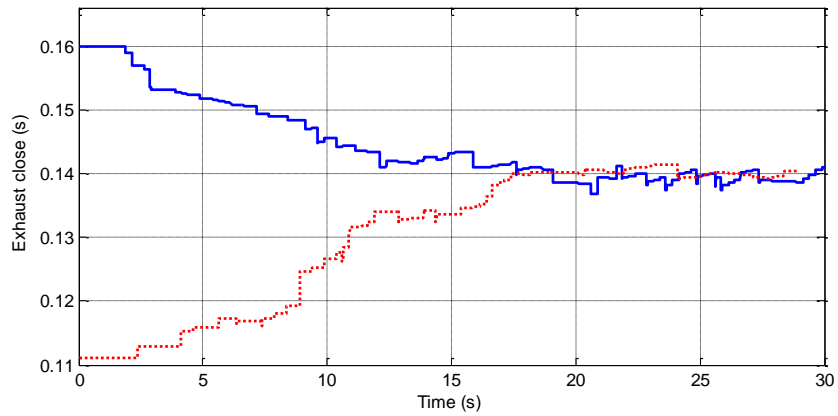

(b) Exhaust close timings

(c) Reservoir pressures

Figure 6.6 Exhaust Timing Control Results

Figure 6.7 shows two example engine cycles during this exhausting adjustment. As seen in the first earlier cycle, the exhaust open and close times are not at the end of pumping and the end of breathe-in. The later cycle shows these two signals have been adjusted to approach the required times.
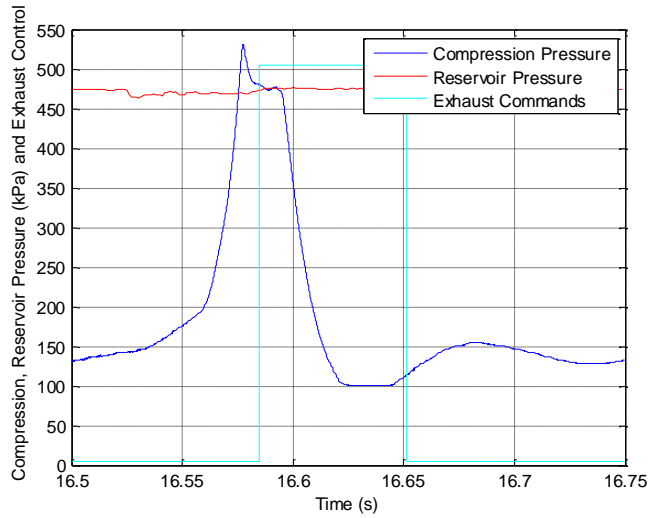

(a) Initial exhaust timings
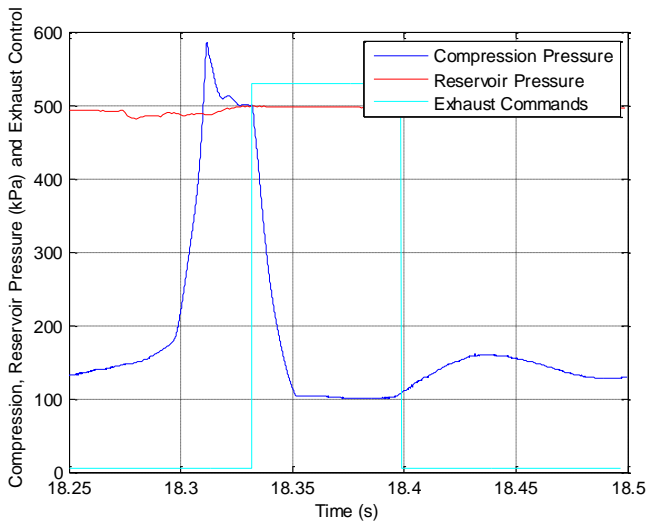

(b) Post-adjustment exhaust timings

Figure 6.7 Individual adjustments of the exhausting timings

6.3.2 Injection control results

To test the injection control, initial injection durations were set to 18.5*ms* and 12.5*ms* in two separate runs. As shown in Figure 6.8, air/fuel injection durations in both test runs are controlled and approach 15.5*ms* while the reservoir pressure is around 60 *psig*, as a result of breathe-in duration optimization. The changing of durations slows down as they approach the optimal value. Given by Eq. (6.2), the regulation of the injection durations is done by measuring the breathe-in durations in the compression chamber. Figure 6.8(a) shows the breathe-in durations along with the change of the air/fuel injection durations. The desired breathe-in duration is 40 *ms*.
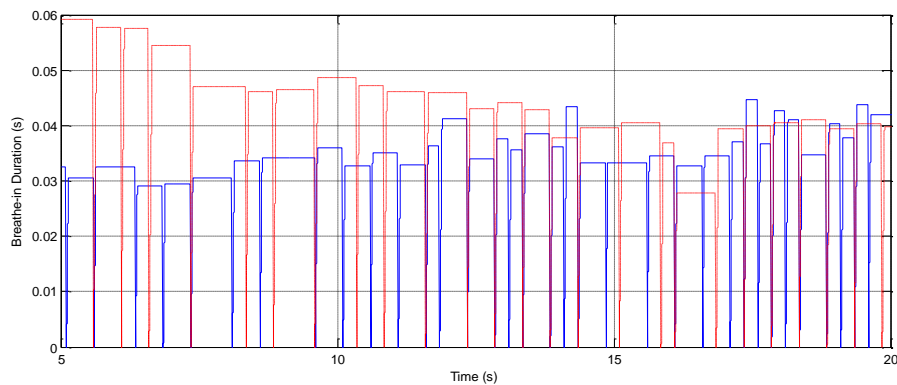

(a) Measured breathe-in durations
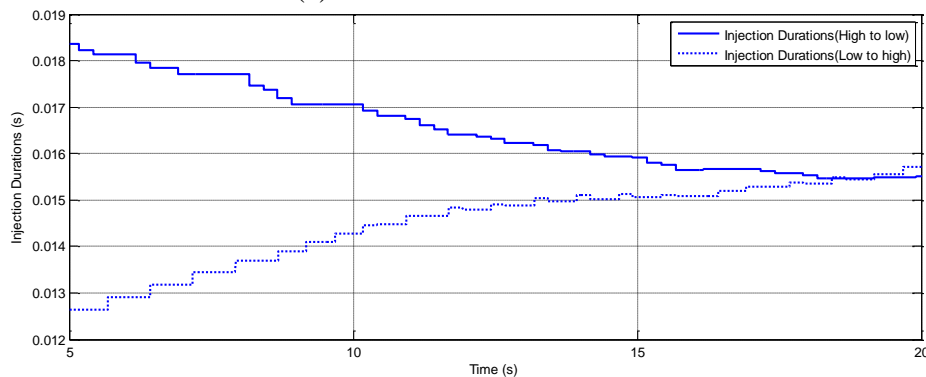

(b) Injection duration adjustment

Figure 6.8 Injection control results

6.4   Full engine control results

Individual tests of injection and exhaust control have shown a satisfactory level of performance. By utilizing the proposed control methodology in a virtual-cam based control context, the major goal of this work is to fulfil the following: 1) improve the overall engine efficiency to be better than the manually tuned results; 2) operate the engine over a wide range of reservoir pressures (loads); 3) the operational frequency can be modulated upon request.
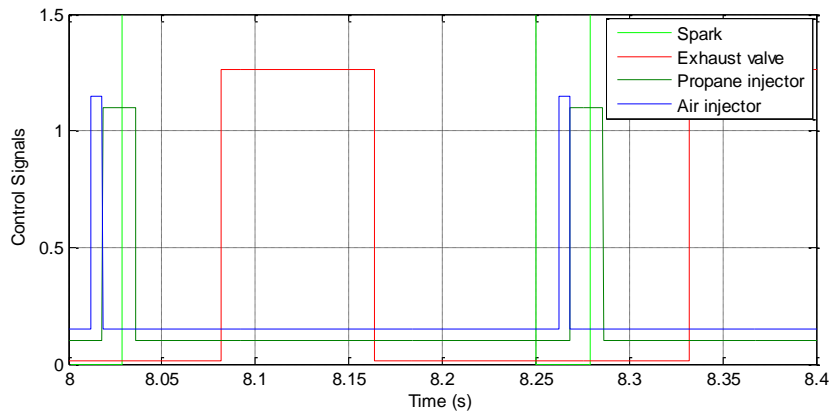
(a) Control signals
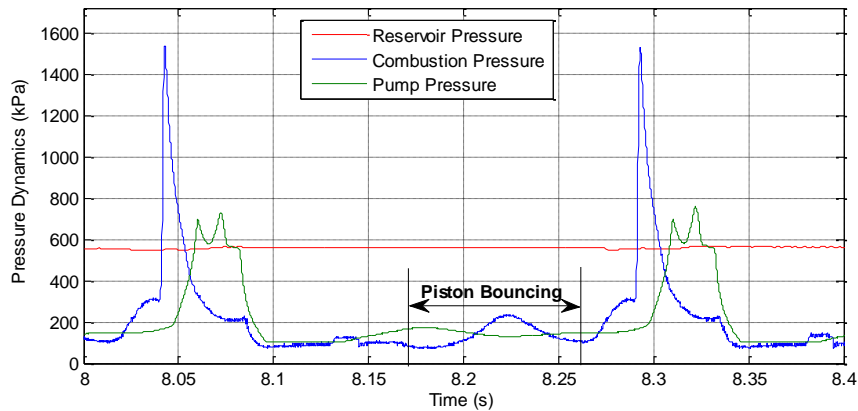
(b) Pressure dynamics

Figure 6.9 Engine control and its dynamics

A typical sequence of control signals sent to the device is shown in Figure 6.9(a). During the air and fuel injections, pressure in the combustion chamber rises. The high inertance liquid piston presents such a high dynamic load it allows the combustion chamber to expand very little such that high air/fuel mixture pressure remains upon spark plug is ignited. This feature eliminates the conventional compression stroke in conventional IC engines. Once the air/fuel mixture combusts, compression pressure rises while the piston is pushed towards the pump side. Once the compression pressure rises above the reservoir pressure, pressurized air in the compression chamber pushes the check valve open resulting in a pump. The exhaust valve opens right after the pumping is done and closes at the end of the breathe-in procedure on the pump side. The engine dynamics are shown in Figure 6.9(b).

In the duration between when the exhaust valve is closed and when the next injection starts, the combustion chamber is sealed so that it acts as an unintended bounce chamber. It can be seen from the combustion pressure in this duration, as shown in Figure 6.9(b). This behavior is very harmful to the next combustion because the air or combustion products leftover in this "bounce chamber" change the air/fuel mixture ratio in the next injection and misfiring may occur. Ideally, the exhaust valve is closed right at the moment when the diaphragm returns to the combustion side and fully contacts with the combustion head so there is zero volume between diaphragm and the combustion head. However, this precise timing is practically difficult to achieve due to following reasons: 1) the diaphragm used in this application is very flexible. It is not clear if the diaphragm is completely flat when it collides with the flat surface of the combustion side.

2) the exhaust valve protrudes out of the flat surface of the combustion head while it is opened, and it pushes against the diaphragm during a portion of its return. Therefore, this design makes it even harder to "catch" the diaphragm at a "zero" volume between diaphragm and the combustion head. However, a relatively precise timing of closing the exhaust valve can alleviate this problem by minimizing the volume. Hence, consistent and continuous combustions will partially rely on the performance of exhaust valve timing control.

The control work is conducted in the Matlab's real-time workshop at a sample rate 10Hz. Table 6.1 lists the constant gains in control laws described by Eq. (6.2,6.3,6.4,5.11). The pressure control of the propane buffer tank is also included.

Table 6.1: Constant gains used in control laws:

| Parameter	Value	Equation	Description
$D_{desired}$	40 ms	$D_{inj}[k+1] =$	Desired breathe-in duration in all tests
K_d	0.01	$D_{inj}[k] + K_d(D_{desire} - D_{breathe}[k])$	A constant gain to weight the adjustment of the injection duration based on breathe-in duration
β_o	0.1	$\theta_o[k+1] =$ $\theta_{oa}[k] + \beta_o(\theta_{oi}[k] - \theta_{oa}[k])$	A constant gain for adjusting opening timing of the exhaust valve
β_c	0.05	$\theta_c[k+1] =$ $\theta_{ca}[k] + \beta_c(\theta_{ci}[k] - \theta_{ca}[k])$	A constant gain for adjusting closing timing of the exhaust valve
K_P	0.075	$P_{desired}$ $= P_{prop\_r} + K_p(P_{res\_r} - P_{res})$	A constant gain for adjusting propane pressure in the buffer tank. The reference propane pressure is 16 *psig* when the reservoir pressure is 60 *psig*.

6.4.1 Efficiency assessment

The efficiency assessment is expected to achieve the following results: 1) higher efficiency than the best one in the manually tuned test [35]; 2) similar or higher

efficiency but over a much wider range of reservoir pressures than that from the manually tuned tests.

Efficiency calculations are performed in the same way as described in section 5.4.2. Only adiabatic efficiencies are calculated for comparison because the corresponding isothermal efficiencies are always about two times that of the adiabatic ones and show the same trends. The first example is chosen to have a similar reservoir pressure range to the one with the best efficiency in the manually tuned test, shown in Figure 6.10. The data reflects consistent cycle-to-cycle combustion events, resulting in a reservoir pressure increase from 543 to 589 *kPa* (about 64 to 71 *psig*). The reservoir pressure increase is very close to the data used in the efficiency calculations for the manually tuned results in the last chapter.
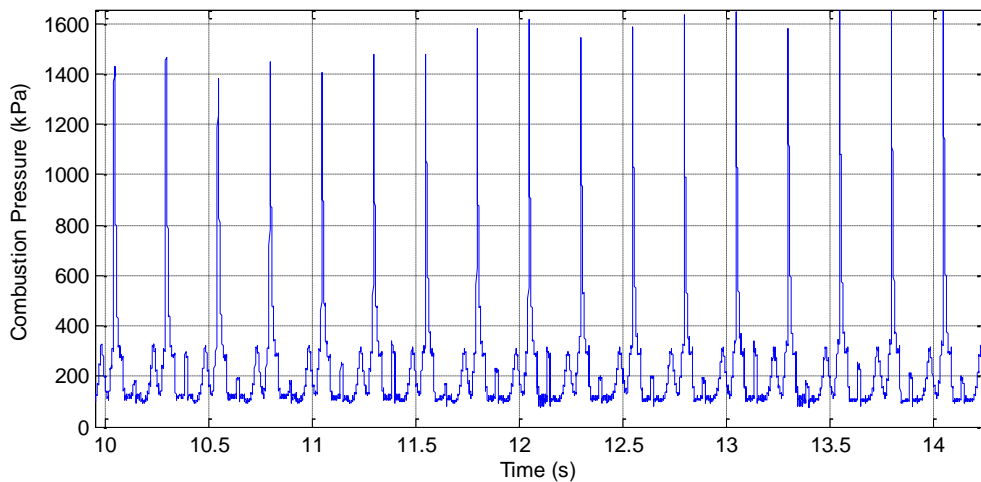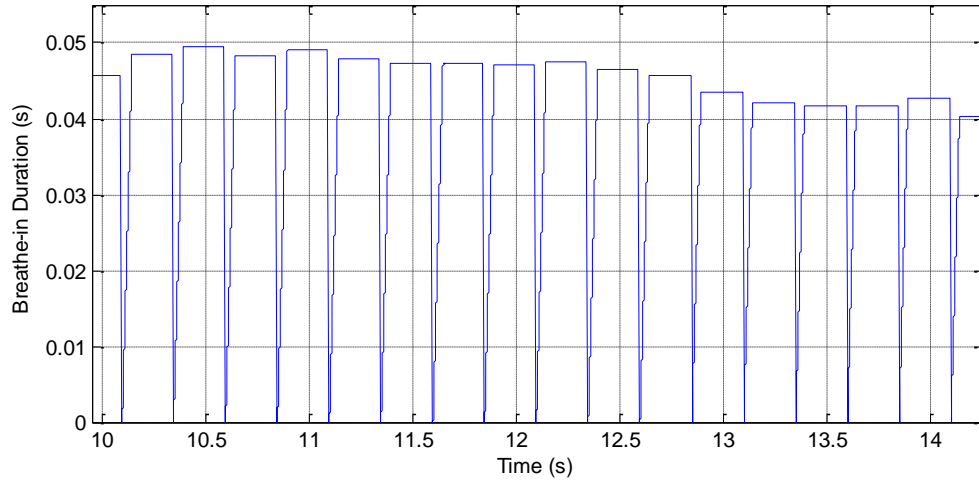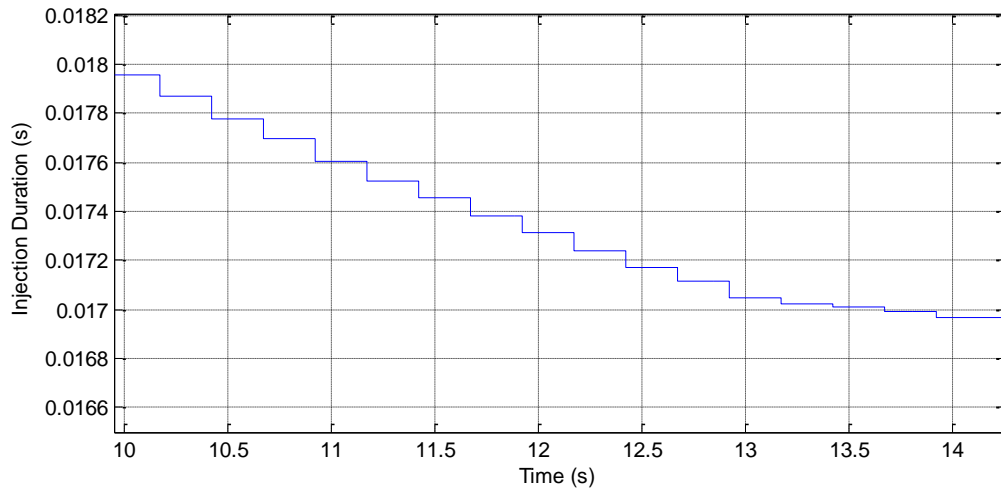

(a) Combustion pressures
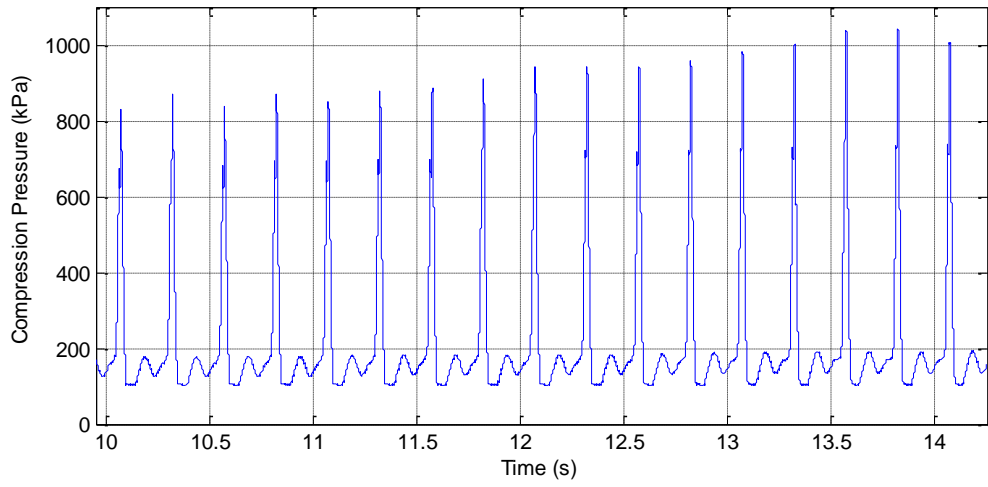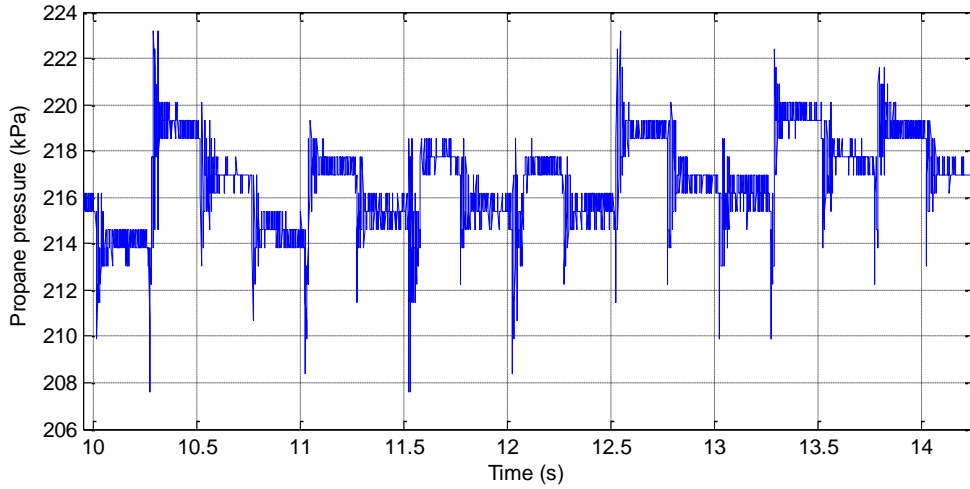
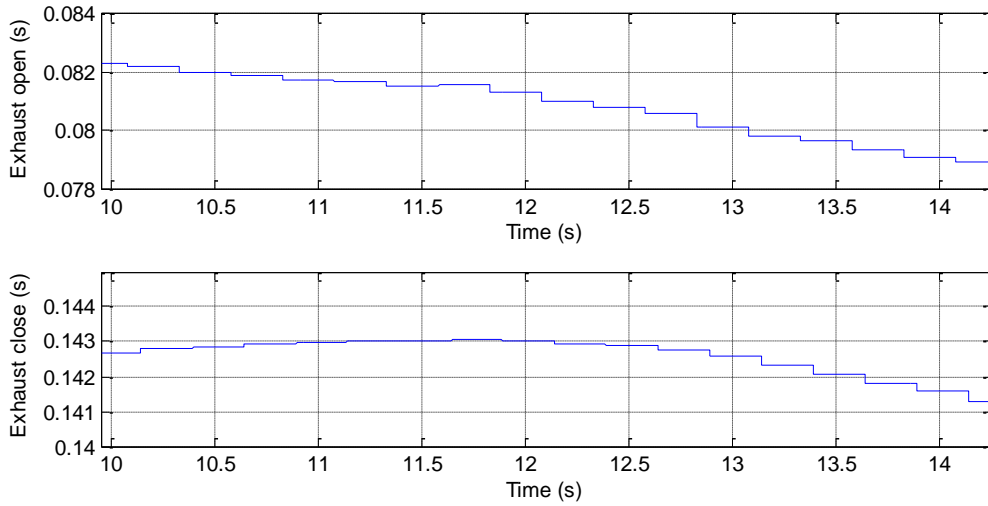(b) Compression pressures
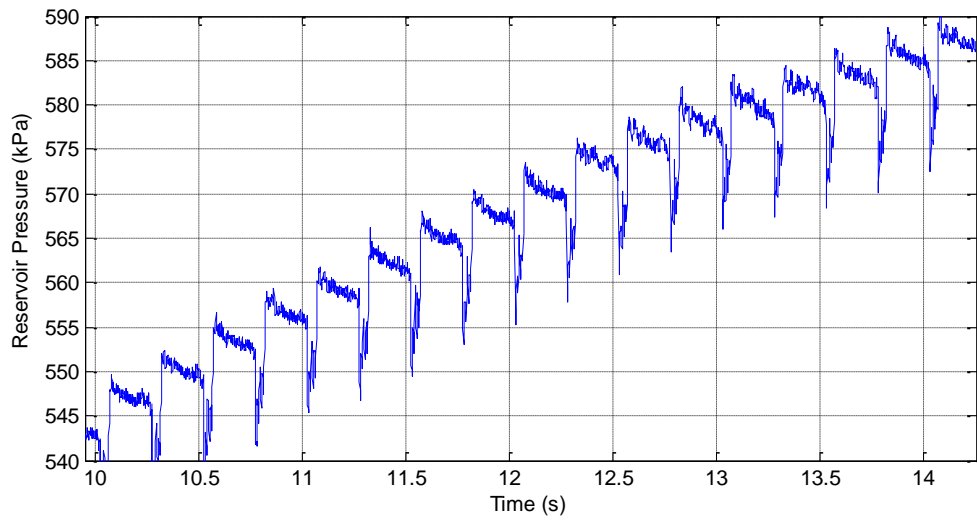
(c) Reservoir pressures

(d) Breathe-in durations

(e) Injection durations

(f) Propane pressures in the buffer tank

(g) Exhaust valve timings

Figure 6.10 Experimental results with full control

As shown in Figure 6.10 (a)-(c), pressure dynamics are similar to those shown in Figure 5.9. Using the propane pressures measured in the buffer tank, the adiabatically determined net energy gain in the reservoir for the pump is calculated by Eq. (5.11). The average energy gain in this test is about 2.33 *J*, slightly less than 2.4 *J* achieved in Eq.

(5.16). In the manually tuned test, the injection duration was 18 ms to ensure consistent combustion and positive net pumping for the reservoir pressure increase of 64 *psig* to 71 *psig*. Therefore, the initial injection duration for the closed-loop test is set to 18 *ms* as well. Figure 6.10(e) shows the injection duration adjustment, where the injection duration continuously decreased while the reservoir pressure increased. This results from the injection control law of Eq. (6.2), which decreases the injection duration according to the measured breathe-in durations, shown in Figure 6.10(d). The shorter injection durations means that less energy input or less fuel investment is required for similar pumping performance. Peak pressures in the combustion chamber are generally lower than those in Figure 5.9(a), as a result of less propane was injected. Average propane pressure in the buffer tank (216 *kPa*), see Figure 6.10(f), is also lower than the one (225 *kPa*) shown in Figure 5.11. This further indicates less propane injection due to the lower upstream propane pressure during the fuel injection. In the buffer tank, the average propane pressure drop during the injection is about 1.65 *kPa*, whereas the propane pressure drop is about 2 *kPa* as shown in Figure 5.11.

As a summary of the above discussion, similar energy output (pressure gain in the reservoir) is achieved while the energy input (fuel investment) is reduced by the closed-loop controller. As a result, the adiabatic efficiency calculated from this test is,

$$\eta_{avg,adb} = \frac{2.33J}{58.1J} = 4.01\% \tag{6.5}$$

Finally, exhaust control timings are shown in Figure 6.9(g). The adjustment of the exhausting timings is gradually done along with increasing of the reservoir pressure.

6.4.2 Wide range of operation

By implementing the virtual-cam based controller, the reservoir is expected to receive compressed air over a wider range than a fixed timing manually tuned controller. In the test using fixed timings, the typical range of consistent pumping (before two or more misfiring occur in a row) is around 7 *psig* by 15-20 pumps over 2.5-3 seconds. It is because the exhaust timings are critical to scavenge the air or combustion products in one cycle so that the air/fuel mixture will not be largely affected in the next cycle. Misfiring will be likely to occur if the engine runs longer than 3 seconds.

The wide operation range achieved by using the closed-loop controller includes two features: 1) the engine can be operated at wide reservoir pressure range (30 *psig* to 90 *psig*); 2) increase of the reservoir pressure is expected to be wider than the longest one in the open loop test, i.e. 6.5 *psig*.

The following figures show one example using the proposed controller to achieve wide range of the reservoir pressure. The engine is combusted and pumped at a very low reservoir pressure (29 *psig*) and positive pumps continuously increase the reservoir pressure to 53 *psig*. The reservoir pressure has a 24-psi gain without any misfiring.
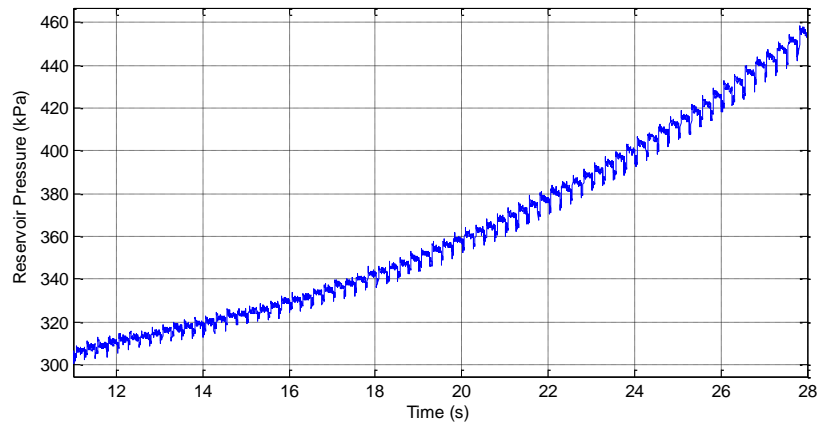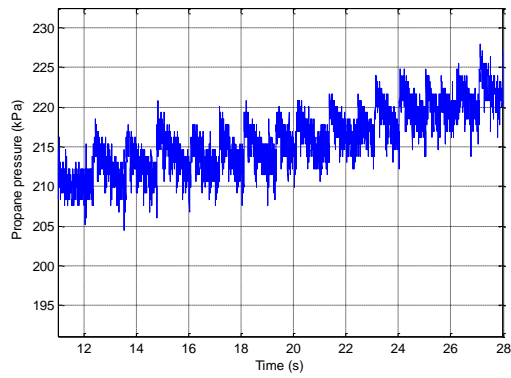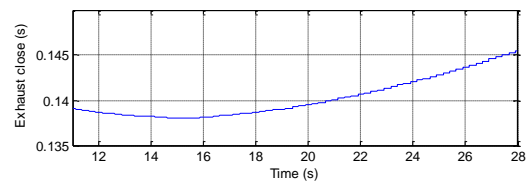
(a) Reservoir pressure dynamics
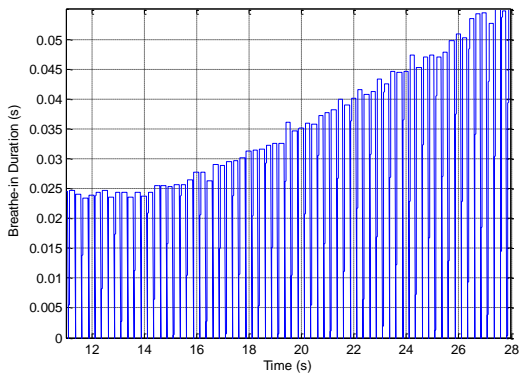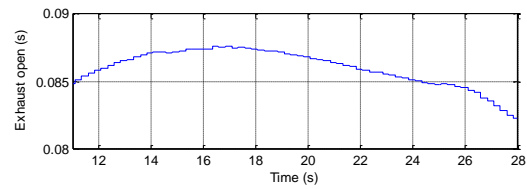

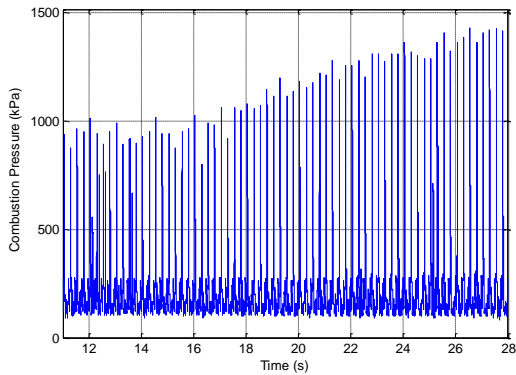(b) Breathe-in durations
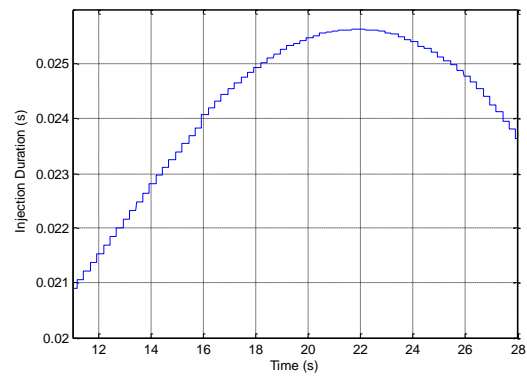
(c) Injection durations
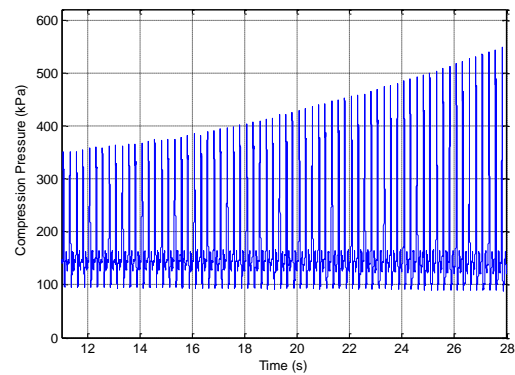

(d) Propane upstream pressure

(e) Exhaust timings

(f) Combustion pressure   (g) Pump pressure

Figure 6.11 Low pre-combustion pressure results

At low reservoir pressures, relatively long injection durations are required for the low air upstream pressures. From Figure 6.11(b), it can be seen that the breathe-in duration is much lower than the desired value (40 *ms*) when the reservoir pressure is only 30-40 *psig*. Therefore, the injection control law gives an injection duration increase resulting in longer breathe-in durations (better pump performance). Once the reservoir pressure is increased, the required air injection duration becomes shorter, indicated by decrease of the injection duration from 22nd second.

The injection controller controls the propane upstream pressure in the buffer tank to achieve the desired air/fuel ratio. As shown in Figure 6.11(d), the propane pressure is continuously increased along with the reservoir pressure. Continuous combustions in this test verify the validity of such air/fuel control method. Consistent combustion is also a strong indicator of good exhaust close times achieved to avoid/alleviate "contaminated air/fuel mixture".

In this run over 26 seconds, the average adiabatic efficiency is about 3.11%. This number is low relative to above result due to a low pre-combustion pressure (low

effective compression ratio). As will be seen, the efficiency increases as the reservoir pressure increases until other factors begin to limit this pre-combustion pressure effect.
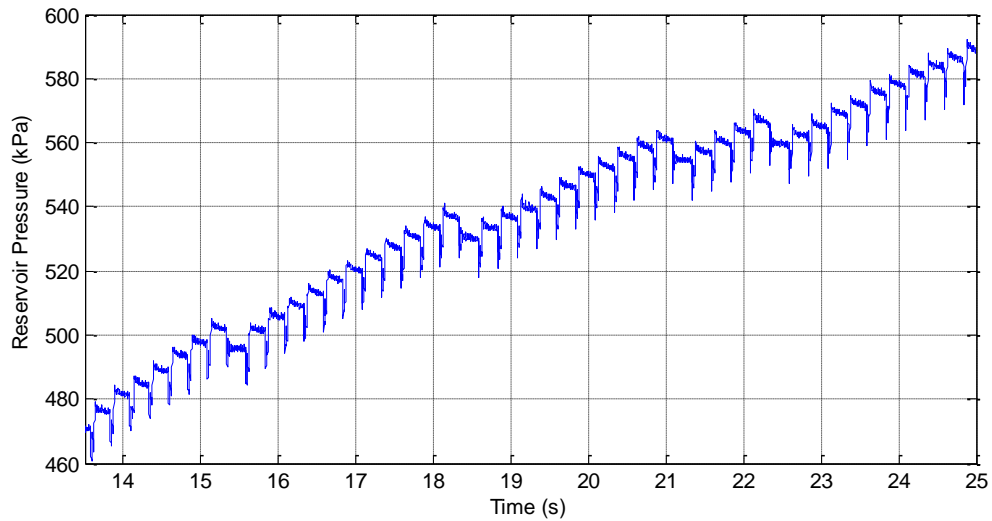
(a) Reservoir pressure
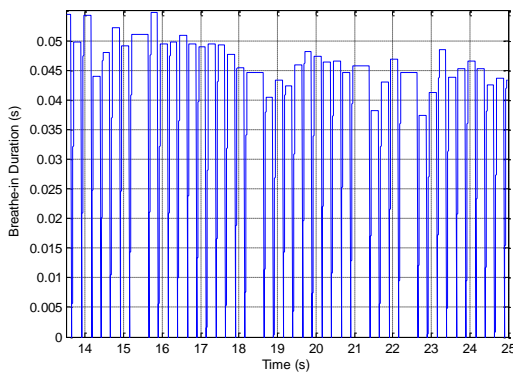
(b) Breathe-in durations
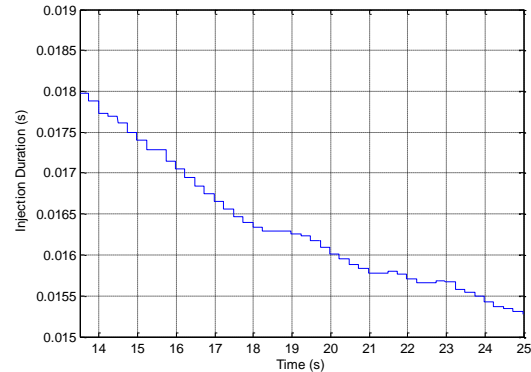
(c) Injection durations

Figure 6.12 High efficiency over a wide reservoir pressure range

Although misfires occurred in this test, the overall engine efficiency is calculated to be 4.32% including the negative efficiencies resulting from misfiring. This is significant because it shows that the achievable efficiency is high even under very

realistic running conditions. Starting the operation from a reservoir pressure of 53 *psig* and injection duration of 18 *ms*, the engine is able to provide enough energy for strong combustions resulting in strong pumps. The injection duration is continuously reduced to about 15.2 *ms* while the reservoir pressure rises up to 72 *psig*. This run has a relatively higher reservoir pressure to start with and it has a better efficiency than the best one from manually tuned test. However, it does not necessarily mean that higher reservoir pressure always helps the pump performance. The next example shows results from a run with even higher reservoir pressure.
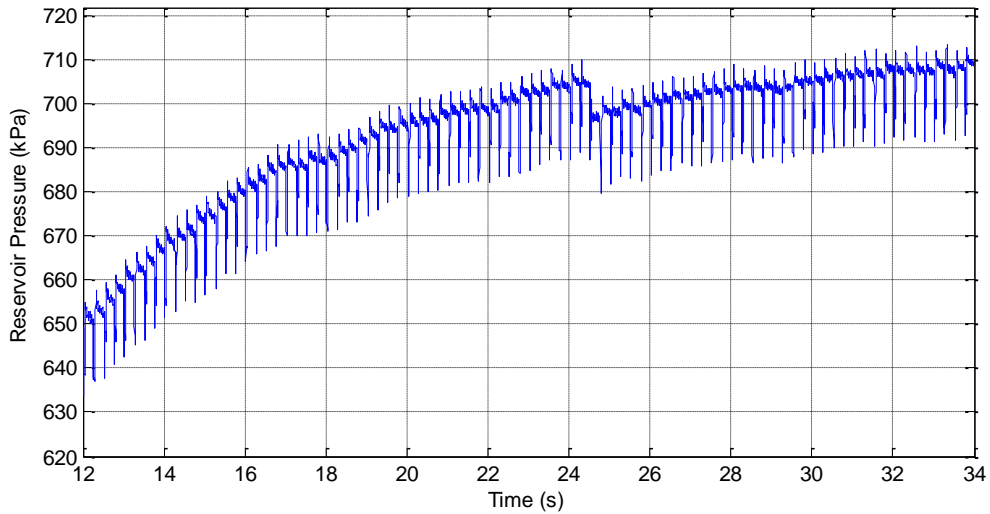
Figure 6.13(a) shows the reservoir pressure starts from about 80 *psig*. However, the pumps get weak as the reservoir pressure increases to about 85-90 *psig* because the reservoir is also acting as the load for the air compressor. Although the engine is controlled to have consistent combustion and pump, the efficiency is low, as seen from the low breathe-in durations in Figure 6.13(b) while the injection duration is high. Reservoir pressure stays around 88-90 *psig* at the end of test, indicating that the engine hits its highest pumping capability.

This test provided a better understanding of the pumping capability of the engine. When the reservoir pressure increases, the optimal injection duration is decreased. Under the high upstream pressure, the injection duration is also desired to be short so that the initial combustion chamber volume (upon combustion) is not too large because a large initial combustion volume results in a smaller expansion ratio upon pumping. However, the air/fuel injectors are subject to a limitation of open/close dynamic response. When the

reservoir pressure goes up to a certain level, the air/fuel injectors are not able to respond

fast enough to ensure a small initial combustion volume.

(a) Reservoir pressure
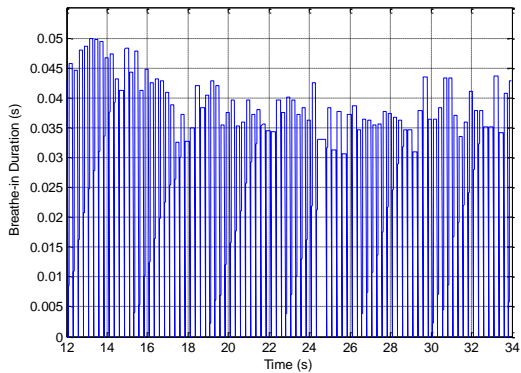
(b) Breathe-in durations
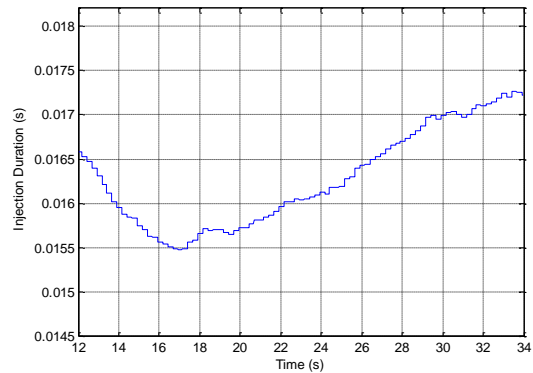
(c) Injection durations

Figure 6.13 Upper limit for pump

Ideally, all the air in the compression chamber can be pumped into the reservoir if

the check valve is fast enough. This is the reason that the HIFLPC utilizes the high

inertance piston to achieve slower dynamics of the piston. This test may indicate that the

dynamics of the pump check valve was strongly influenced by the high reservoir pressure

and it might present much more flow loss under higher reservoir pressure during the pumping.

As summary, Table 6.2 lists more calculated efficiencies and powers from experimental results using the virtual-cam based controller. In these examples, there is no misfiring occurred and every cycle has a positive gain in the reservoir. Both adiabatic and isothermal efficiencies are shown for comparison with those in the open-loop test. All tests were operated at 4 Hz.

Table 6.2. Efficiency and reservoir pressure gain results

Event	Reservoir pressure range (*psig*)	Cycles	Average propane investment (*J*)	Average Adiabatic Power (W)	Adiabatic Efficiency	Isothermal Efficiency
1	42.7 to 51	17	55.8	9.76	4.37%	8.11%
2	46.6 to 59.7	25	58.35	10.48	4.49%	8.29%
3	48.4 to 57	19	55.32	9.05	4.09%	7.68%
4	52.1 to 64.1	23	56.11	10.44	4.57%	8.33%
5	52.1 to 72.1	46	56.7	9.83	4.32%	8.02%
6	55.2 to 62.9	15	59.9	10.4	4.40%	8.22%
Average	*42.7 to 72.1*	*26*	*57.11*	*9.99*	*4.37%*	*8.11%*
Open-loop	64.1 to 70.8	14	72.4	9.6	3.35%	6.45%

From Table 6.2, it can be seen that a wide operation range was achieved by the closed-loop controller. The overall reservoir pressure range is from 42 *psig* to 72 *psig* with an average adiabatic efficiency of 4.37%. The efficiency improvement over the manually tuned results is about 30%. The improvement is mainly from the reduction of the propane investment because the average power outputs in both are similar. By using the injection control duration control, average fuel investment was reduced to 57.11J whereas 72.4J of fuel was used in the manually tuned results. Number of the average

cycles with consistent combustion and pumping is increased from 14 (open-loop results) to 26, indicating the exhaust controller greatly improved the engine performance.

6.4.3 Frequency control

(a) 2Hz   (b) 4Hz
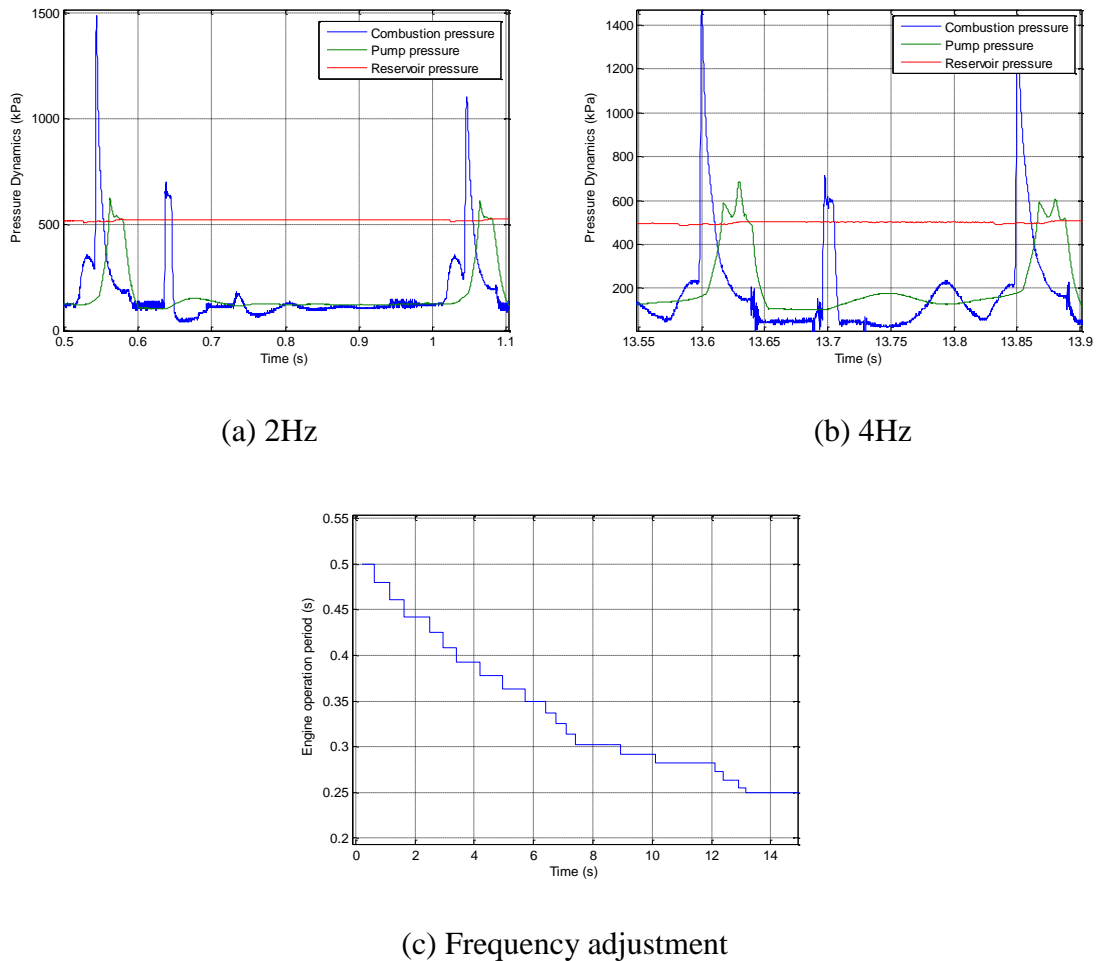

(c) Frequency adjustment

Figure 6.14 Frequency control results

Frequency control is conducted in a straightforward way. That is, operating frequency can be changed by changing the duration between the exhaust closing time of θ_{ca} and the end of the current cycle where $\theta = 2\pi$. It is essentially to wait a certain

amount of time, after one cycle is finished, before starting the next one. The frequency control is to shorten the wait time by 20% in each cycle. Therefore, the operational frequency and power output from the engine can be increased.

Figure 6.14 shows the frequency control results. The initial operation frequency is 2Hz, shown in Figure 6.14(a). By shortening the duration between the time to close the exhaust valve and the time to start the next injection, operational frequency is increased to 4 Hz as seen in Figure 6.14(b). These results are shown to demonstrate frequency control ability of the virtual-cam based control method. The overall engine operational frequency adjustment is shown in Figure 6.14(c).

6.5   Conclusions

This chapter presented the implementation of the virtual-cam based control methodology onto HIFLPC. A pressure-based control approach was proposed to replace the piston position measurement. For air/fuel injection control and exhaust control, only one pressure sensor on the compression chamber was used. Experimental results of the injection control, exhaust control and overall engine operation were shown. These results validated the proposed methodology and a satisfactory level of engine performance was achieved.

Chapter VII

CONCLUSTIONS

This dissertation presents a virtual-cam based approach to relate free-piston motion to actuated engine valve control within a clear and familiar intuitive physical context. The herein described approach was validated in simulation of a free liquid-piston engine compressor (FLPEC) and was experimentally implemented on a high-inertance free liquid piston compressor (HIFLPC). The basic control scheme, however, can be used for general free-piston engine control. Specifically, the cycle-to-cycle dynamic control method, exhaust control and injection control are not device/application specific and can be used for general free-piston engine control with no or only minor modifications.

In order to test the performance of the virtual-cam based control methodology, thorough experimental tests were conducted on the HIFLPC. Implementation of the closed-loop controller was used not only to evaluate the performance of the control method, but also to actually improve the engine performance. Since there is no rigid piston used in this application, a pressure-based control approach was used to examine the engine dynamics. A high-pressure injection scheme was proposed and successfully implemented on the HIFLPC. It provided a simple and effective injection solution, which did not require conventional intake and compression strokes needed in IC engines, for small air compressor applications. Moreover, a novel term of "breathe-in duration" is used for evaluating the pump performance so that measurement of the stroke length and calculation of expansion ratio are replaced by it. The experimental results show satisfactory engine performance in three categories: 1) overall engine efficiency is

significantly improved (>30%) as compared to the results from manually tuned tests; 2) wide operation range in term of the reservoir pressure was achieved; 3) the controller was shown to be capable of adjusting the engine operational frequency upon request.

Untethered robotic systems, especially those with power needs in the neighbourhood of 100 Watts, are typically DC servo motors powered by NIMH or Li-ion batteries. However, the low energy density of batteries prohibits long term use of human-scale mechanical work in a self-contained robot package [38]. The HIFLPC was designed with the purpose of surpassing the combined system energy densities (power supply and actuation) of state of the art power supplies (batteries) and actuators (electric motors). As shown in experimental results (see Table 6.2), the achievable engine efficiency of the HIFLPC can range from 4.37% (adiabatic) to 8.11% (isothermal). Table 7.1 shows an energetic comparison between the electrical approach (batteries/DC motors), chemofluidic approach (H_2O_2/pneumatic actuators) and the HIFLPC approach. From Table 7.1, it can be seen that the overall system energy density of the HIFLPC is significantly higher than those of the electrical and chemofluidic systems due to the high achievable engine efficiency.

Table 7.1 Energetic comparison between domains

Domain	Energy Source	Specific Energy Density	Actuation	Overall Conversion Efficiency	Overall System Energy Density
Electrical	Batteries	~730 kJ/kg[39]	DC Motors	~50%-90%	~365-657kJ/kg
Chemofluidic	H_2O_2	~400 kJ/kg [40]	Pneumatic Actuator	~45% [40]	~180 kJ/kg
Petrochemical (HIFLPC)	C_3H_8	~46,350 kJ/kg	Pneumatic Actuators	~4.37%-8.11%	**~1,013-1,880 kJ/kg**

Beside the success of the control performance itself, the closed-loop controller helped show the potential of the HIFLPC and aided at arriving at potential design improvements for the next prototype and other free-piston engine compressors. For example, optimal engine efficiencies were achieved when reservoir range was between 50 *psig* and 75 *psig*. Therefore, it suggests that the reservoir pressure should be maintained in this range by taking advantage of the start-on-demand feature of free-piston engines. From the exhaust control results, it can be seen that the current design of the combustion head and the exhaust valve present a challenge with regard to scavenging. Although carefully controlled exhaust timings can alleviate this problem, minor re-design of the engine configuration would solve it altogether. For instance, a convex combustion shape facing towards the diaphragm ensures that a pre-extended diaphragm would bounce less when it hit the combustion head. The placement of the exhaust valve can also be altered so that it would never push against diaphragm when the latter is returning to the combustion side.

The virtual-cam based control methodology is proposed in a general free-piston engine control context. With slight modifications to suit the specific HIFLPC application, it yielded good engine performance. Based on the experimental results, this control framework should be capable of serving as a favourable control scheme for other free-piston engines. Although it offers satisfactory performances, this control method can be improved. The following is a list of possible improvements:

1. Sensor drift and noise can affect the threshold of the event trigger in the controller. The controller consequently may be miss-triggered in some engine

cycles. Therefore, a fault-tolerant mechanism could be implemented to deal with such cases.

2. In any cycles, it is nearly impossible to calculate the optimal injection duration or exhaust timings by just measuring pump pressure and reservoir pressure. As a result, there is no good solution to evaluate how close the adjusted injection durations or exhaust timings are to the ideal/optimal ones in this particular cycle. In other words, the proposed control method cannot guarantee convergence of those durations and timings. It is desired to have a way to obtain optimal value in real-time (or predict beforehand) so that the control performance can be further improved by adjusting control parameters to known ideal ones. One potential solution would employ model predictive control. The difficulty here is a lack of closed-from solutions to the highly nonlinear system. At a minimum, an approach with guaranteed convergence toward optimal values would yield a more robust control approach.

3. The proposed control framework naturally bridges the system level control to the low level control. However, such topics as camless engine control and dynamics control of the actuators have not been investigated in this work. Integration of these kinds of low level controls into the proposed framework should be included in future work.

4. Lastly, the experimental setup in this work is based on PC implemented computer control. Since the application of the HIFLPC is intended to provide compressed air on-board for untethered robots, on-board integration of the

controller needs to be conducted in the near future.

As a summary, this dissertation introduces a virtual-cam based control framework for free-piston engines. The virtual cam and virtual camshaft naturally connect the system level control with the low level control. It puts valve timing control, low-level valve dynamics control and frequency control into one place without losing the unique control flexibility of free-piston engines. An adaptive control structure is developed for the cycle-to-cycle engine operations. This method adjusts the parameters of the virtual cam so that the optimal exhaust valve timings and air/fuel injection duration can be achieved. Additionally, a pressure-based control approach is proposed for air/fuel injection control and exhaust control. The experimental results validate the proposed methodology and a satisfactory level of engine performance is achieved. More importantly, this control methodology is designed for general free-piston control purpose so that this method can be applied to other free-piston engine applications with no or only minor modifications.

REFERRENCES

[1] Pescara, R. P., "Motor Compressor Apparatus," U.S. Patent No. 1,657,641, Jan. 31, 1928.

[2] J. Riofrio, E. J. Barth, "Design and analysis of a resonating free liquid-piston engine compressor," IMECE 2007, November 11-15, 2007, Seattle, WA.

[3] J. Riofrio, E. J. Barth, "Experimental assessment of a free elastic-piston engine compressor with separated combustion chamber," Bath/ASME Symposium on Fluid Power and Motion Control, FPMC 2008, 10-12 SEPTEMBER 2008.

[4] Mikalsen, R., and Roskilly, A. P., "A Review of Free-Piston Engine History and Applications," Applied Thermal Engineering, vol. 27, pp. 2339-2352, March 2007.

[5] Nakahara, M., (2001) "Free Piston Kikai-Kouzou to Rekisi". Shinko-Techno Gihou, Vol.13, No. 25 & 26.

[6] Toutant WT. "The Worthington-Junkers free-piston air compressor," Journal of the American Society of Naval Engineers, 1952:64(3): 583-594.

[7] Underwood, A. F., "The GMR 4-4 'Hyprex' Engine: A Concept of the Free-Piston Engine for Automotive Use," SAE Technical Paper Series, 570032, vol. 65, pp. 377-391.1957.

[8] Specht DH. "Evaluation of free piston-gas turbine marine propulsion machinery in GTS William Patterson," SAE Paper 620280, 1962.

[9] Klotsch, P., (1959) "Ford Free-Piston Engine Development," SAE Technical Paper Series, 590045, vol. 67, pp. 373-378.

[10] Achten, P. A., Van Den Oeven, J. P. J., Potma, J., and Vael, G. E. M. "Horsepower with Brains: the design of the CHIRON free piston engine," SAE Technical Paper 012545. 2000.

[11] Tikkanen, S. Vilenius, M. "Hydraulic Free piston engine – challenge for control,' European Control Conference ECC99, Karsruhe, Germany, 1999.

[12] Tikkanen S., Vilenius M., "Control of dual hydraulic free piston engine," Int. J. Vehicle Autonomous Systems, Vol. 14, No. 1, 2006. pp: 3-23.

[13] T.A. Johansen, O. Egeland, E.A. Johannessen, R. Kvamsdal, "Free-Piston Diesel Engine Timing and Control – Toward Electronic Cam- and Crankshaft," IEEE Transactions on Control Systems Technology, VOL. 10, NO.2, March 2002, pp. 177-190.

[14] Johansen, T. A., Egeland, O., Johannessen, E. A., and Kvamsdal, R., "Dynamics and Control of a Free-Piston Diesel Engine," ASME Journal of Dynamic Systems, Measurement, and Control, Vol. 125, pp. 468-474, 2003.

[15] Aichlmayr HT. "Design Considerations, Modeling, and Analysis of micro-Homogeneous Charge Compression Ignition Combustin Free-Piston Engines, PhD Thesis, University of Minnesota, 2002.

[16] P. Nemecek, O. Vysoky, "Control of two-stroke free-piston generator," 2007.

[17] Mikalsen R, Roskilly AP. "The control of a free-piston engine generator. Part 1: Fundamental analyses," Appl Energy (2009).

[18] Mikalsen R, Roskilly AP. "The control of a free-piston engine generator. Part 2: Engine dynamics and piston motion control," Appl Energy (2009).

[19] A.G. Stefanopoulou, J.S. Freudengberg, J.W. Grizzle, "Variable Camshaft Timing Engine Control," IEEE Transactions on Control Systems Technology, Vol.8, No.1, march 2000, pp: 23-34.

[20] Gray, C., "A review of variable engine valve timing," In: Proc. of the SAE Conference, 1988.

[21] W. Hoffmannann, K. Peterson, A.G. Stefanopoulou, "Iterative Learning Control for Soft Landing of Electromechanical Valve Actuator in Camless Engines," IEEE Transactions on Control Systems Technology, Vol.11, No.2, march 2003, pp: 174-184.

[22] J. D. Powell, "Engine control using cylinder pressure: past, present and future," Journal of Dynamic Systems, Measurement, and Control, Vol.115 June 1993, pp. 343-350.

[23] S. Park, P. Yoon and M. Sunwoo, "Cylinder Pressure-Based Spark Advance Control for SI Engines", JSME International Journal Series B, Vol. 44, No. 2 (2001), pp.305-312.

[24] Riofrio, J. A., and Barth, E. J., "A Free Piston Compressor as a Pneumatic Mobile Robot Power Supply: Design, Characterization and Experimental Operation," International Journal of Fluid Power, vol. 8, no. 1, pp 17-28, February 2007.

[25] Goldfarb, M., Barth, E. J., Gogola, M. A., and Wehrmeyer, J. A., "Design and Energetic Characterization of a Liquid-Propellant-Powered Actuator for Self-Powered Robots," IEEE/ASME Transactions on Mechatronics, vol. 8, no. 2, pp. 254-262, June 2003.

[26] McGee, T. G., Raade, J. W., and Kazerooni, H., "Monopropellant-Driven Free-piston Hydraulic Pump for Mobile Robotic Systems," ASME Journal of Dynamic Systems, Measurement, and Control, vol. 126, pp. 75-81, March 2004.

[27] J. Riofrio, E. J. Barth, "Design and analysis of a resonating free liquid-piston engine compressor," IMECE 2007, November 11-15, 2007, Seattle, WA.

[28] Richer, E., and Hurmuzlu, Y., "A High Performance Pneumatic Force Actuator System: Part I – Nonlinear Mathematical Model," Transactions of ASME, vol. 122, pp. 416-425, September 2000.

[29] K. Annamalai, I. K. Puri, "Combustion Science and Engineering," CRC, pp.195-196, 2006.

[30] Takagi, Y., "A New Era in Spark-ignition Engines Featuring High-pressure Direct Injection". Twenty-Seventh Symposium on Combustion Institute, pp. 2055-2066, 1998.

[31] Chang, C.F., Fekete, N.P., Amstutz, A., Powell, D., 1995. "Air-fuel ratio control in spark-ignition engines using estimation theory". IEEE Transactions on Control Systems Technology, Vol .3 No .1 pp. 22-31.

[32] Won, M., Choi, S.B., Hedrick, J.K., 1998. "Air-to-fuel ratio control of spark ignition engines using Gaussian network sliding control". IEEE Transactions on Control Systems Technology, Vol. 3 No. 1 pp. 678-687.

[33] Hendricks, E., "Engine Modeling for Control Applications: A Critical Survey." Meccanica, vol. 32: pp. 387-396, 1997.

[34] Willhite, J. A., Yong, C. and Barth, E. J., (2011) "The high inertance free piston engine compressor part 1: dynamic modeling," ASME Journal of Dynamic Systems, Measurement and Control, submitted.

[35] Willhite, J. A. Yong, C. and Barth, E. J., (2011) "The high inertance free piston engine compressor part 2: design and experimental evaluation," *ASME Journal of Dynamic Systems, Measurement and Control*, submitted.

[36] Chang, C.F., Fekete, N.P., Amstutz, A., Powell, D., 1995. "Air-fuel ratio control in spark-ignition engines using estimation theory". IEEE Transactions on Control Systems Technology, Vol .3 No .1 pp. 22-31.

[37] Won, M., Choi, S.B., Hedrick, J.K., 1998. "Air-to-fuel ratio control of spark ignition engines using Gaussian network sliding control". IEEE Transactions on Control Systems Technology, Vol. 3 No. 1 pp. 678-687.

[38] Kuribayashi, K., (1993) "Criteria for the evaluation of new actuators as energy converters," Advanced Robotics, vol. 7, no. 4, pp. 289-37.

[39] JCI-SAFT (2010 June). "Rechargeable LiFePO4 lithium-ion battery Super-Phosphate™ VL 45E Fe Very High Energy cell". SAFT Batteries. SAFT Batteries. http://www.saftbatteries.com/doc/Documents/defence/Cube769/VL45EFe.e3741a09-74fd-4df4-8687-12997f445ef5.pdf

[40] Fite, K. B., and Goldfarb, M., "Design and Energetic Characterization of a Proportional-Injector Monopropellant-Powered Actuator," IEEE/ASME Transactions on Mechatronics, vol. 11, no.2, pp. 196-204, April 2006.
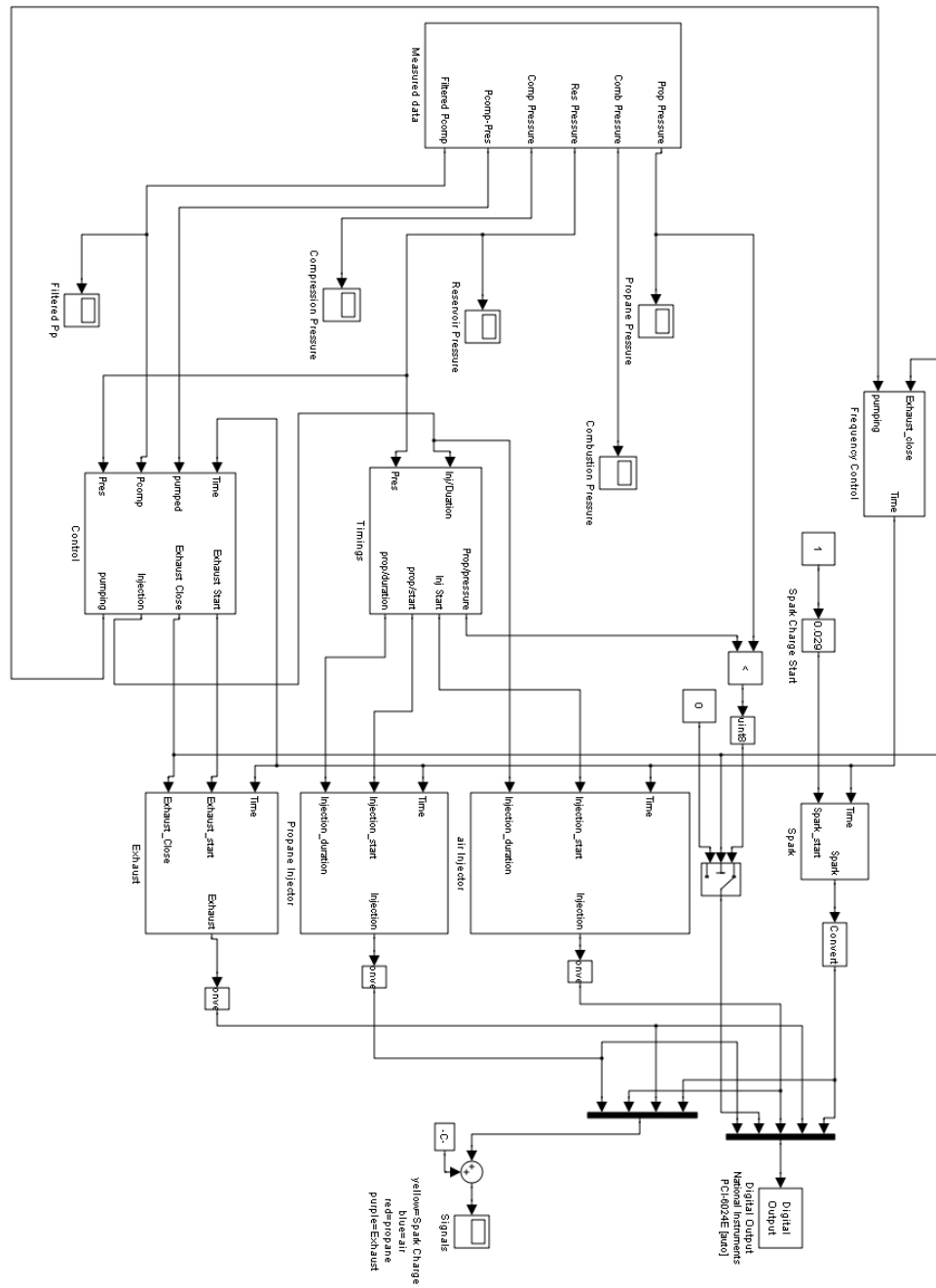
APPENDIX A

MATLAB REAL-TIME WORKSHOP DIAGRAMS

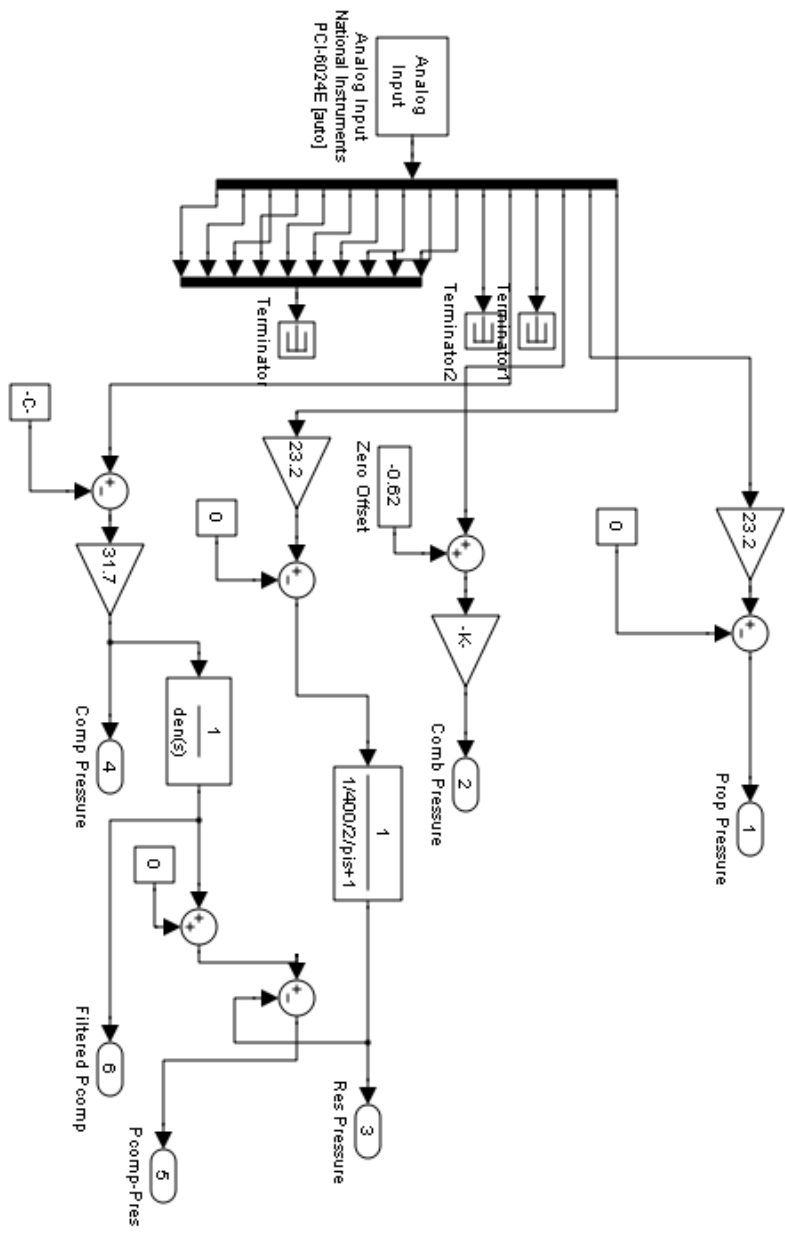Figure A-1: MATLAB Simulink real-time workshop block diagram of HIFLPC
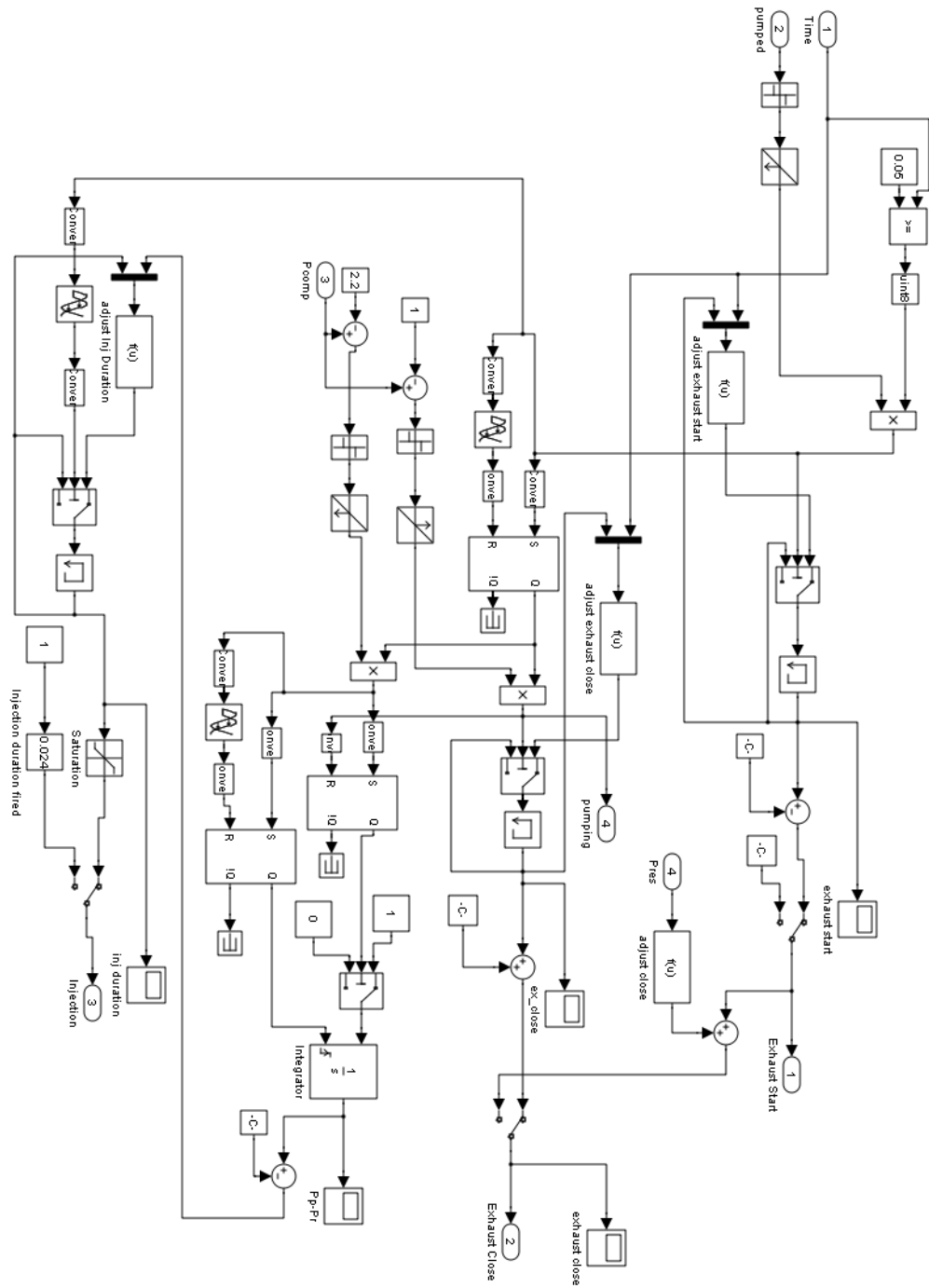
Figure A-1-1: Sensor data acquisition block

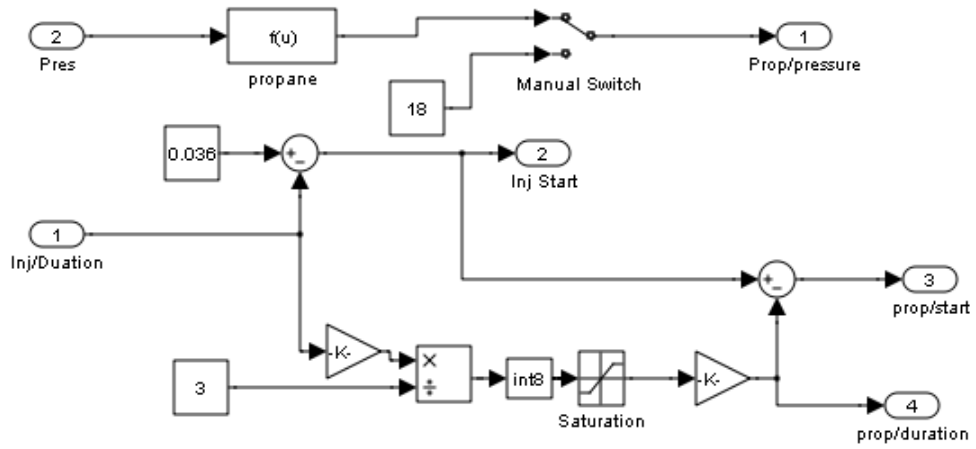Figure A-1-2: Injection duration and exhaust timing control block
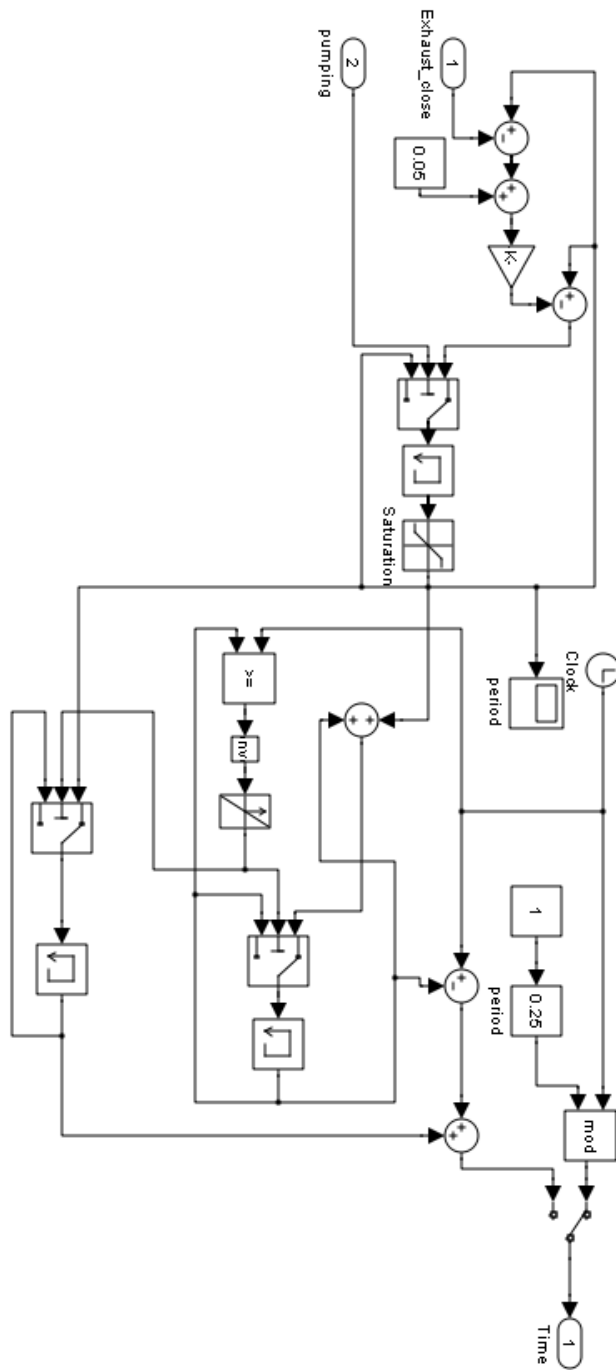
Figure A-1-3: Injection control block

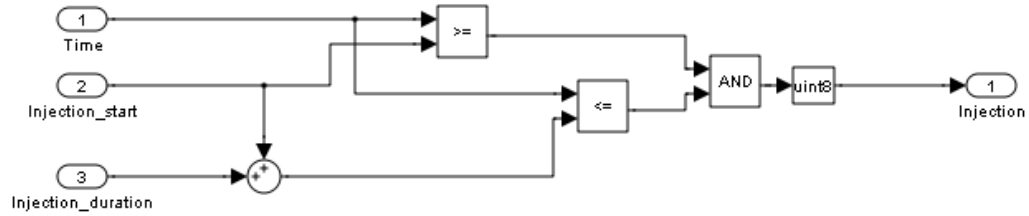Figure A-1-4: Virtual-cam and frequency control block

137

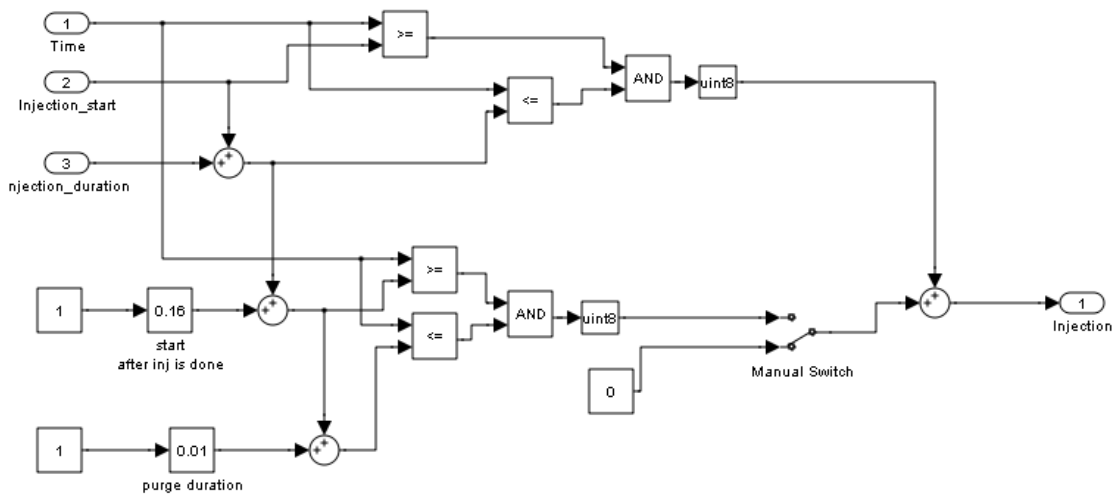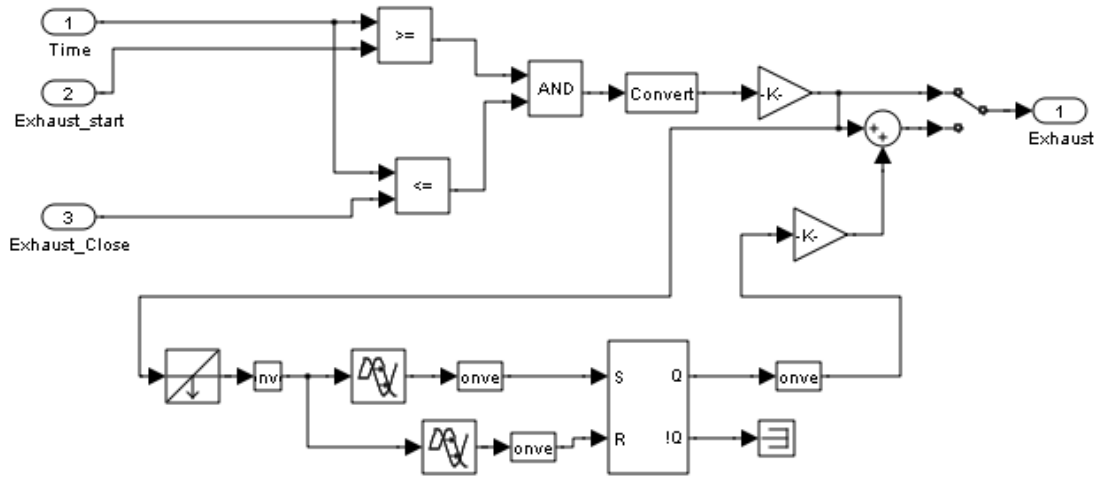Figure A-1-5: Air injector timing control block

Figure A-1-6: Fuel injector timing control block

Figure A-1-7: Exhaust valve actuator control block